

2011

A Novel Experimental Approach Using A Reconfigurable Test Setup For Complex Nonlinear Dynamic Systems

Aaron Rank
University of Central Florida

 Part of the [Engineering Commons](#)

Find similar works at: <https://stars.library.ucf.edu/etd>

University of Central Florida Libraries <http://library.ucf.edu>

This Masters Thesis (Open Access) is brought to you for free and open access by STARS. It has been accepted for inclusion in Electronic Theses and Dissertations, 2004-2019 by an authorized administrator of STARS. For more information, please contact STARS@ucf.edu.

STARS Citation

Rank, Aaron, "A Novel Experimental Approach Using A Reconfigurable Test Setup For Complex Nonlinear Dynamic Systems" (2011). *Electronic Theses and Dissertations, 2004-2019*. 1882.
<https://stars.library.ucf.edu/etd/1882>

A NOVEL EXPERIMENTAL APPROACH USING A RECONFIGURABLE TEST SETUP
FOR COMPLEX NONLINEAR DYNAMIC SYSTEMS

by

AARON RANK
B.S. Valparaiso University, 2008

A thesis submitted in partial fulfillment of the requirements
for the degree of Master of Science
in the Department of Civil, Environmental, and Construction Engineering
in the College of Engineering and Computer Science
at the University of Central Florida
Orlando, Florida

Summer Term
2011

Major Professor: Hae-Bum Yun

© 2011 AARON RANK

ABSTRACT

Experimental nonlinear dynamics is an important area of study in the modern engineering field, with engineering applications in structural dynamics, structural control, and structural health monitoring. As a result, the discipline has experienced a great influx of research efforts to develop a versatile and reliable experimental methodology. A technical challenge in many experimental studies is the procurement of a device that exhibits the desired nonlinear behavior. As a result, many researchers have longed for a versatile, but accurate, testing methodology that has complete freedom to simulate a wide range of nonlinearities and stochastic behaviors.

The objective of this study is to develop a reconfigurable test setup as a tool to be used in a wide range of nonlinear dynamic studies. The main components include a moving mass whose restoring force can accurately be controlled and reprogrammed (with software) based upon measured displacement and velocity readings at each time step. The device offers control over nonlinear characteristics and the equation of dynamic motion. The advantage of having such an experimental setup is the ability to simulate various types of nonlinearities with the same test setup. As a result, the data collected can be used to help validate nonlinear modeling, system identification, and stochastic analysis studies.

A physical test apparatus was developed, and various mechanical, electrical, and programming calibrations were performed for reliable experimental studies. To display potential uses for the reconfigurable approach, examples are presented where the device has been used to create physical data for use in change detection and deterioration studies. In addition, a demonstration is presented of the device's ability to physically simulate a large-scale orifice viscous damper, commonly used in vibration mitigation in bridges and buildings. For a large-scale viscous damper, physical testing is required to ensure structural design properties. However, due to the large scale of the dampers, expensive dynamic loading tests can be carried out at a very

limited number of facilities. Using the reconfigurable test setup, the dynamic signature of the large-scale viscous damper can accurately be simulated with pre-collected data.

The development of a system capable of emulating the restoring force of a nonlinear device with software is a novel approach and requires further calibration for increased reliability and accuracy. A discussion regarding the challenges faced when developing the methodology is presented and possible solutions are recommended.

The methodology introduced by this apparatus is very promising. The device is a valuable experimental tool for researchers and designers, allowing for physical data collection, modeling, analysis, and validation of a wide class of nonlinear phenomena that commonly occur in a wide variety of engineering applications.

I dedicate this work to all those who are special to me and have made a positive impact upon
my life.

ACKNOWLEDGEMENTS

I would first and foremost like to express my sincere appreciation for the guidance, assistance, and support by my advisor, Professor Hae-Bum “Andrew” Yun. He has been a source of knowledge, inspiration, and motivation. As an engineer and a researcher, he serves as a great role model. I am honored to be his first graduate student and can only look forward to future collaborative efforts with him.

I would also like to thank the other members of my committee, Professors Necati Catbas and Kevin Mackie, for providing me with valuable guidance and instruction during my graduate studies. So too are the efforts of my friends and colleagues working in the structural health monitoring lab: Bryan Paul and Yoonhwak “Danny” Kim. Special thanks to Professor John P. Caffrey and Miguel Hernandez at the University of Southern California for helping in the early prototyping of the Reconfigurable Test Setup. Thanks also must go to those whom I’ve met during this process at UCF: Chris O’Riordan-Adjah, who was wonderful to work under as a graduate teaching assistant; Paul DiCicco, Weston Haggren, and Erwin Rodriguez for assisting in studying efforts over a range of graduate courses; Mr. Juan Cruz for assistance staging the lab components; and Cyrus Hillsman and Ryan O’Kelley for their assistance in the design and fabrication of the riser.

I must thank my family for supporting and inspiring me throughout my educational career. My parents, Rick and Linda, for constantly encouraging and providing me with sound advice throughout my studies from Waterford High, to Valparaiso University, and eventually at UCF. You are both wonderful people and I never would have gotten to this point without you. I am honored to be your son. I must send my love and well wishes to my brother and sister, Matt and Steffi, for being a great sources of amusement throughout this process. I would also like to acknowledge my grandparents: Ed and Joan and Dottie and Arvin who have served as great

examples of how one should live their lives.

Last but certainly not least, there is my girlfriend Andrea who has been especially kind in putting up with the graduate-study lifestyle. Without her, I could never have gone through this process with such an upbeat attitude and comfortable home-life. You've been especially wonderful during this process. Special kudos to little *Jack* for always being up for a "fight" when I arrive home.

TABLE OF CONTENTS

LIST OF FIGURES	x
LIST OF TABLES	xii
1 INTRODUCTION	1
1.1 Motivation and Objective	1
1.2 Approach	2
1.3 Scope	3
2 BACKGROUND	5
2.1 Dynamic Modeling	5
2.1.1 Forcing Function Types	7
2.1.2 Relationships between Measurements	9
2.1.3 Types of Uncertainty	11
2.2 System Identification	14
2.2.1 Parametric System Identification by Least Squares Estimation	16
2.2.2 Non-Parametric System Identification with Restoring Force Method	17
2.3 Previous Reconfigurable Test Approaches	20
2.3.1 Yun and Masri Apparatus	21
2.3.2 Caffrey Apparatus	24
3 ANALYTICAL STUDY: SYSTEM IDENTIFICATION FOR NONLINEAR OSCILLATORS	28
3.1 Simulation of Nonlinear Dynamic Models	28
3.2 Measurement Uncertainty: Analysis and Discussion	31
3.2.1 System Identification without Uncertainty	34
3.2.2 Measurement Uncertainty in the Force Vector	34
3.2.3 Violation of the Deterministic LSE Model	35
3.3 Modeling Order: Analysis and Discussion	37
4 DESCRIPTION OF THE RECONFIGURABLE TEST SETUP	45
4.1 Hardware	45
4.1.1 Restoring Force Generator	45
4.1.2 Optical Table	50
4.1.3 Moving Mass	51
4.1.4 Linear Servo Motor	51
4.1.5 Measurement Sensors	52
4.1.6 Data Acquisition Systems	53

4.2	Software	54
4.2.1	Reconfigurable Test Setup Control Code	55
4.2.2	Restoring Force Calculator Code	63
5	PHYSICAL STUDY: CALIBRATION	71
5.1	Calibrating the Restoring Force Calculator	75
5.1.1	Input Data Smoothing	75
5.1.2	Interaction between the Restoring Force Electromagnet and the Linear Servo Motor	81
5.1.3	Effects of Excitation Frequency	84
5.2	Electromagnet Calibration	86
5.3	Actuator Noise and Post Filtering	88
6	PHYSICAL STUDY: APPLICATIONS	92
6.1	Damage Simulation	92
6.2	Physical Simulation of Nonlinear Viscous Damper	97
6.2.1	Background of Viscous Dampers	97
6.2.2	Simplified Mathematical Modeling	103
6.2.3	Velocity Dependent Modeling using the Reconfigurable Test Setup . . .	106
7	SUMMARY AND CONCLUSIONS	109
7.1	Summary	109
7.2	Challenges Presented in the Physical Simulation of Restoring Properties with Software	110
7.3	Future Studies Planned using the Reconfigurable Test Setup	113
7.3.1	Sample Applications	114
8	APPENDIX	118
	LIST OF REFERENCES	132

LIST OF FIGURES

Figure 1.1	Verification process flow chart.	3
Figure 2.1	Model of a nonlinear single degree of freedom (SDOF) system.	6
Figure 2.2	Displacement vs. restoring force phase plots for a linear and Duffing model.	7
Figure 2.3	Various excitation types considered in this study.	10
Figure 2.4	Relationships between displacement, velocity, and acceleration	11
Figure 2.5	A non-parametric system identification with different model orders (Yun et al., 2009).	14
Figure 2.6	Photographs of a nonlinear viscous damper (Yun et al., 2008).	22
Figure 2.7	Photographs of the Yun and Masri Apparatus Yun and Masri (2008). . .	24
Figure 2.8	Photograph of the Caffrey nonlinear test apparatus (Caffrey et al., 2004). .	25
Figure 2.9	Photograph of the time-varying friction force actuator (Caffrey et al., 2004). .	26
Figure 3.1	Simulink model of linear SDOF system undergoing forced excitation. . .	30
Figure 3.2	Simulink model of Duffing system undergoing forced excitation.	31
Figure 3.3	Comparison between noise-less and noisy measurements.	33
Figure 3.4	System identification with Least Squares Estimation with various uncertainties.	38
Figure 3.5	Sample scatter plots of identified dynamic system parameters with Least Squares Estimation and the Restoring Force Method.	44
Figure 4.1	Modeling of a nonlinear single degree of freedom system with the Reconfigurable Test Setup.	46
Figure 4.2	Photograph of the assembled Reconfigurable Test Setup.	46
Figure 4.3	Three-dimensional model of the Reconfigurable Test Setup's main components.	47
Figure 4.4	System architecture and wiring diagram of the Reconfigurable Test Setup. .	47
Figure 4.5	Pictorial flowchart of the Reconfigurable Test Setup.	48
Figure 4.6	Physical components of the restoring force generator (electromagnet). . .	49
Figure 4.7	Image of an optical table (Courtesy of Thorlabs, Inc., Newton, NJ). . . .	50
Figure 4.8	Photograph of the moving mass.	51
Figure 4.9	Photograph of the linear servo motor.	52
Figure 4.10	Direct measurement sensors.	53
Figure 4.11	Snapshot of the user interface menu.	55
Figure 4.12	LabVIEW code for user interface.	57
Figure 4.13	LabVIEW code for motion control.	59
Figure 4.14	LabVIEW code for data acquisition.	61

Figure 4.15	LabVIEW code for measurement calibration.	62
Figure 4.16	LabVIEW code for graphical analysis.	64
Figure 5.1	Pictorial locations of RFC and IRFC measurements.	73
Figure 5.2	Displacement vs. restoring force phase plot for a gap-space nonlinearity.	74
Figure 5.3	Sample nonlinear models created by the Reconfigurable Test Setup.	76
Figure 5.4	Comparison of input data smoothing.	79
Figure 5.5	Error bar plot comparing number of smoothing terms.	81
Figure 5.6	Interaction between the restoring force electromagnet and the linear servo motor.	83
Figure 5.7	Error bar plot comparing gap-space models with various stiffnesses.	84
Figure 5.8	Error bar plot comparing various excitation frequencies.	86
Figure 5.9	Displacement vs. velocity phase plots undergoing various frequencies.	87
Figure 5.10	Plot of input voltage values and the corresponding measurements recorded by the restoring force gauge.	88
Figure 5.11	Fast Fourier Transforms comparing sources of high-frequency noise.	90
Figure 5.12	Comparison between unfiltered and filtered measurements.	91
Figure 6.1	Creation of data to be used in a change detection analysis.	93
Figure 6.2	Decaying rate of coefficients k_1 and k_3	96
Figure 6.3	Time-lapse exponential decay of k_1 term.	98
Figure 6.4	Time-lapse exponential decay of k_3 term.	99
Figure 6.5	Components of a typical fluid orifice viscous damper (Soong and Dargush, 1997).	100
Figure 6.6	Photographs of viscous dampers installed in-field.	102
Figure 6.7	Simplified mathematical model of a nonlinear viscous damper.	105
Figure 6.8	Velocity vs. restoring force phase plots for various nonlinear viscous dampers.	105
Figure 6.9	Instability when simulating velocity dependent models.	106
Figure 6.10	Sample nonlinear viscous damper models created by the Reconfigurable Test Setup.	108
Figure 7.1	Installation of viscous dampers upon a long-span bridge.	115
Figure 7.2	Elevation view showing the location of shock absorbers installed on a vehicle chassis.	117
Figure 7.3	Model of a mounted turret (Chen and Wereley, 2004).	117

LIST OF TABLES

Table 2.1	Previous Options for Physically Creating Nonlinear Dynamic Data	23
Table 3.1	System Identifications of Linear and Duffing Models with No Uncertainty	34
Table 3.2	System Identification of a Duffing Model with Force Noise	35
Table 3.3	System Identification of a Linear Model with Displacement Noise	36
Table 3.4	System Identification of a Duffing Model with Displacement Noise	36
Table 3.5	System Identification of a Duffing Model with Velocity Noise	37
Table 3.6	System Identification of a Duffing Model with Acceleration Noise	37
Table 3.7	Mean Identified Coefficients via Least Squares Estimation and the Restoring Force Method	40
Table 3.8	Modeling Order Comparison Between Least Squares Estimation and the Restoring Force Method	41
Table 4.1	LabVIEW Components of the Reconfigurable Test Setup DAQ System . .	54
Table 4.2	Motion Planner Control Code	58
Table 4.3	Reconfigurable Test Setup Control Code Calibration Factors	62
Table 4.4	Current Nonlinear Feedback Types	70
Table 5.1	Types and Sources of Restoring Force Measurements	72
Table 5.2	Restoring Force Calculator Smoothing over 20 Iterations	78
Table 5.3	Comparison of Number of Smoothing Points	82
Table 5.4	Comparison of Gap-Space Models with Varied Stiffness	85
Table 5.5	Effects of Excitation Frequency	86
Table 6.1	Comparison between Update Rates	95

1 INTRODUCTION

1.1 Motivation and Objective

Experimental nonlinear dynamic systems is an important area of study in modern engineering. As a result, many researchers have spent effort researching various topics within the field, including: buildings under strong earthquake excitations, bolted joints whose deformations induce friction forces, aerospace structures incorporating joints, and computer disk drives (Ibrahim and Pettit, 2005). In the structural engineering field, applications include structural design, structural dynamics, structural control, and structural health monitoring (SHM). Despite the diversity in the field, each research project shares a common component - data collection - requiring the use of a carefully designed, controlled, and documented testing device capable of reproducing the desired dynamic behavior.

The researcher may choose to procure a device capable of replicating the desired nonlinear characteristics. For instance, Yun et al. (2009) employed large-scale orifice viscous dampers for data collection purposes in a change detection study. However, these devices are very expensive to procure, large space is required to house, and very heavy-duty machinery is needed to excite them. A great limitation with the use of a nonlinear viscous damper is that these devices are usually capable of producing one predetermined type of nonlinear behavior. For instance, a viscous damper is incapable of physically simulating a nonlinear spring. The same is also true of a nonlinear spring as it is unable to simulate a nonlinear damper.

An alternative to the utilization of a pre-fabricated device is for the researcher to build their own apparatus. However, much time is often spent designing, fabricating, and calibrating the experimental device before efforts can be placed on the targeted scope of the project. If the desire to study an alternative dynamic behavior arises, another test setup must be assembled.

An approach by Yun and Masri (2008) to conduct a stochastic uncertainty analysis included the use of an actively controlled magnetorheological (MR) damper. By varying input current into the device, Yun and Masri were able to control the dynamic behavior of the device, including uncertainty. While Yun and Masri were able to calibrate their system identification and change detection algorithms with the complex, reconfigurable nonlinear system, a number of limitations prevent the use of a MR damper in another project; the range of dynamic models is not interchangeable. Even though the nonlinear characteristics (in other words, the system parameters) can be modified, the overall equation of motion data cannot (Yun and Masri, 2008).

Another reconfigurable test approach was studied by Caffrey et al. (2004). To create a dynamic response, a time-varying dry-friction is applied in conjunction with a spring. However, similar to the use of a MR damper, Caffrey's device is not able to model a great range of nonlinear dynamic response types as the equation of motion is invariable.

With the previous discussion in mind, the purpose of this investigation is to produce a reconfigurable test setup with the ability to model a variety of stochastic time-varying, nonlinear dynamic characteristics where the user has the ability to not only vary the nonlinear characteristics, but also the equation of motion.

1.2 Approach

This study will contain two distinct components: an analytical study and a physical study. The analytical study has been completed to analyze the effects of uncertainty with regards to system identification. First, a number of models will be created using software. From these simulations, synthetic data sets of input force, restoring force, acceleration, velocity, and displacement will be found. Next, known amounts of uncertainty will be synthetically added. System identifications will be performed by Least Squares Estimation and the Restoring Force Method. An analysis will be performed to determine the effects of the uncertainty with regards

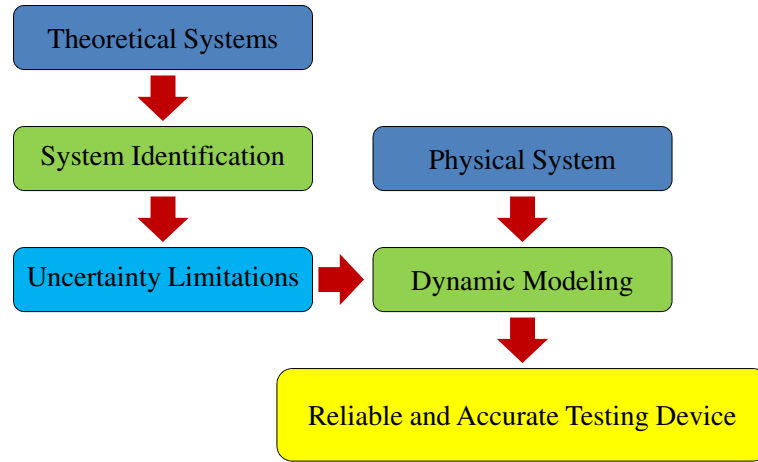


Figure 1.1: Verification process flow chart.

to system identification and physical modeling.

In a physical study, a reconfigurable test apparatus will be fabricated using an electromagnetic device controlled by a feedback controller. Once the physical apparatus is constructed, various mechanical, electrical, and programming calibrations will be conducted to quantify the accuracy and limitations for reliable experimental studies. The culmination of the research results in a case study where the Reconfigurable Test Setup is used to replicate a series of linear and nonlinear dynamic behaviors, including a gap-space nonlinearity and an orifice viscous damper. The usage of the reconfigurable approach is further documented by the creation of change detection and deterioration data. The entire verification process is outlined in Figure 1.1.

1.3 Scope

Chapter 2 of the paper is a brief introduction to necessary background information on the study, including: dynamic models, dynamic loading, orthogonality, system identification, uncertainties present in structural dynamics, and history regarding the development of previous techniques used to physically simulate nonlinear behavior. Chapter 3 analyzes system identification algorithms on a number dynamic models with varied measurement and system uncer-

tainties. An analysis is made regarding their effects upon an identification and physical model creation. Chapter 4 discusses the components of the Reconfigurable Test Setup. Chapter 5 describes a number of studies conducted to calibrate and improve the accuracy of the Reconfigurable Test Setup. Chapter 6 presents practical uses for the Reconfigurable Test Setup, including the physical simulation of time variant and invariant deterioration of a nonlinear model. Also discussed are the efforts made using device to simulate a primarily velocity-dependent nonlinear model, a viscous damper. Chapter 7 discusses number of suggestions for implementation on future evolutions of the Reconfigurable Test Setup to improved physical simulation performance.

2 BACKGROUND

In an effort to provide all readers with pertinent background information regarding the subject, a lengthy “background” chapter was included in this report. Each section of this chapter can be viewed as a separate entity, solely designed to provide the reader a basic introduction to the study, classification, and identification of dynamic systems.

2.1 Dynamic Modeling

The number of independent displacements required to define the positions of all included masses relative to their original position is called “degrees of freedom.” By the aid of computer analysis software, mechanical structures, such as buildings and bridges, can be simplified into models using a number lumped masses with various degrees of freedom. The Reconfigurable Test Setup system has been designed to represent a single mass, single-degree of freedom (SDOF) nonlinear system.

The physical modeling of a SDOF system is a challenging endeavor. A constant-mass, SDOF system can be represented by:

$$m\ddot{u}(t) + r(u(t), \dot{u}(t)) = f(t) \quad (2.1)$$

where $f(t)$ is the exciting force, m is the mass, and $r(u(t), \dot{u}(t))$ is the restoring force component which is a function of displacement and velocity. Equation 2.1 can be used to represent numerous models where displacement and velocity exhibit a wide variety of relationships to function as the restoring force. A simplified mathematical model can be seen in Figure 2.1.

Equation 2.1 can be rewritten as:

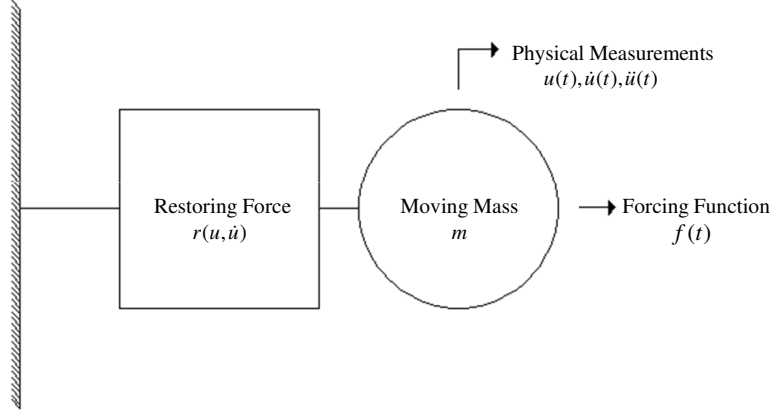


Figure 2.1: Model of a nonlinear single degree of freedom (SDOF) system.

$$r(u(t), \dot{u}(t)) = f(t) - m\ddot{u}(t) \quad (2.2)$$

in order to solve for the components of the restoring force.

When a dynamic model behaves linearly, Equation 2.1 can be expressed as

$$m\ddot{u} + c\dot{u} + ku = f(t) \quad (2.3)$$

where c and k represent the damping and stiffness constants, respectively. A phase plot showing the displacement and restoring force relationship is seen in Figure 2.2(a). For simplification in future notation, $u(t)$ has been shortened to u , $\dot{u}(t)$ to \dot{u} , and $\ddot{u}(t)$ to \ddot{u} .

A classical simple example of a nonlinear system is the Duffing oscillator. The equation of motion is described as:

$$m\ddot{u} + c\dot{u} + k_1u + k_3u^3 = f(t) \quad (2.4)$$

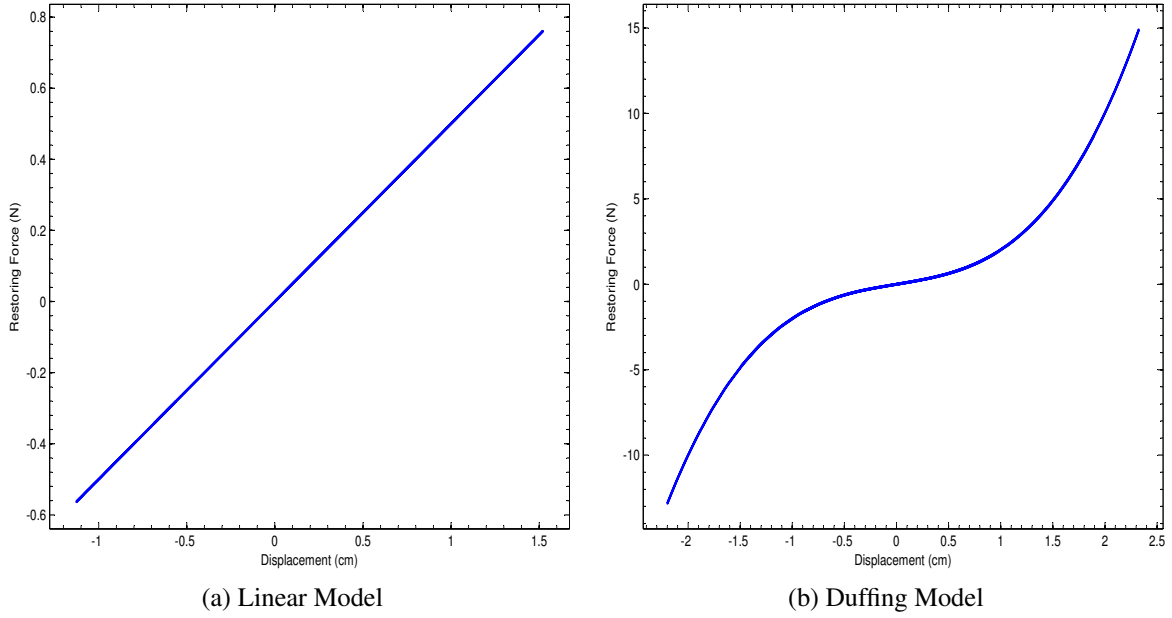


Figure 2.2: Displacement vs. restoring force phase plots for (a) linear and (b) Duffing models. A linear model exhibits a linear relationship between restoring force and displacement, while a Duffing model has cubic tendencies.

where k_1 and k_3 are stiffness coefficients. Note that because displacement has an exponential term, the properties of a Duffing system are usually dominated by the displacement cubed term at large excitation levels. A Duffing model provides an example of a nonlinear spring and its displacement and restoring force relationship is shown in Figure 2.2(b).

2.1.1 Forcing Function Types

A dynamic structure is generally excited with two types of loading: free and forced vibrations. In a free vibration, the overall motion of the system is only excited by an initial input influence. A forced vibration, on the other hand, will continuously provide external excitation. The Reconfigurable Test Setup provides only a displacement-based force excitation.

In order to investigate the amplitude and frequency dependency of nonlinear systems, different types of excitation can be applied. The first type forcing function considered in this study

is monotonic sinusoidal excitation, given by the equation:

$$f(t) = A \sin(2\pi ft) + B \quad (2.5)$$

where A is the scale, B is the offset, and f is the frequency. The resulting forcing function is given in Figure 2.3(a). A sine function will generate data measurements of the model according to *one amplitude and one frequency*.

The second type of forcing function considered in this study is beat excitation, given by:

$$f(t) = A(\sin(2\pi ft) + \sin(2\pi(f + \Delta_f)t)) + B \quad (2.6)$$

where f and Δ_f are frequencies that determine the amplitude gain, respectively, and $\Delta_f \ll f$. The resulting motion is given by Figure 2.3(b). Beat excitation will generate data measurements of the dynamic model according to *a range of amplitudes and one frequency*.

The third type of forcing function considered in this study is sine-sweep or “chirp” excitation, given by the equation:

$$f(t) = A \left[\sin \left(2\pi \left(\frac{1}{2} \right) \left[\frac{f_2}{t_f} \right] t + f_1 \right) t \right] + B \quad (2.7)$$

where f_1 and f_2 are the beginning and ending frequencies, respectively, and t_f is the final testing time. The resulting forcing function is shown in Figure 2.3(c). Chirp excitation will generate data measurements of the dynamic model according to *one amplitude and a range of frequencies*.

Beat and chirp excitation will only provide a variation of amplitudes and frequencies, respectively. However, many dynamic models behave exhibit different characteristics under a

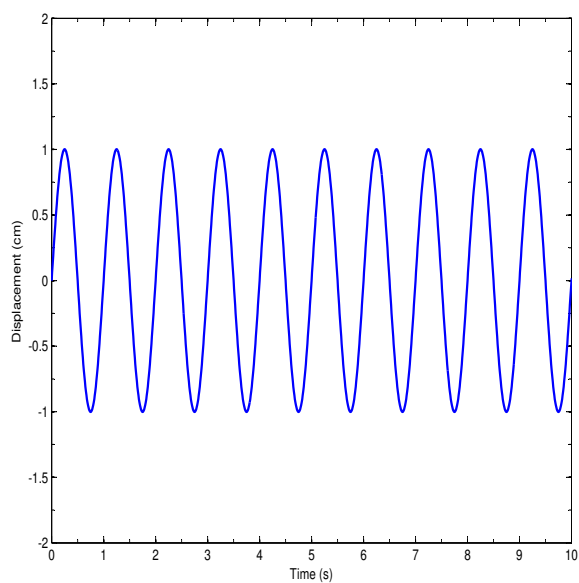
range of amplitudes and frequencies. To generate a number of possible behavior outcomes under a range of excitation amplitudes and frequencies, a broadband random distribution force can be utilized. Its motion is governed by the equation:

$$f(t) = Ay(t) + B \quad (2.8)$$

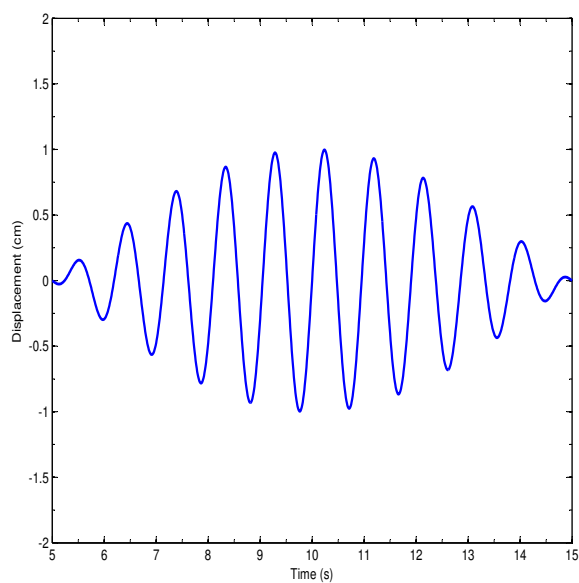
where $y(t)$ is a $\{t \times 1\}$ vector whose distribution follows the standard normal (the size depends upon the sampling rate and total sampling time). As compared to a simple sine excitation where uniform displacement, velocity, and acceleration values would be obtained for each test, random excitation will produce constantly altered values at each time step. Therefore, using a forcing function with variable properties is advantageous to use when a large sample of data undergoing various amplitudes and frequencies is desirable. A plot showing a broadband random force vs. time is shown in Figure 2.3(d).

2.1.2 Relationships between Measurements

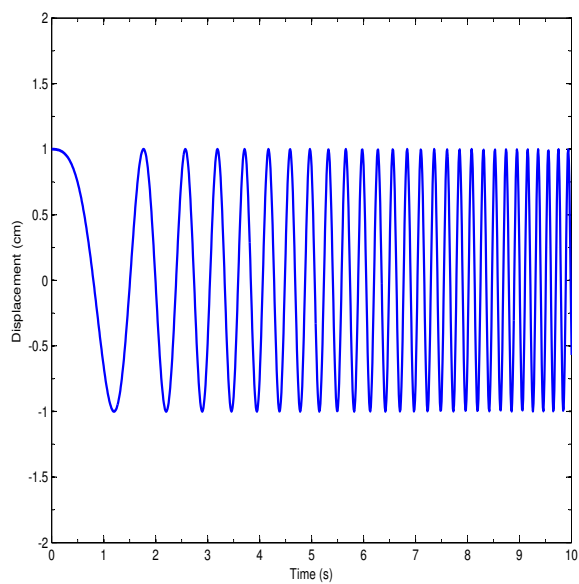
For the response of dynamic systems, the displacement and velocity are orthogonal, with the phase difference of $\pi/2$. Thus a velocity vs. displacement phase plot will be result in a circle (Figure 2.4(a)), meaning no statistical correlation exists. A similar representation of the phase plot can be seen if the magnitudes of displacement and velocity are graphed with time (Figure 2.4(b)). Displacement and acceleration have a phase difference of π , meaning that the two are inversely proportional (i.e. one's maximum occurs simultaneously at the other's minimum) and have a correlation in their values. By taking acceleration, velocity, and displacement measurements of the system, system identification methods can be used to describe the dynamic profile of the model.



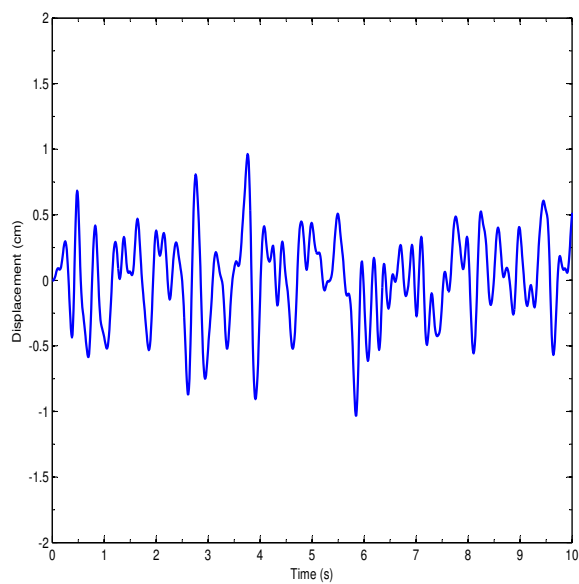
(a) Sine Excitation



(b) Beat Excitation



(c) Chirp Excitation



(d) Broadband Random Excitation

Figure 2.3: Various excitation types considered in this study.

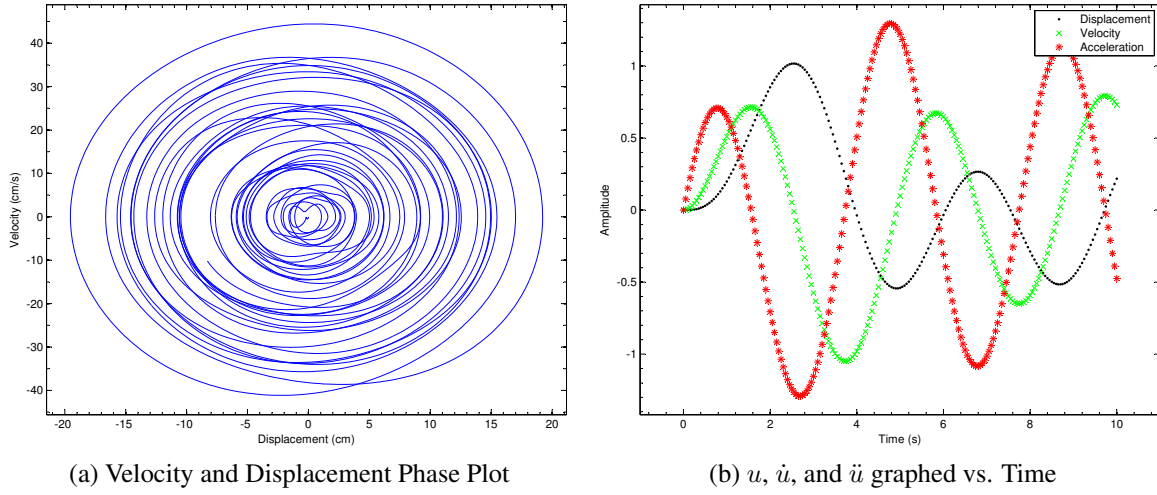


Figure 2.4: Plots demonstrating the relationships between displacement, velocity, and acceleration. (a) shows the orthogonality between displacement and velocity. (b) details shows the difference in phases between each: displacement and velocity differ in phase by $\pi/2$ and displacement and acceleration differ in phase by π .

2.1.3 Types of Uncertainty

A number of types of uncertainty may exist in the field of structural dynamics. In the construction, design, and/or modeling of structure, sources of uncertainties include: imperfections, external load effects, and the interaction between loads and the structure. These types of uncertainties have a significant influence on the structural response. Therefore, it is extremely useful to study their influences and are critical for the design and maintenance of a structure (Balthazar et al., 2008).

Two distinct types of ambiguity are generally considered in engineering risk analysis: inherent randomness (or aleatory uncertainty) and subjective (or epistemic) uncertainty (Ayyub and Klir, 2006). Of the two, epistemic uncertainty is of main concern with the implementation of the Reconfigurable Test Setup. Epistemic uncertainty primarily exists due to the lack of complete information about regarding a engineering endeavor. This uncertainty can be reduced if additional knowledge is gained. However due to various technological and feasibility restrictions,

the intrinsic uncertainty often cannot be reduced (Ang and Tang, 1975).

Within this discussion, epistemic uncertainty can be further partitioned into uncertainties that may exist in the physical simulation of a dynamic model: measurement uncertainty and system uncertainty.

Measurement Uncertainty

In a physical system, measurements are taken by sensors which are polluted by noise from a variety of sources. Furthermore only displacement or acceleration is measured in many *in situ* health monitoring applications. When other response states are then derived from the recorded data, thereby proliferating the effects of measurement noise (Yun et al., 2009). However because the Reconfigurable Test Setup utilizes direct measurements for displacement, velocity, and acceleration, no propagation will occur as the effects will be additive. The uncertainty of these measurements is time-uncorrelated (white noise) because the amount of noise present will remain constant throughout an experiment given the carefully controlled settings of the laboratory.

System Uncertainty

System characteristic uncertainty can also add a degree of error into a system identification. However, as opposed to measurement uncertainty which is primarily polluted by a time-uncorrelated noise, system uncertainty (with respect to system models) is often caused in two ways: excessive model-order reduction and environmental effects (Yun and Masri, 2008, 2009). In the confines of the laboratory, environmental changes are assumed negligible and are therefore not considered in the Reconfigurable Test Setup study.

Excessive model-order reduction may cause error in system identifications because in many applications, it is not possible to characterize the dynamic motion of each system by a simple

equation. Consider the true system parameters are designated as \mathbf{p} . The significance of system uncertainty due to modeling error can be categorized with regards to the correlation of the system complexity, $O(\mathbf{p})$, and the model complexity, $O(\mathbf{q})$. The relationship between $O(\mathbf{p})$ and $O(\mathbf{q})$ will fall into one of three conditions (Yun and Masri, 2008):

1. $O(\mathbf{p}) > O(\mathbf{q})$, where the system complexity is greater than the model complexity (i.e. underfitting)
2. $O(\mathbf{p}) = O(\mathbf{q})$, where the system complexity is equal to the model complexity (i.e. perfect fitting)
3. $O(\mathbf{p}) < O(\mathbf{q})$, where the system complexity is less than the model complexity (i.e. overfitting)

Because the components of \mathbf{p} are usually unknown, the modeling is generally either underfit or overfit. Depending upon the system identification method, a statistical bias may be introduced into the identification with an imperfect model (Mendel, 1995). In a physical simulation sense, system uncertainty in the Reconfigurable Test Setup may exist due to the under or over simplification of complex models.

In the Restoring Force Method (to be discussed in Section 2.2.2) the restoring force of a dynamic system is modeled with a series of coefficients. Yun and Masri (2008) compared the identification results using fifth order polynomials versus twentieth order polynomials for a magneto-rheological (MR) damper. The MR damper was identified with the model orders of 5 and 20 out of the highest order of 20 ($O(5/20)$ and $O(20/20)$, respectively) to investigate the effects of model-order reduction. Figure 2.5(a) shows the velocity-force plot of the measured response. Figure 2.5(b) shows with a reduced-ordered model, although the majority of the traces of the velocity-force plot can be identified, the details of the traces fail to be identified due to

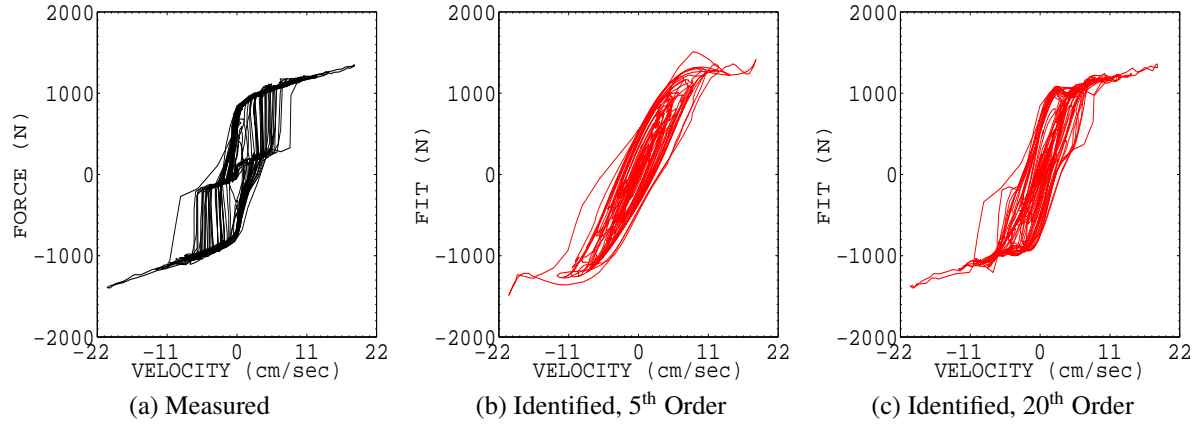


Figure 2.5: A non-parametric system identification with different model orders (Yun et al., 2009).

the highly nonlinear behavior of the MR damper. Figure 2.5(c) shows that with the higher $O(20/20)$, the discontinuous nonlinearity is much more accurately identified (Yun and Masri, 2008). It must be noted the solution time required to solve for the twentieth order polynomials was much larger than to generate a solution with fifth order polynomials.

In most real-world applications of non-parametric system identifications, the desired modeling precision will dictate the modeling order. While a higher-ordered analysis will provide the most accurate representation of nonlinear characteristics, reliable change detection with the use of reduced-ordered models of orthogonal basis functions prove to be more time and cost efficient than a higher-order analysis (Yun et al., 2009). System identification with orthogonal basis functions will be evaluated in Section 3.3.

2.2 System Identification

The purpose of a system identification technique is to determine the dynamic properties of a system by creating a mathematical model based upon recorded data. Over time, researchers have created a number of the methods to describe the behavior of a system and two levels of identification have been developed: general system identification and component level identi-

fication. In general system identification, the goal is to detail how the overall structure will respond to excitation (Hart and Yao, 1976). For instance, Yun et al. (2008) utilized the Natural Excitation Technique in conjunction with Eigensystem Realization Algorithm to extract modal parameter information of a long-span suspension bridge. With this data, mode shapes and frequencies for the entire bridge can be found under various types of excitation. For specific information regarding these studies, the reader is referred to Yun et al. (2008) and Nayeri et al. (2009).

This study, on the other hand, will focus upon component level system identification, where the objective is to quantify and model the restoring capabilities of a system. More specifically this study will concentrate upon the single mass, single degree of freedom case, thus its application will include the physical modeling of springs and dampers (Tasbihgoo et al., 2007).

A number of confines exist on parametric identification. At the start of the determination, various assumptions must be made regarding the predicted behavior of the system and cannot be changed throughout the identification process. Thus by making these assumptions, the system is being “forced” to behave a certain way. Consequently, substantial error will arise if the assumptions made at the start do not closely match the actual behavior of the system. For example, if a Duffing model was analyzed as a linear model in the form of Equation 2.3, a poor classification would result because a very influential term is omitted (displacement-cubed).

The confines of parametric system identification can be alleviated by the use of non-parametric identification, which will be explained in Section 2.2.2. Unlike parametric system identification, non-parametric system identification techniques do not require *a priori* information about the restoring capabilities of a dynamic model.

2.2.1 Parametric System Identification by Least Squares Estimation

To perform parametric system identification, Least Squares Estimation (LSE) will be used. LSE is an optimal estimator for determining the optimal value of $\{\theta\}$ with only the presence of input force measurement uncertainty. The unknown dynamic coefficients are estimated in a batch solution (thus requiring all data to be recorded before parameters can be found). A limitation of this method is that the results of the identification are a singular value for each coefficient. Thus, system changes that occur during measurement collection are averaged into the final identification. Similarly, the method assumes that no uncertainty exists in recorded measurements, only in the applied force. Thus if the measurements taken are not completely “clean” (which cannot always be assured) and are desired to be utilized in a LSE identification, the assumptions will be violated.

The equation for Least Squares Estimation that describes a dynamic system begins with the generic linear model:

$$\{Z(t)\} = [H(t)]\{\theta\} + \{V(t)\} \quad (2.9)$$

where $\{Z(t)\}$ is an $\{N \times 1\}$ vector detailing the applied force, $[H(t)]$ is a $[N \times n]$ matrix collection of measurements, $\{\theta\}$ is a $\{n \times 1\}$ vector giving the dynamic coefficients, and $\{V(t)\}$ is a $\{N \times 1\}$ giving the uncertainty present in the force. The goal of Least Squares Estimation is to find the most likely value of $\{\theta\}$, designated as $\{\hat{\theta}\}$. A cost function can be applied to Equation 2.9 such that

$$J(\hat{\theta}) = [Z(t) - \hat{Z}(t)]^T [W(t)] [Z(t) - \hat{Z}(t)]^T \quad (2.10)$$

is minimized, where $[W(t)]$ is a weighting matrix used to place more emphasis upon selected

measurements and is required to be symmetric and positive definite. Through linear manipulation, the weighted least squares solution to Equation 2.9 that optimizes Equation 2.10 is

$$\{\hat{\theta}_{WLS}\} = [H(t)^T W(t) H(t)]^{-1} H(t)^T W(t) Z(t) \quad (2.11)$$

Should all measurements be considered equally (i.e. $[W(t)]$ is equal to the identity matrix, $[I(t)]$), Equation 2.11 can be simplified into:

$$\{\hat{\theta}_{LS}\} = [H(t)^T H(t)]^{-1} H(t)^T Z(t) \quad (2.12)$$

In a parametric identification, the method described by Equation 2.12 will provide an accurate computation of the values of $\{\theta\}$. However there are a few limitations on this model: (1) Least Squares Estimation assumes that $[H(t)]$ is deterministic. Frequently this is not the case as some level of noise is usually present in any measured value; and (2) The force vector, $\{Z(t)\}$, and the force uncertainty vector, $\{V(t)\}$ become incorporated when Equation 2.9 is transformed into Equation 2.11. In many real-world applications the exact amount of noise is unknown, but always present. Because of the derivation of the equation, uncertainty in $\{Z(t)\}$ exists.

2.2.2 *Non-Parametric System Identification with Restoring Force Method*

The system identification procedures considered in the previous section were parametric, meaning the only terms describing the dynamic properties were those included in their respective equations. A common technical challenge in system identification applications is accurate mathematical representation (or modeling) of a nonlinear dynamic system is usually unknown. The restrictions of having to make assumptions in a parametric identification technique can be alleviated by using non-parametric methods that do not require *a priori* knowledge (meaning a reasonable estimation about the system's behavior) about the system, and the modeling

processes are data-driven. For this reason, the method remains valid even if the system is transformed (often through deterioration) into another type of nonlinearity. Because the analysis method is model-free, however, physical interpretation with most non-parametric approaches is not straightforward since there are no direct relationships between the identified model and system characteristics. For example, in Artificial Neural Networks (ANN) the model complexity is not uniquely defined, even with a successful identification (Masri et al., 2000). System identification results obtained by RFM, however, are able to be physically interpreted as verified in Yun and Masri (2008), Yun and Masri (2009), and Yun et al. (2009).

Introduced by Masri and Caughey (1979), the Restoring Force Method is an approach used to identify a variety of dynamic phenomena. The restoring force of Equation 2.2 can be approximated by a series of two-dimensional Chebyshev polynomials:

$$r(u(t), \dot{u}(t)) \approx \hat{r}(u(t), \dot{u}(t)) = \sum_{i=0}^{MX} \sum_{j=0}^{NY} \bar{C}_{ij} T_i(\bar{u}) T_j(\bar{\dot{u}}) \quad (2.13)$$

where T_n is the n^{th} order Chebyshev Polynomial and the normalized values of u and \dot{u} are the normalized displacement and velocity in the range $[-1, 1]$ given by:

$$\bar{u} = \left[\frac{u - \left(\frac{u_{max} + u_{min}}{2} \right)}{\left(\frac{u_{max} - u_{min}}{2} \right)} \right]$$

$$\bar{\dot{u}} = \left[\frac{\dot{u} - \left(\frac{\dot{u}_{max} + \dot{u}_{min}}{2} \right)}{\left(\frac{\dot{u}_{max} - \dot{u}_{min}}{2} \right)} \right].$$

By restricting the range from $[-1, 1]$, orthogonality in the Chebyshev polynomials is preserved (Datta and Mohan, 1995). \bar{C}_{ij} is the normalized Chebyshev coefficient given by

$$C_{ij} = \begin{bmatrix} (2/\pi)^2 v & i \text{ and } j \neq 0 \\ (2/\pi^2) v & i \text{ or } j = 0 \\ (1/\pi^2) v & i = j = 0 \end{bmatrix},$$

where

$$v = \int_{x=-1}^1 \int_{y=-1}^1 f(x, y) T_i(x) T_j(y) w(x) w(y) \, dx dy$$

but for convenience of computation and by making the transformation $x = \cos \theta$, $y = \cos \phi$, v is discretized into:

$$v = \sum_{k=-1}^{MX2} \sum_{l=-1}^{MY2} f_{kl} \cos [i(\Delta\theta)(k-1)] \cos [j(\Delta\phi)(l-1)] \Delta\theta \Delta\phi$$

where

$$\Delta\theta = \frac{\pi}{MX2}$$

$$\Delta\phi = \frac{\pi}{NX2}$$

and

$$f_{kl} = f(\cos \theta_k, \cos \phi_l)$$

$$\theta_k = (k-1)\Delta\theta$$

$$\phi_l = (l-1)\Delta\phi$$

where $MX2$ and $MY2$ are user defined parameters (essentially giving the “resolution” of the analysis) based upon discretization resolution.

Once the normalized Chebyshev coefficients are identified, they can be converted into an equivalent power series, resulting in:

$$\hat{r}_p(u(t), \dot{u}(t)) = \sum_{i=0}^{MX} \sum_{j=0}^{NY} \bar{a}_{ij} \bar{u}^i \bar{\dot{u}}^j = \sum_{i=0}^{MX} \sum_{j=0}^{NY} a_{ij} u^i \dot{u}^j \quad (2.14)$$

where \bar{a}_{ij} is a normalized power series coefficient, a_{ij} is a de-normalized power series coefficient and $\hat{r}_p(u(t), \dot{u}(t))$ is the restoring force identified with a power series (Mason and Handscomb, 2002; Yun et al., 2009). The normalized power-series coefficients, \bar{a}_{ij} , and denormalized power-series coefficients, a_{ij} , are convenient for physical interpretation because they are directly related to parametric stiffness or damping characteristics. On the other hand, the orthogonal Chebyshev polynomials, \bar{C}_{ij} , have a number of desirable features that are ideal for condition assessment and health monitoring purposes: (1) they are statistically unbiased with respect to model complexity; and (2) the distributions of orthogonal coefficients can be reliably used to detect changes (even if a reduced-order model is used in the system identification process).

2.3 Previous Reconfigurable Test Approaches

In the experimental nonlinear dynamics field, researchers defend new findings based upon acquired data. Thus the procurement of a device capable of providing the desired dynamic restoring force is essential. However, a number of confines exist on attaining many of these apparatuses:

- The devices are often very large. In the case of a nonlinear viscous damper - nearly 15 feet long and weighing many tons - thus creating many logistical (transportation, storage, etc) difficulties.
- In addition, many of these devices require large forcing inputs (some as high as 650 kip) for excitation which many facilities simply do not have.

- Should a different model be desired to examine, either the properties of the current device must be altered (if it is even possible) or a new device must be procured.

In the past, a number of viable options exist for the creation of physical dynamic data. The researcher may choose to procure a specific physical device capable of simulating the target dynamic model. Although physical data will be able to be captured, a number of drawbacks to this approach exist: these devices often require large space to house and specific machinery to excite. Furthermore, the range of dynamic models produced by the device is most likely very rigid. Photographs of a 250 kip viscous damper used for research purposes at the University of California, Berkeley can be seen in Figure 2.6 (Yun et al., 2008).

Alternatively, the researcher may choose to create a custom device, but much time and effort will be spent designing, assembling, and calibrating the device. Rapid prototyping, which involves repeated and automatic assembling of physical objects, shows promise in quickly manufacturing a number of physical devices. (Wright, 2000). The drawback, however, is that for every system change desired, a new device must be created.

The Yun and Caffrey apparatuses can be considered previous generations of the Reconfigurable Test Setup, an extended summary of their features are presented in Sections 2.3.1 and 2.3.2. Each of the discussed approaches are described in Table 2.1.

2.3.1 Yun and Masri Apparatus

In a 2008 experimental study aimed at verifying a change detection method with the presence of system uncertainty, Yun and Masri utilized a SDOF magnetorheological (MR) damper, for the creation of change detection data. A MR damper is a semi-active energy dissipation device commonly used in a variety of civil engineering applications. The properties of the damper's output force can be precisely controlled by the input current it receives. By varying the input current by broadband random excitation, the MR damper could effectively create a



(a)



(b)

Figure 2.6: Photographs of a viscous damper on a testing machine at the University of California, Berkeley (Yun et al., 2008).

Table 2.1: Previous Options for Physically Creating Nonlinear Dynamic Data

Modeling Device	Advantages	Disadvantages
Acquiring a specific device	Will fit exact needs of research or desired use	Device may be difficult to acquire, house, excite
Creation of a custom device	Will fit exact needs of research or desired use	Much time and effort required to design, fabricate, and calibrate each component Device will often not have utility after the study is complete
Rapid Prototyping	A variety of dynamic models can be physically created	To achieve a wide range of dynamic models, a large number of devices may need fabrication Dynamic model deterioration difficult to implement
Yun and Masri Apparatus	Ability to vary dynamic parameters Ability to simulate deterioration	Requires the procurement of a MR damper and other specialized equipment Inability to vary the equation of motion
Caffrey device	Ability to model various dynamic systems On-board DAQ, parameter variation, and excitation control	Inability to vary the stiffness Inability to vary the equation of motion

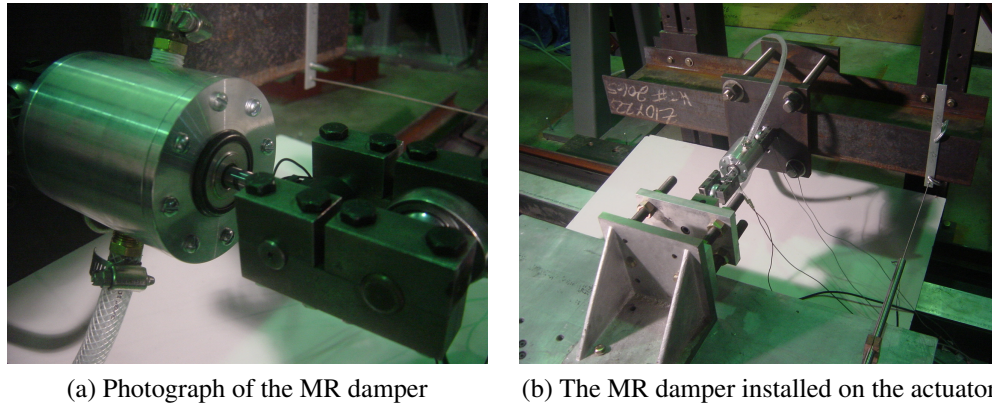


Figure 2.7: Elements of the Yun and Masri (2008) experimental setup that allows for the modification of dynamic properties.

number of physical data sets required for intended research goals. Photos of a MR damper can be seen in Figure 2.7 (Yun and Masri, 2008).

The dynamic modeling of restoring properties by an electromagnet served as partial inspiration for the Reconfigurable Test Setup. Similar to the MR damper, variation of the input current allows for control over the restoring properties. However a MR is limited in its range of dynamic models that it can simulate, as the device is not manufactured for this purpose. For example, a MR damper is incapable of replicating a nonlinear spring.

2.3.2 *Caffrey Apparatus*

A reconfigurable testbed was pioneered by Caffrey et al. (2004). It is capable of modeling a variety of generic, nonlinear phenomena such as dry-friction, time-varying hysteretic phenomena, elastic nonlinearities, and nonlinear viscous forces. The goal of the Caffrey study was to simulate the nonlinear response of SDOF systems with generic type of nonlinearities to utilize and calibrate an on-line identification algorithm.

Photographs of the Caffrey apparatus are shown in Figures 2.8 and 2.9. To provide the stiffness to the system, a spring was utilized. To simulate the damping characteristics of the

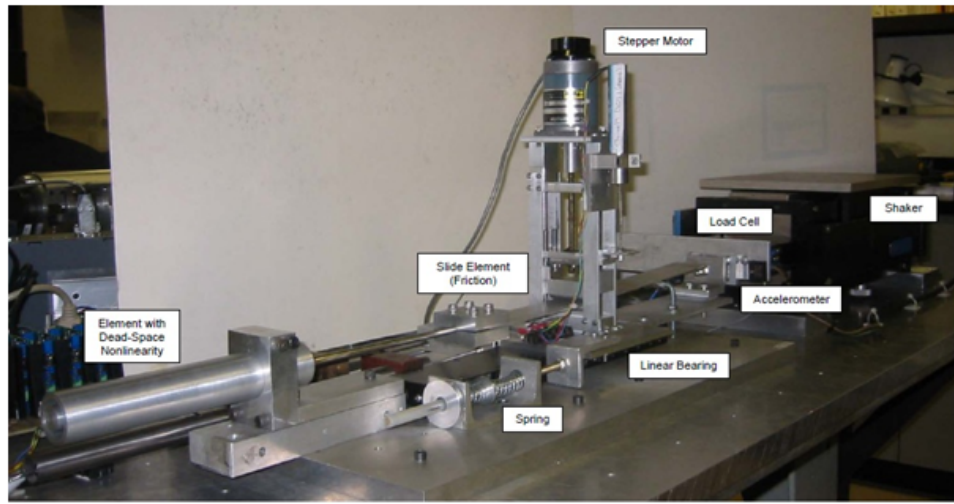


Figure 2.8: Photograph of the Caffrey nonlinear test apparatus (Caffrey et al., 2004).

system, a time-varying normal force was applied to a bar between two edges that produces a dry friction. The degree of damping was controlled by the amount of normal force applied upon the bar by a computer-controlled electro-mechanical device.

By collecting data at varying degrees of damping and comparing the results, the researchers could calibrate their proposed reduced-order nonlinear model. By varying the amount of dry friction, the dynamic properties of the system change, thereby allowing the device to simulate a number of different dynamic models at once, essentially simulating the properties that it normally would have taken an inventory of hundreds of different physical nonlinear systems. Thus, the Caffrey apparatus is advantageous to employ when one needs access to a number of different damping characteristics (Caffrey et al., 2004). However, it does have limited bounds in the variety of dynamic models it can emulate.

The goal of the Reconfigurable Test Setup project is to simulate a variety of real-world systems requiring great versatility in its restoring force components. In the Caffrey device, the stiffness of the system was limited to the stiffness of the spring, thereby greatly limiting its application. To model a specific real-world application, the researcher would need to find a

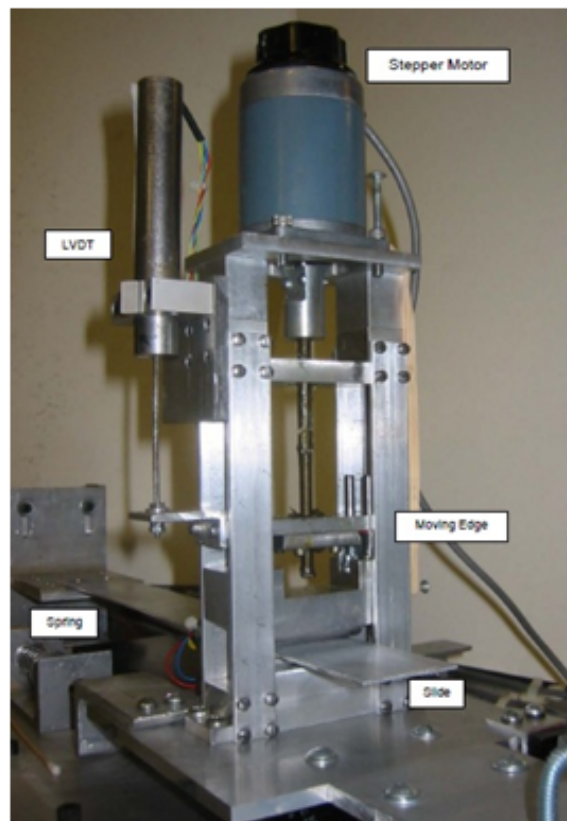


Figure 2.9: Photograph of the time-varying friction force actuator (Caffrey et al., 2004).

spring with the exact stiffness, thereby limiting the modeling capabilities of the apparatus to the amount of springs in researcher's inventory.

The Caffrey device, despite lacking complete dynamic modeling flexibility, does provides a framework of components required in the Reconfigurable Test Setup, including a: (1) embedded DAQ system; (2) restoring force control program; and (3) on-board system identification techniques. Each of these components are crucial inclusions of a functional reconfigurable testbed.

3 ANALYTICAL STUDY: SYSTEM IDENTIFICATION FOR NONLINEAR OSCILLATORS

The Reconfigurable Test Setup involves the replication of nonlinear dynamic models. Because this study pertains to the *physical* simulation of restoring force, uncertainties will be present. The physical and software components of the setup, introduced in Chapter 4, were chosen to limit uncertainty as much as possible. Despite these measures, unknown levels of measurement uncertainty may pollute recorded signals. Additionally as the Reconfigurable Test Setup continually expands its range of experimental applications, reduced ordered modeling is a realistic and beneficial option, especially in data creation for change detection or deterioration studies of highly nonlinear devices.

To explore the limits and constraints of the various parametric and nonparametric system identification methods to be used, a number of dynamic models were created theoretically. In each of these models, the dynamic model properties are inputs into the system. Various types of uncertainty will then be intentionally added to models in order to analyze and quantify the limitations of system identification and discuss its effects upon force replication.

3.1 Simulation of Nonlinear Dynamic Models

Two types of dynamic restoring force types will be analyzed in the theoretical study: linear and Duffing. By including these two types of nonlinearities, a broad spectrum of dynamic systems will be covered. Numerous types of dynamic models exist but by including a type whose motion is governed by a particular term and one whose motion is equally controlled by all terms, the limitations and strengths of system identification can be demonstrated.

To create the theoretical models, Simulink, a dynamic systems analysis tool that operates simultaneously with MATLAB, was utilized. Embedded into each Simulink code is a variety

of solution methods that are able to numerically approximate solutions for a differential equation. The Runge-Kutta method was chosen to solve the theoretical models because it is an accurate procedure for obtaining an approximate solution to dynamic problems. The Runge-Kutta method gives an accurate approximation of the system of terms that can be determined in a computer-friendly manner - first and second order analysis - whose calculations are already required (to generate acceleration, velocity, and displacement). In these calculations, a fourth-order Runge-Kutta procedure (Zill et al., 2006) takes the form:

$$\begin{aligned}
y_{n+1} &= y_n + \frac{h}{6}(k_1 + 2k_2 + 3k_3 + k_4) \\
k_1 &= f(x_n, y_n) \\
k_2 &= f(x_n + \frac{1}{2}h, y_n + \frac{1}{2}hk_1) \\
k_3 &= f(x_n + \frac{1}{2}h, y_n + \frac{1}{2}hk_2) \\
k_4 &= f(x_n + h, y_n + hk_3) \\
y' &= f(x, y)
\end{aligned} \tag{3.1}$$

where h is a fixed step size that is small enough to ensure a smooth fitting between the data points, particularly important since the Runge-Kutta method is a numerical approximation. Should the step size be large, error would compound very quickly and result in faulty and unstable results. The values of x_n and y_n are displacement and velocity values, respectively, with the starting values equal to the specified initial conditions.

A linear model follows the relationship specified by Equation 2.3 and its behavior is governed by the values of the stiffness and damping coefficients. To model in Simulink, Equation 2.3 can easily be manipulated to be solved for in terms of acceleration:

$$\ddot{u}(t) = \frac{f(t)}{m} - \frac{c}{m}\dot{u}(t) - \frac{k}{m}u(t) \tag{3.2}$$

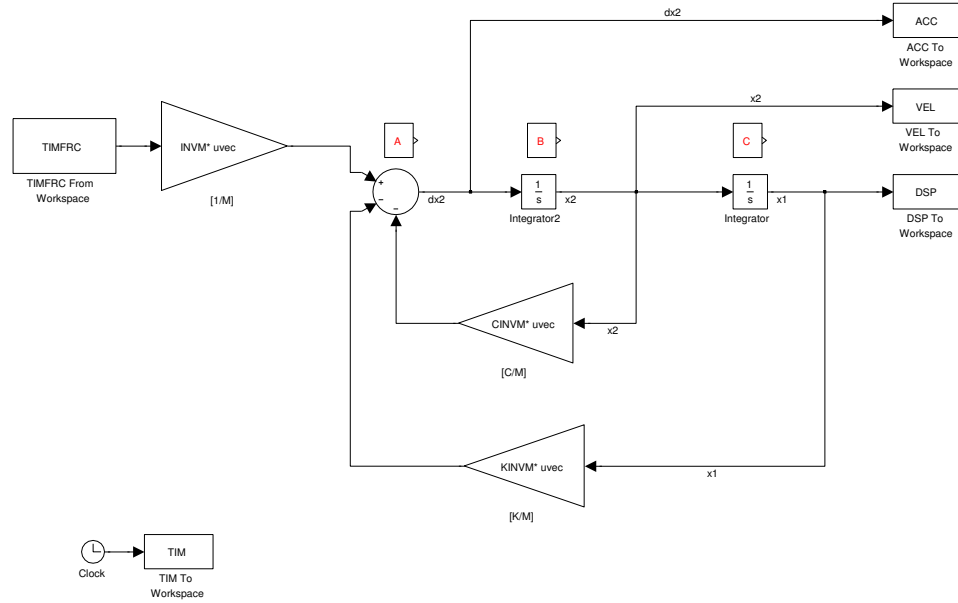


Figure 3.1: Simulink model of linear SDOF system undergoing forced excitation.

The Simulink model for a linear system is seen in Figure 3.1 where the equal sign of Equation 3.2 can be considered the circular summation command in the center of the figure (labeled as “A”). On the right hand side, acceleration is integrated twice - resulting in velocity (labeled as “B”) and displacement (labeled as “C”). The velocity and displacement are multiplied by their respective coefficients and proceed into the circular summation command. The process is then repeated with the previous values found for displacement and velocity. The output of the simulation is a series of displacement, velocity, and acceleration measurements.

To create a Duffing Model in Simulink, Equation 2.4 was modified into:

$$\ddot{u}(t) = \frac{f(t)}{m} - \frac{c}{m}\dot{u}(t) - \frac{k_1}{m}u(t) - \frac{k_3}{m}u(t)^3 \quad (3.3)$$

where the values of c , k_1 , and k_3 (the viscous damping and stiffness coefficients, respectively) and are each input at the onset of the modeling process. The Simulink model for Duffing Model is seen in Figure 3.2 and can be interpreted similarly to Figure 3.1.

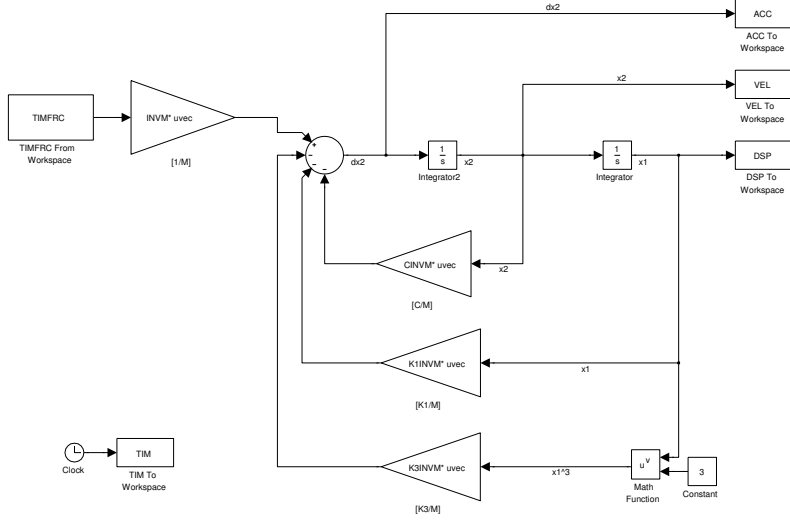


Figure 3.2: Simulink model of Duffing system undergoing forced excitation.

3.2 Measurement Uncertainty: Analysis and Discussion

To explore the effects of measurement uncertainty on the system identification methods, broadband white noise (following a normal distribution to the root-mean square of the measurement signal) is intentionally added to the results. A comparison of noise-less and noise-polluted displacement vs. time measurements of identical, generic linear models can be seen in Figure 3.3. In this analysis, the parametric system identification technique, Least Squares Estimation will be explored and its limitations and strengths will be analyzed. To discuss these limitations, the results must be compared by quantifiable means. Normalized mean-square-error (NMSE) was utilized and is calculated by

$$NMSE(\hat{f})(\%) = \frac{100}{N\sigma_f^2} \sum_{i=1}^N (f_i - \hat{f}_i)^2 \quad (3.4)$$

where f_i is the measured force, \hat{f}_i is the identified force, N is the number of data points, and σ_f^2

is the variance of the measured force (Worden, 1990). NMSE will provide a unitless indicator that details the difference between the actual and created force values to give a measurement of the “goodness of fit” and is reported as a percentage of error from the target value (f_i). The value in using this type of analysis is the magnitude, regardless of sign, of the difference between the actual and identified force is calculated, resulting in a non-subjective error examination (Yun et al., 2008). The lower the result of the NMSE, the better the particular identification technique performed in that particular instance. A valid comparison between NMSE’s can only be made between trials of an equal sampling time as additional or less sampling time may lead to improved or reduced goodness of fit results.

The following parameters will be used in each simulation:

- Each simulation will last 300 seconds with a time step of 0.01 seconds and be repeated for 100 iterations.
- Each model was excited by a broadband random root-mean-square force, with a frequency range of 0.1 HZ to 5 HZ. The force has a scale of 1.0 and an offset of 0.0.
- Model Input Parameters

For the linear case, $m = 1.0$ kg, $c = 0.05$ kg/s, and $k = 1.0$ kg/s².

For the Duffing case, $m = 1.0$ kg, $c = 0.05$ kg/s, $k_1 = 1.0$ kg/s², and $k_3 = 1.0$ kg/mm²/s².

and each of the following sections will contain two parts:

1. First, the specific details of the case study will be presented along with the actual results.
2. A discussion will be included to analyze the meaning and ramifications of the findings.

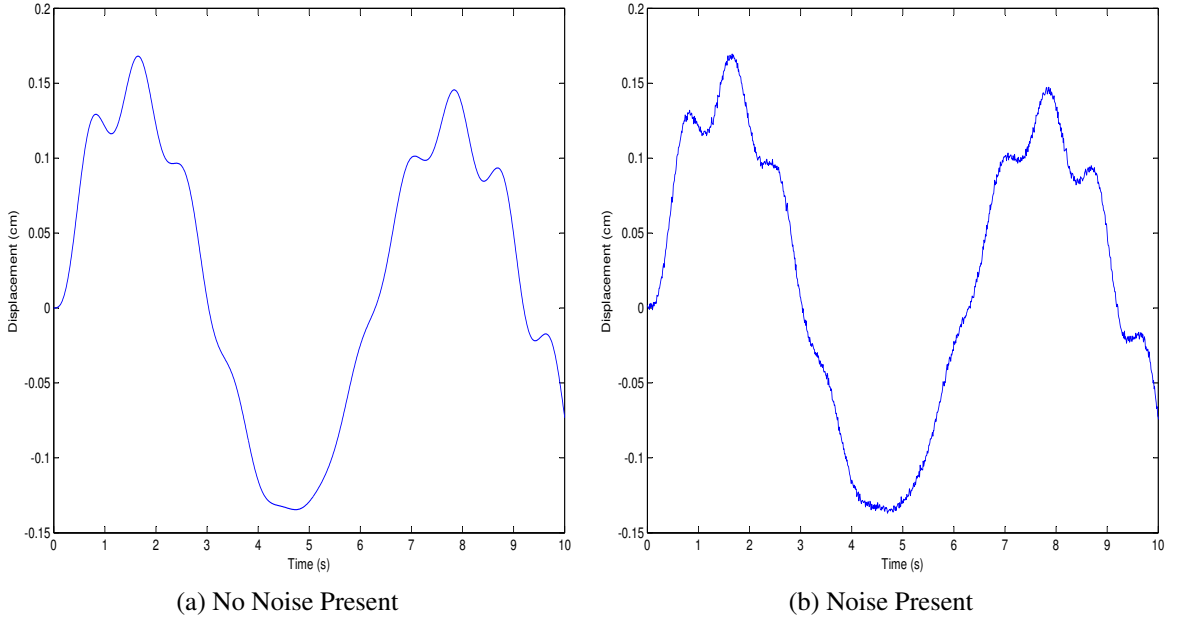


Figure 3.3: Dynamic response of a generic linear model (a) without noise and (b) with 5% RMS broadband white noise in the displacement measurements.

To be able to quantifiably discuss the repercussions of measurement uncertainty present in measurements, all recorded data (displacement, velocity, acceleration, input force, and restoring force) will be normalized by the equation:

$$DAT_{norm} = \frac{DAT_{act} - DAT_{mean}}{\sigma} \quad (3.5)$$

where DAT_{act} is the actual data recorded, DAT_{mean} is the mean of the data, and σ is the standard deviation of the data. DAT_{norm} is then compiled into the measurement ([H]) matrix of Equation 2.12 and solved as previously described. The results are normalized system identifications, which are then denormalized to achieve the actual system identification values. By making the noise introduction process unitless, direct comparisons can be made between final system identification values with noise affecting different measurements. For instance, placing 5% RMS broadband white noise upon displacement measurements has different units and consequences

Table 3.1: System Identifications of Linear and Duffing Models with No Uncertainty

Linear Model			Duffing Model		
Parameter	True	Identification	Parameter	True	Identification
m	1.00	1.0000	m	1.00	1.0000
c	0.05	0.0500	c	0.05	0.0500
k	1.00	1.0000	k ₁	1.00	1.0000
NMSE	0.0000		k ₃	1.00	1.0000
			NMSE	0.0000	

than adding 5% RMS Gaussian white noise upon the velocity. Henceforth, all data in the following case studies will be normalized, allowing system identifications for different scales of data to be compared.

3.2.1 System Identification without Uncertainty

To begin, system identifications were performed on linear and Duffing models data without measurement uncertainty. Least Squares Estimation was utilized and the results are shown in Table 3.1. This study is designed to serve as a basis for later comparison.

Discussion

With no uncertainty, LSE provides an exact match for the input system parameters and the identified force is exactly equal to the actual force (shown in Figure 3.4(a)). This analysis verifies that without measurement uncertainty, LSE can accurately identify the parametric coefficients and the resulting restoring force. This analysis also proves that the system identification methods were implemented correctly and without uncertainty present, the NMSE returned is zero. Furthermore, the parameter inputs are correctly identified to the fourth decimal place.

3.2.2 Measurement Uncertainty in the Force Vector

In this analysis, force control uncertainty was introduced. Although including noisy force control does not violate the assumptions of Least Squares Estimation, it may cause a discrep-

Table 3.2: System Identification of a Duffing Model with 5% RMS Gaussian Noise acting on the Forcing Function for 100 iterations

Parameter	True	Mean	Std. Dev.
m	1.00	1.0001	0.0005
c	0.05	0.0500	0.0002
k_1	1.00	1.0000	0.0010
k_3	1.00	1.0001	0.0006
Mean NMSE		0.2499	
Std. Dev. NMSE		0.0021	

ancy in the identification of the restoring force. The goal of this exercise is to determine the effect that force control noise has upon parameter identification process. Duffing model measurements were polluted with 5% RMS Gaussian white noise acting upon the input force vector over a period of 100 iterations. During each iteration, the model was subjected to a broadband random force for 300 seconds with a time step of 0.01 seconds. The system identification results and mean NMSE are shown in Table 3.2.

Discussion

Despite the presence of measurement noise in the input force vector, system identifications of the parametric coefficients are within a ten-thousandth of a decimal point of the “true” values. A non-zero NMSE is calculated because the recalculated force will not exactly replicate the noisy input force. In this study, the noise acting upon the force input follows a normal distribution. Because LSE seeks to minimize the square of the identified errors, the identified force will produce a smooth estimation of the force that is generally unresponsive to the noise in the input force. This is demonstrated in Figure 3.4(b).

3.2.3 Violation of the Deterministic LSE Model

In this analysis, known amounts of measurement uncertainty was synthetically introduced into the displacement, velocity, and acceleration data. The basic function of a least square

Table 3.3: System Identification of a Linear Model with 5% RMS Gaussian Noise acting on Displacement Measurements for 100 iterations

Parameter	True	Mean	Std. Dev.
m	1.00	0.9892	0.4940×10^{-3}
c	0.05	0.0501	0.2824×10^{-3}
k	1.00	0.9859	0.6033×10^{-3}
Mean NMSE		1.1766	
Std. Dev. NMSE		0.0100	

Table 3.4: System Identification of a Duffing Model with 5% RMS Gaussian Noise acting on Displacement Measurements for 100 iterations

Parameter	True	Mean	Std. Dev.
m	1.00	0.8836	0.0022
c	0.05	0.0501	0.0007
k_1	1.00	0.9122	0.0050
k_3	1.00	0.8673	0.0029
Mean NMSE		11.5724	
Std. Dev. NMSE		0.1782	

estimation is to minimize the square of the error when estimating the model parameter. For this reason, the estimator is very sensitive to outliers caused by a non-deterministic measurement set. Although including noisy measurements of displacement, velocity, and acceleration, violates the assumptions of LSE, the goal of this analysis is to determine the effect that measurement noise takes on system identification. These results will be compared to the results of Sections 3.2.1 and 3.2.2.

First, a linear model with 5% RMS Gaussian white noise in the displacement measurements is presented. Next, Duffing model measurements polluted with 5% RMS Gaussian white noise acting upon the displacement, velocity, and acceleration data in individual measurements is shown. The system identification results are shown in Tables 3.3, 3.4, 3.5, and 3.6.

Discussion

The introduction of noise into any of the measurement vectors is a violation of the assump-

Table 3.5: System Identification of a Duffing Model with 5% RMS Gaussian Noise acting on Velocity Measurements for 100 iterations

Parameter	True	Mean	Std. Dev.
m	1.00	1.0000	0.3223×10^{-4}
c	0.05	0.0500	0.1443×10^{-4}
k_1	1.00	1.0000	0.7372×10^{-4}
k_3	1.00	1.0000	0.3167×10^{-4}
Mean NMSE		0.0031	
Std. Dev. NMSE		2.361×10^{-5}	

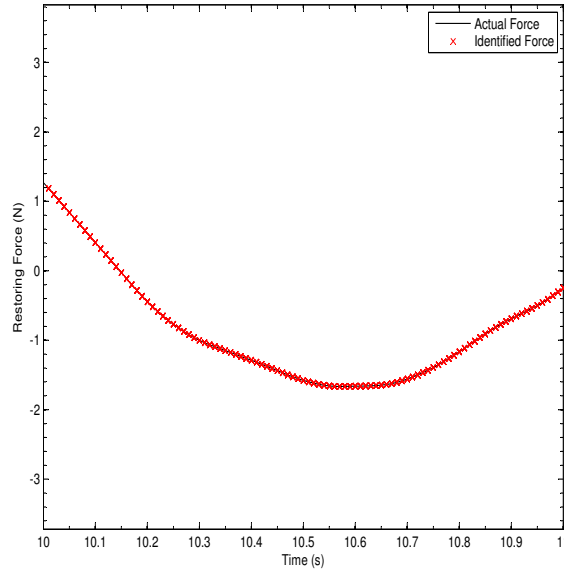
Table 3.6: System Identification of a Duffing Model with 5% RMS Gaussian Noise acting on Acceleration Measurements for 100 iterations

Parameter	True	Mean	Std. Dev.
m	1.00	0.9438	0.0013
c	0.05	0.0501	0.0005
k_1	1.00	0.9416	0.0026
k_3	1.00	0.9446	0.0016
Mean NMSE		5.5475	
Std. Dev. NMSE		0.0423	

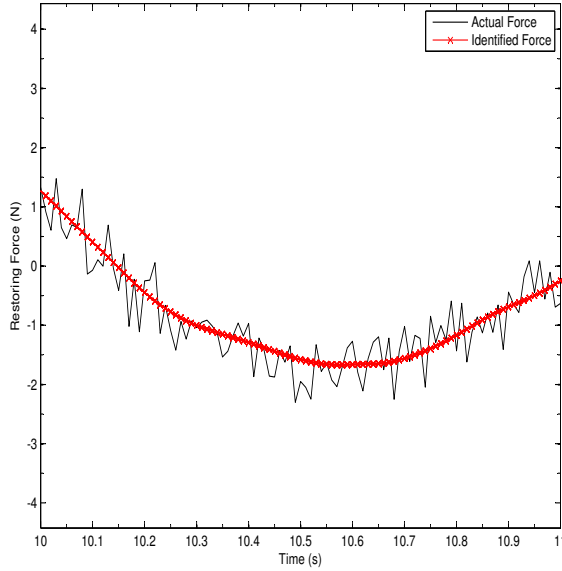
tions of LSE. LSE assumes that in a particular model, a certain input will result in a deterministic output at every time step. Because this is not the case, error is introduced into the solution. The repercussions of this violation result in an identified coefficient value that is different from the original input, regardless of which measurement vector contains noise. Figure 3.4(c) demonstrates that with noisy measurement inputs, the resulting identified force deviates from the input force.

3.3 Modeling Order: Analysis and Discussion

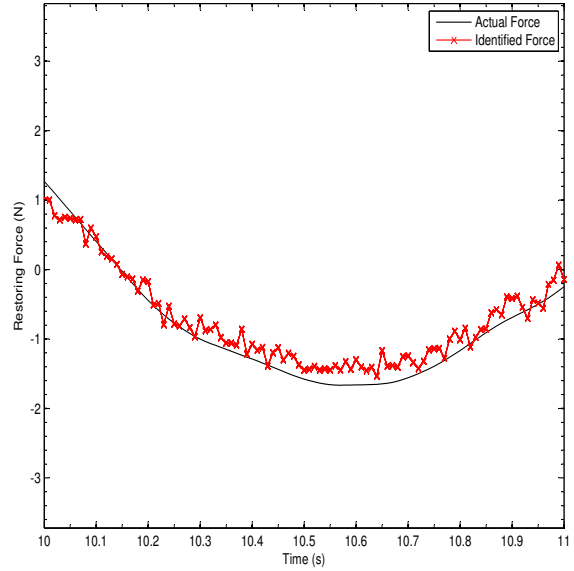
In this analysis, system identifications of a nonlinear Duffing model are performed using Least Squares Estimation and the Restoring Force Method. The modeling parameters used were, $m = 1.0$ kg, $c = 0.5$ kg/s, $k_1 = 1.0$ kg/s², and $k_3 = 0.15$ kg/mm²/s². Each analysis will be performed three times with different modeling orders: underfit, perfect fit, and overfit (for



(a) No Measurement Uncertainty



(b) Noise in Input Force



(c) Noise in Measurement Vector

Figure 3.4: System identification with Least Squares Estimation of dynamic models: (a) without measurement uncertainty; (b) with 5% uncertainty in the input force; and (c) with 5% uncertainty in the displacement measurements. Plot (a) provides a smooth identified force that follows the input force. Plot (b) is not a violation of Least Squares Estimation and produces a smooth identified force that roughly follows the mean of the noisy force. Plot (c) is a violation of Least Squares Estimation and produces a noisy identified force.

background into modeling order, see Section 2.1.3). Because a Duffing model has a third-order nonlinear term, a “perfect” model will include a third-order analysis. Underfit was chosen to be a first-order identification, and overfit will be a sixth-order identification.

It is obvious that a reduced-ordered identification will result in much more error than a perfect model and generally, a higher-ordered analysis will provide a more accurate identification. However, the goal of this study is to determine which type of identification performs the best for change detection purposes. Three types of identification polynomials will be considered: power series via Least Squares Estimation, normalized Chebyshev polynomials via the Restoring Force Method, and power series via Least Squares Estimation. To be able to properly control the modeling order of Least Squares Estimation, the restoring force was estimated by a power series:

$$r(u(t), \dot{u}(t)) \approx \hat{r}(u(t), \dot{u}(t)) = \sum_{i=0}^{MX} \sum_{j=0}^{NY} A_{ij} u(t)^i \dot{u}(t)^j \quad (3.6)$$

where MX and NY are the modeling orders of displacement and velocity, respectively, and A_{ij} is the identified coefficient. To determine A_{ij} , $u(t)^i \dot{u}(t)^j$ was input into the [H] (measurement) matrix of Equation 2.12. Table 3.7 displays the mean and standard deviations of the identified coefficients over 100 iterations. Table 3.8 shows the stochastic effects of model-order reduction.

Discussion

Table 3.8 compares the identified coefficients of the perfect fit case to the underfit and overfit model-orders. The results are showcased as a percentage, given by the equation $\frac{\text{Perfect Fit}}{\text{Case}}$. A valid change detection method should produce similar identified coefficients regardless of the modeling-order. Ideally, the *mean and standard deviations* of each set of identified coefficients should be 100% of each other.

Table 3.7: Mean Identified Power Series Coefficients via Least Squares Estimation, Chebyshev Polynomial Coefficients via Restoring Force Method, and Power Series Coefficients via Restoring Force Method Coefficients for a Duffing Model for 100 Iterations.

Underfit Case

<i>Term</i> (i,j)	Power Series via LSE		Chebyshev Polynomials via RFM		Power Series via RFM	
	<i>Mean</i>	<i>Std. Dev.</i>	<i>Mean</i>	<i>Std. Dev.</i>	<i>Mean</i>	<i>Std. Dev.</i>
(1,0)	1.2271	0.0071	5.3663	0.2539	1.5803	0.0679
(0,1)	0.4707	0.0056	1.9633	0.2262	0.4126	0.0477

Perfect Fit Case

<i>Term</i> (i,j)	Power Series via LSE		Chebyshev Polynomials via RFM		Power Series via RFM	
	<i>Mean</i>	<i>Std. Dev.</i>	<i>Mean</i>	<i>Std. Dev.</i>	<i>Mean</i>	<i>Std. Dev.</i>
(1,0)	1.0639	0.0168	5.3663	0.2593	1.3468	0.0845
(0,1)	0.4762	0.0106	1.9633	0.2262	0.5150	0.0450
(3,0)	0.0988	0.0043	0.3039	0.1178	0.0435	0.0132

Overfit Case

<i>Term</i> (i,j)	Power Series via LSE		Chebyshev Polynomials via RFM		Power Series via RFM	
	<i>Mean</i>	<i>Std. Dev.</i>	<i>Mean</i>	<i>Std. Dev.</i>	<i>Mean</i>	<i>Std. Dev.</i>
(1,0)	1.1114	0.0384	5.3363	0.2947	0.8693	0.0738
(0,1)	0.5094	0.0215	2.1348	0.2626	0.4794	0.0403
(3,0)	0.0827	0.0207	0.2011	0.1048	0.2011	0.0301

Table 3.8: Modeling Order Comparison. Each (%) column shows the percentage of $\frac{\text{Perfect Fit}}{\text{Case}}$.

Power Series via Least Squares Estimation

<i>Term</i> (i,j)	<i>Mean (Case)</i>		<i>Std. Dev. (Case)</i>	
	Underfit (%)	Overfit (%)	Underfit (%)	Overfit (%)
(1,0)	86.70	95.72	236.61	43.75
(0,1)	101.17	93.48	189.29	49.30
(3,0)	N/A	119.48	N/A	20.77

Chebyshev Polynomials via Restoring Force Method

<i>Term</i> (i,j)	<i>Mean (Case)</i>		<i>Std. Dev. (Case)</i>	
	Underfit (%)	Overfit (%)	Underfit (%)	Overfit (%)
(1,0)	100.00	100.56	100.00	87.99
(0,1)	100.00	92.97	100.00	86.14
(3,0)	N/A	84.28	N/A	112.40

Power Series via Restoring Force Method

<i>Term</i> (i,j)	<i>Mean (Case)</i>		<i>Std. Dev. (Case)</i>	
	Underfit (%)	Overfit (%)	Underfit (%)	Overfit (%)
(1,0)	85.22	154.93	124.45	114.50
(0,1)	124.81	107.43	94.33	111.62
(3,0)	N/A	21.63	N/A	43.85

The power series coefficients determined from Least Squares Estimation and the power series coefficients determined from the Restoring Force Method both show bias. For the Least Squares power series coefficients, similar mean values were identified for each model-order. However, the standard deviation for the first-order stiffness (1,0) term went from 236.61% in an underfit model to 43.75% for the overfit case. The overfit case performed similarly, as the coefficient decreased from 189.29% to 49.30%. The first order damping coefficient (0,1) yielded similar results. Because the standard deviations were widely distributed, confidence intervals are difficult to establish, which are critical in a health monitoring application.

The power series coefficients computed from the Restoring Force Method also showed a statistical bias, especially in the third order stiffness (3,0) term. The mean coefficient for the perfect case was identified at 21.63% of the overfit case. Similarly, its standard deviation was identified at 43.85% of the perfect case. Using this data, the variation of the identified parameters suggests that a system change has occurred; which, because the same Duffing model was tested for each, has not. The variation is due to the modeling order complexity of the identification.

The normalized Chebyshev polynomials, on the other hand, showed both the mean and standard deviations of the identified coefficients are the roughly the same for all three modeling orders. Because statistical independence is preserved, the orthogonal-based coefficients provide an accurate basis for change detection, even at reduced-orders.

Figure 3.5 provides a good indication of each power series modeling order bias. Although no significant statistical correlations are observed between first-order stiffness and first-order damping (Figures 3.5(a), (c), and (e)), a strong relationship is observed between first-order stiffness and third-order stiffness for both power series identifications (Figures 3.5(b) and (f)). Conversely, the normalized Chebyshev coefficients show no noticeable statistical bias (Figure 3.5(d)). The results of this analysis confirm that the reduced-ordered identified coefficients

using orthogonal basis functions can be reliably used for change detection of an uncertain single mass, SDOF nonlinear system.

As the Reconfigurable Test Setup evolves and is used to simulate complicated nonlinear models, orthogonal based functions should be utilized within the Restoring Force Calculator. It will not be possible to use the normalized Chebyshev polynomials as normalization of displacement and velocity is not possible in real-time. However a number of orthogonal based functions exist, including Hermite and Legendre polynomials (Koekoek et al., 2010).

Another interesting result of this study was when the modeling order was increased to a tenth-order analysis for Least Squares Estimation. The solution process for Least Squares involves inverting the measurement matrix. At high ordered analyses, instability is encountered as a result of a singular matrix because inverting a matrix with singular values is impossible. This is one of the many reasons why in system identification, the model-order should not be blindly increased.

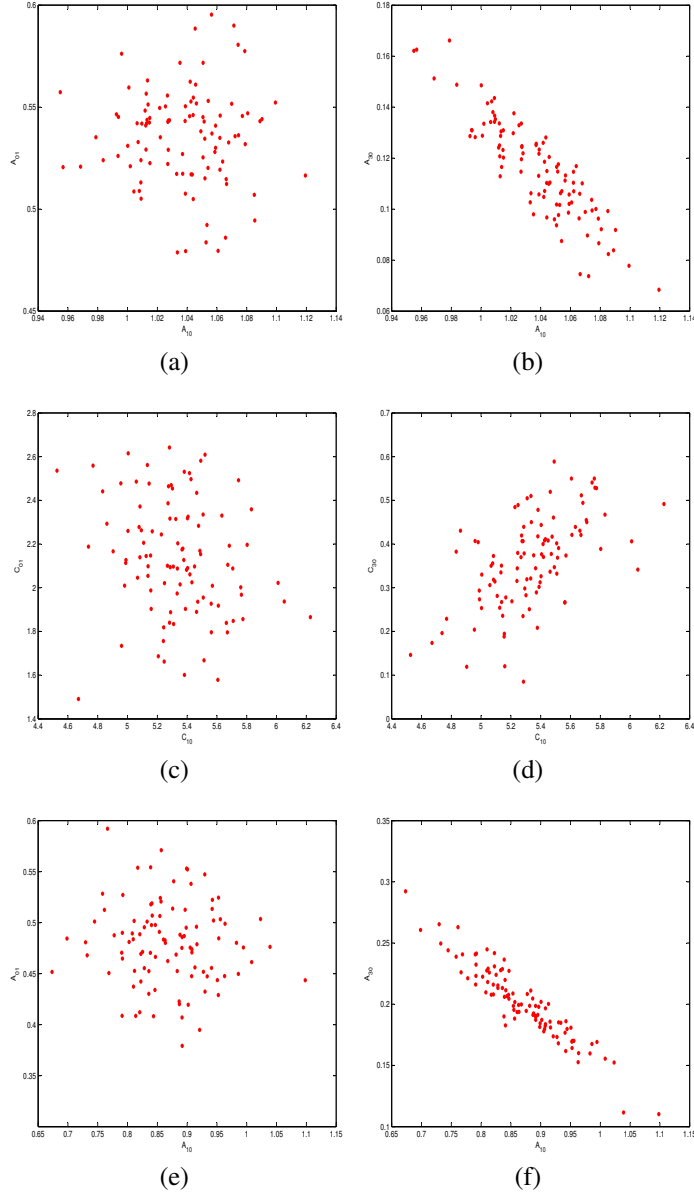


Figure 3.5: Sample scatter plots of power series coefficients from Least Squares Estimation, normalized Chebyshev Coefficients from the Restoring Force Method, and power series via the Restoring Force Method. Each is shown with a modeling order of 6 for displacement and velocity. (a) is of Least Squares Estimation power series coefficients between first-order stiffness and first-order damping. (b) is of Least Squares Estimation power series coefficients between first-order stiffness and third-order stiffness. (c) is of Restoring Force Method normalized Chebyshev coefficients between first-order stiffness and first-order damping. (d) is of Restoring Force Method normalized Chebyshev coefficients between first-order stiffness and third-order stiffness. (e) is of Restoring Force Method power series coefficients between first-order stiffness and first-order damping. (f) is of Restoring Force Method power series coefficients between first-order stiffness and third-order stiffness.

4 DESCRIPTION OF THE RECONFIGURABLE TEST SETUP

The Reconfigurable Test Setup is designed for simulating a SDOF nonlinear dynamic system. Physically, the setup includes a moving mass that is excited by a linear servo motor. The mass is connected at a fixed point to an electromagnetic element that functions as the restoring force for the system. The motion of the linear servo motor and data acquisition (DAQ) is controlled through software, referred to as the Reconfigurable Test Setup Control Code (RTSCC).

As an experiment is performed, the values of displacement and velocity are directly measured in real-time. The recorded data is sent to the restoring force control algorithm, which calculates the “current” value of the restoring force. This process is outlined in Figure 4.1. Figures 4.2 and 4.3 are a photograph and a schematic of the experimental test setup, respectively. A diagram of the operational control and connection types for the setup described in Figure 4.4 seen in Figure 4.5.

4.1 Hardware

In this section, the main physical components of the test apparatus are described. The uses and control of each of these devices will provide precise control, recording, and analysis of each test.

4.1.1 Restoring Force Generator

The simulation restoring force with a calibrated electromagnet is the key breakthrough of the Reconfigurable Test Setup system because of its great modeling versatility. With its use, a broad spectrum of damping and stiffness characteristics can be achieved by varying the amount of supplied current. In this study, this device will be referred to as the “restoring force generator” or the “restoring force electromagnet.”

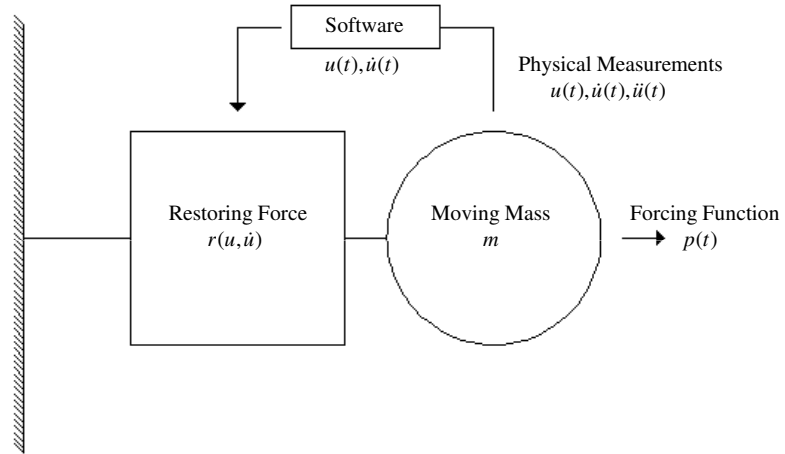


Figure 4.1: Modeling of a nonlinear single degree of freedom system with the Reconfigurable Test Setup.

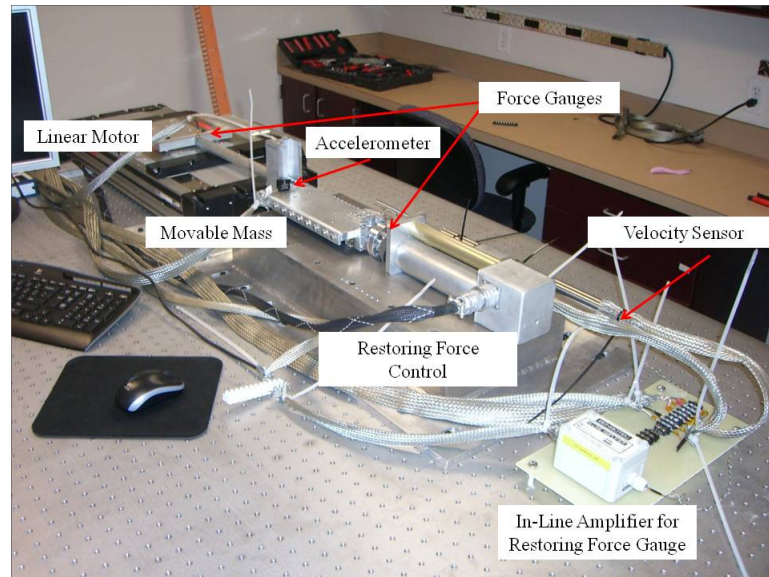


Figure 4.2: Photograph of the assembled Reconfigurable Test Setup.

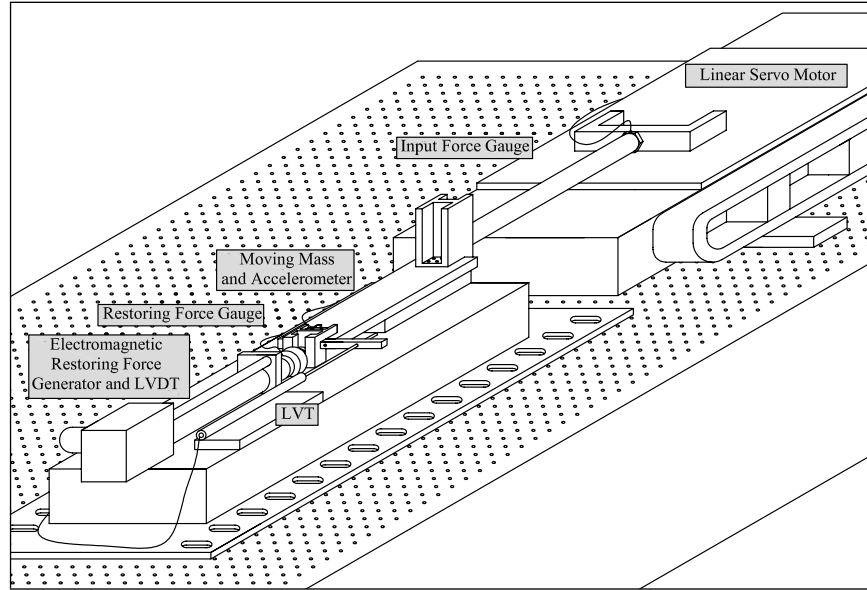


Figure 4.3: Three-dimensional model of the Reconfigurable Test Setup's main components.

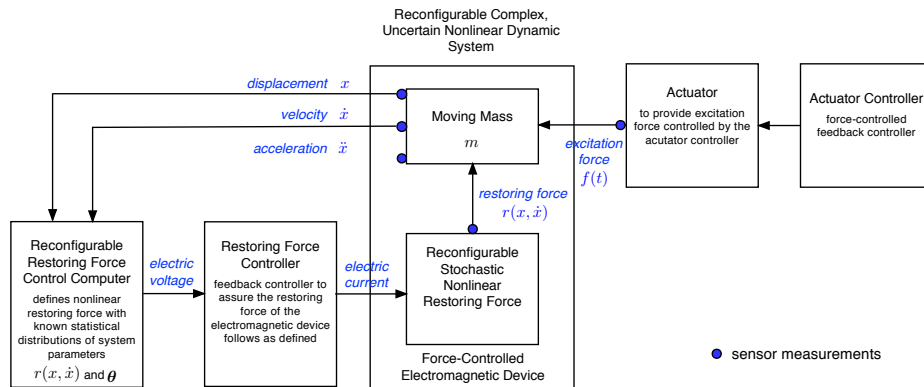


Figure 4.4: System architecture and wiring diagram of the Reconfigurable Test Setup.

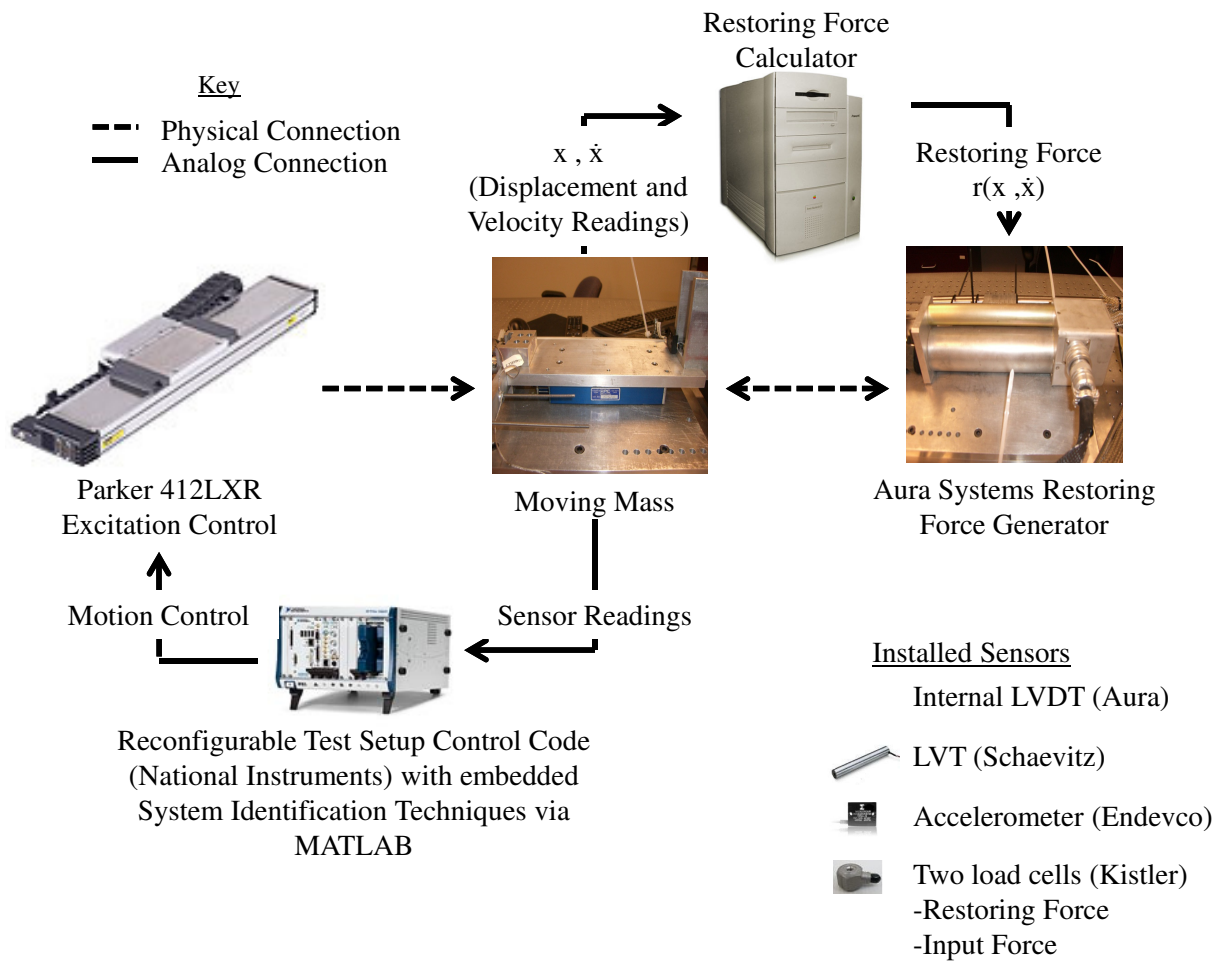


Figure 4.5: Pictorial flowchart of the Reconfigurable Test Setup.

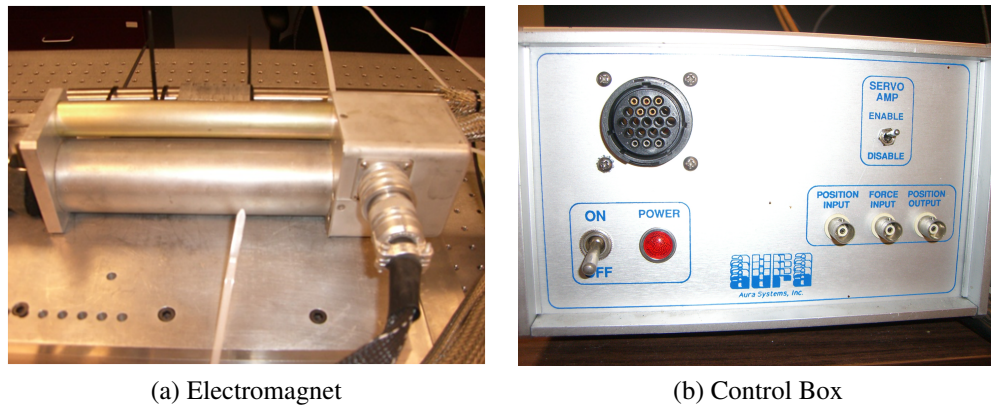


Figure 4.6: Physical components of the restoring force generator (electromagnet).

The restoring force generator is made of two physical components: a force generator and control box. Each is shown in Figure 4.6. To simulate the restoring force, the force generator repels an internal bar by an electromagnetic force to a degree determined by the control program. To provide accurate restoring force results in real-time, the control program samples displacement and velocity measurements at a high rate to ensure that an appropriate force is being applied to a certain displacement and velocity. This is especially critical when dealing with a complex, nonlinear system where the restoring force could vary greatly depending upon small variances of displacement and/or velocity.

In Figure 4.6(b), a number of BNC ports are shown. An internal linear variable differential transformer (LVDT) reads displacement values and its output port is seen on the far right of the photo, labeled “position output.” The value of the restoring force determined by the control program is input into the device through the middle BNC port, labeled “force input.” The left BNC port (“position input”) is not used in this application. The multi-pin, black connection connects the control box to the electromagnet.



Figure 4.7: Image of an optical table (Courtesy of Thorlabs, Inc., Newton, NJ).

4.1.2 Optical Table

To mitigate vibrational interference, an optical table was used. A photograph of the device is shown in Figure 4.7. The function of an optical table is to eliminate relative motion between the components secured to the surface of the table. Thus, the vibrations caused by the linear servo motor will not cause the entire table to vibrate violently. Should isolation not occur, measurement sensors would be subjected to large vibrations introducing large noise components in their respective outputs.

Additionally, minor sources of noise may be caused by uncontrollable sources of vibration such as air conditioners, experimentation in adjacent laboratories, and even the pounding of a researcher's footsteps. The table also isolates the experiment as a whole from ambient background laboratory vibrations, which are typically in the 4 to 100 Hz range in a multistory building. Since large frequency differences preclude energy transfer from one form into another, the resonant frequency of the optical table is well above 100 Hz, thus eliminating the chances of any energy coupling between the tabletop and its support system (Thorlabs, 2010). The optical also serves as a rigid base on which all of the Reconfigurable Test Setup components can be mounted to provide long-term stability.

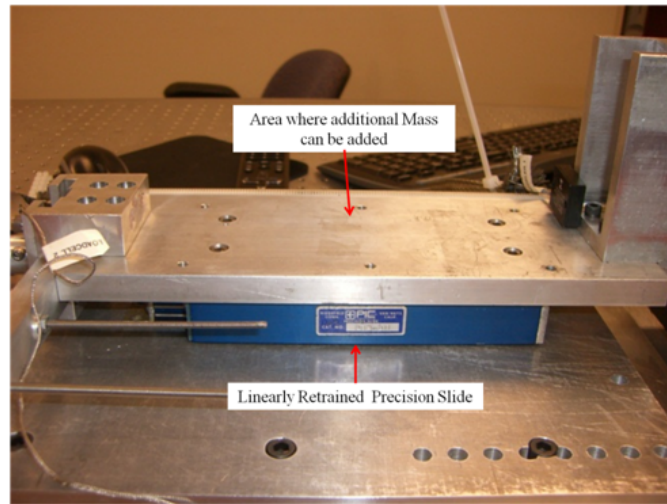


Figure 4.8: Photograph of the moving mass.

4.1.3 Moving Mass

The rigid, oscillating mass functions as the test specimen in the Reconfigurable Test Setup and seen in Figure 4.8. Acceleration, velocity, and displacement measurements are taken from its surface. It also provides the link between the actuator and the restoring force generator. The oscillating mass was raised and leveled to the actuator to avoid secondary forces that may be introduced due to a misalignment of the applied force and moveable mass.

As excitation is provided, the oscillating mass is free to move in a single-degree of freedom manner. The movement is impeded by a negligible amount of frictional forces because it is mounted upon a linear bearing system. As shown in Equation 2.1, dynamic models include an inertia term and to properly replicate a variety of different models, additional mass can easily be installed.

4.1.4 Linear Servo Motor

The excitation force of the Reconfigurable Test Setup system is controlled by a linear servo motor manufactured by Parker Automation. To program the motion of the actuator, Parker's

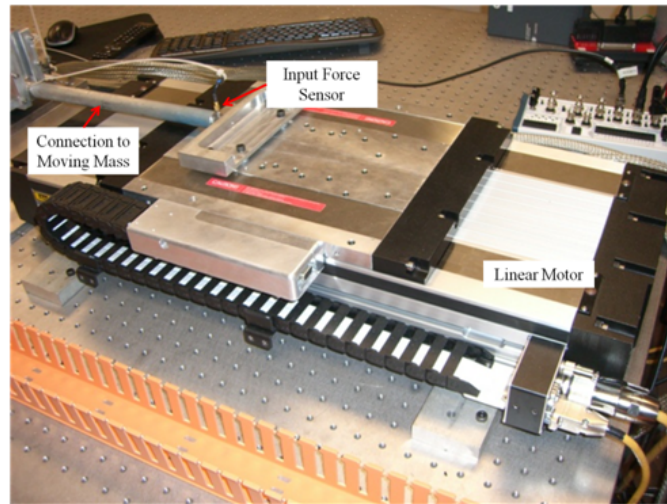


Figure 4.9: Photograph of the linear servo motor.

Motion Planner syntax was used to send a series of commands to the servo designed to “follow” an analog input signal. The script code is embedded into the Reconfigurable Test Setup control code written in LabVIEW. Components of the command code include:

- Following lowpass filter
- Distance scaling
- Motion tare

For further explanation of each of these components, see Section 4.2.1.

4.1.5 Measurement Sensors

The overall purpose of the Reconfigurable Test Setup is to reliably and accurately replicate the restoring properties of a system *in real-time*. Therefore, a crucial component of the Reconfigurable Test Setup is its inclusion of direct measurement sensors. Direct measurements are crucial due to the presence of hysteresis, where the effects of an input are experienced with a lag time, which can cause a misrepresentation of a model’s physical effects (Worden, 1990).

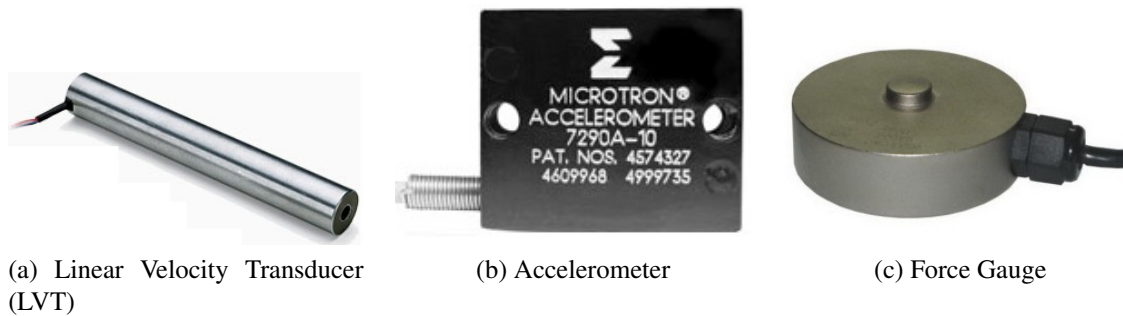


Figure 4.10: Velocity, acceleration, and force sensors used on the Reconfigurable Test Setup for direct measurement. A displacement sensor is also included in the apparatus and is located within the restoring force generator. Photographs courtesy of Schaevitz Technologies, Inc. (Pennsauken, NJ), Endevco Corporation (San Juan Capistrano, CA), and Kistler Instruments (Singapore), respectively.

A collection of sensors was assembled for direct measurement including: a linear variable differential transformer (LVDT) that is housed in the restoring force generator's silver box, a linear velocity transducer (LVT), an accelerometer, and two force gauges: one to measure the excitation force and another to measure the restoring force. Photos of each are shown in Figure 4.10. Wire shielding has been provided to limit external noise contamination and can be best seen in Figure 4.2.

4.1.6 Data Acquisition Systems

To accurately control the test and acquire data, specialized computer equipment was purchased through National Instruments. The function of each piece is summarized in Table 4.1. In order to control each of the components, a software program was written. Chosen for its ability to communicate easily with various types of machinery, National Instrument's graphical computer programming language, LabVIEW, has the ability to control the entire testing process.

Table 4.1: LabVIEW Components of the Reconfigurable Test Setup DAQ System

Device	Use
PXIe 8101 Controller	Contains an Intel Celeron 575 processor that will allow for high speed data collection. Also contains standard USB, Ethernet, and computer monitor connections that are important for setting up the tests.
PXIe 6363 Signal Conditioner	A DAQ device that allows for high data throughput and low latency. Similarly, it features independent analog and digital timing engines (for use in sensor readings), timers. An accurate and powerful internal clock is imperative for structural dynamic tests to allow for accurate displacement, velocity, and acceleration measurements.
PXI 1062Q Chassis	Functions as the “device stable”
BNC 2120 Terminal Block	Allows for BNC input access for sensor recording and contains a signal generator that is used in a variety of purposes.

4.2 Software

The Reconfigurable Test Setup system requires data measurements in two areas: to record physical measurements, deemed the Reconfigurable Test Setup Control Code (RTSCC); and another to calculate the effects of the restoring force, referred to as the Restoring Force Calculator. RTSCC is a computer code written with LabVIEW software. The physical simulation of the restoring force, on the other hand, will be controlled by an algorithm written in C. In this code, physically recorded measurements will be read and utilized to calculate the real-time value of the restoring force.

At this time, the RTSCC and Restoring Force Calculator codes are housed in separate CPU's. Thus, they are running at different internal clocks. Synchronization between the two programs is crucial in the modeling of a nonlinear model's restoring force with software. As this methodology is improved in the future, improvements in this area must be made.

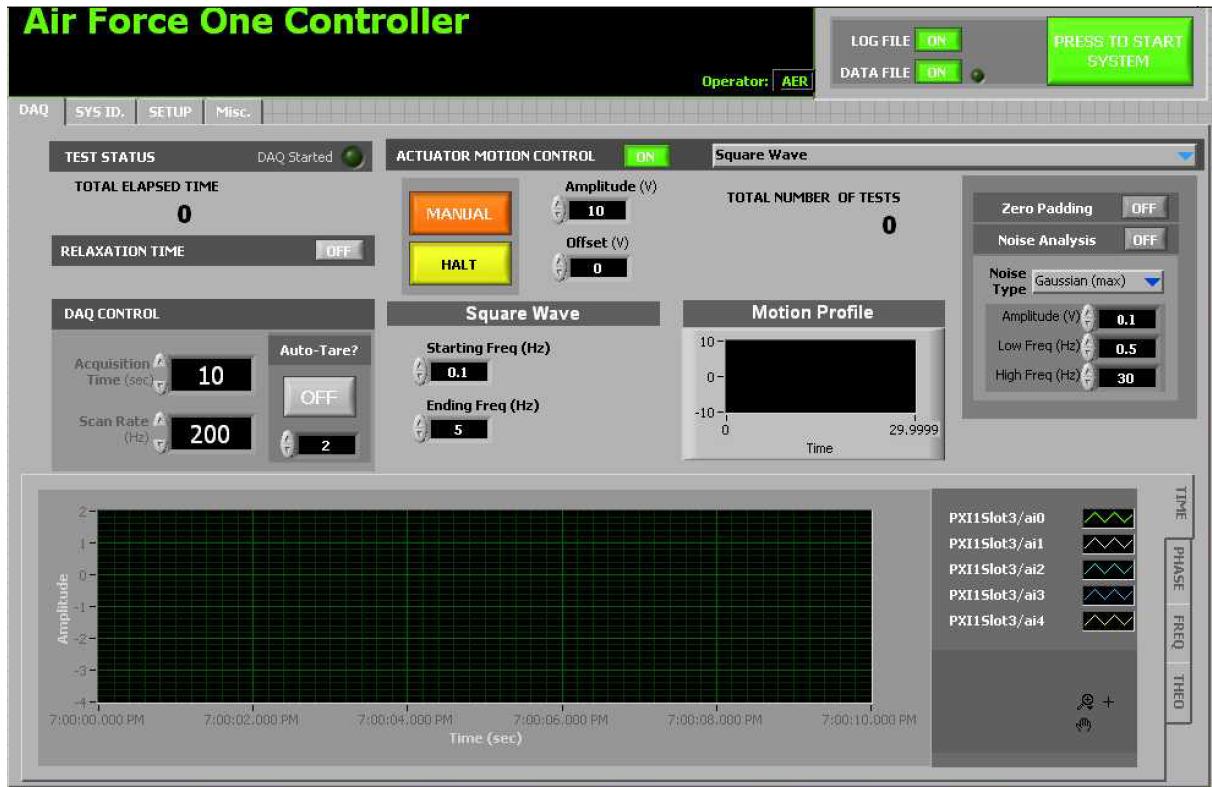


Figure 4.11: Snapshot of the user interface menu.

In following sections, the RTSCC and Restoring Force Calculator codes are described.

4.2.1 Reconfigurable Test Setup Control Code

The program has the capability to record and graph sensor measurements from a number of analog inputs and may automatically interface with MATLAB software to provide system identification analysis. Each element of the LabVIEW is essential in providing reliable and meaningful data. The components of the control code are described and shown in the following sections. A snapshot of the user interface menu is shown in Figure 4.11.

User Interface Coding

When the user chooses the type of actuator motion, the corresponding options for that type of motion will appear on the user interface. Similarly, all other selections from other cases will disappear. For instance if the user chooses monotonic sinusoidal wave excitation, the following user controls will be available for modification: amplitude, offset, frequency and phase. Similar coding also allows the user to:

- Turn on and off data tare
- Turn on and off on-board system identification
 - Parametric with Least Squares Estimation
 - Non-parametric with the Restoring Force Method
- Turn on and off the linear servo motor after completion of data acquisition

This section of LabVIEW code is shown in Figure 4.12.

Linear Servo Motor Control

As previously mentioned, the type of excitation applied to a dynamic system may greatly affect its response. For optimal flexibility, the linear servo motor has been programmed to follow an analog voltage signal that is generated by the LabVIEW control code. Possible analog wave generation types include: monotonic sinusoidal, square, chirp, beat, broadband random with a Gaussian distribution, broadband random with uniform distribution, sawtooth, and triangle. To add further types of motion, the user may also input a file containing displacement locations or define movement in an equation. To ensure accurate physical motion, the analog output

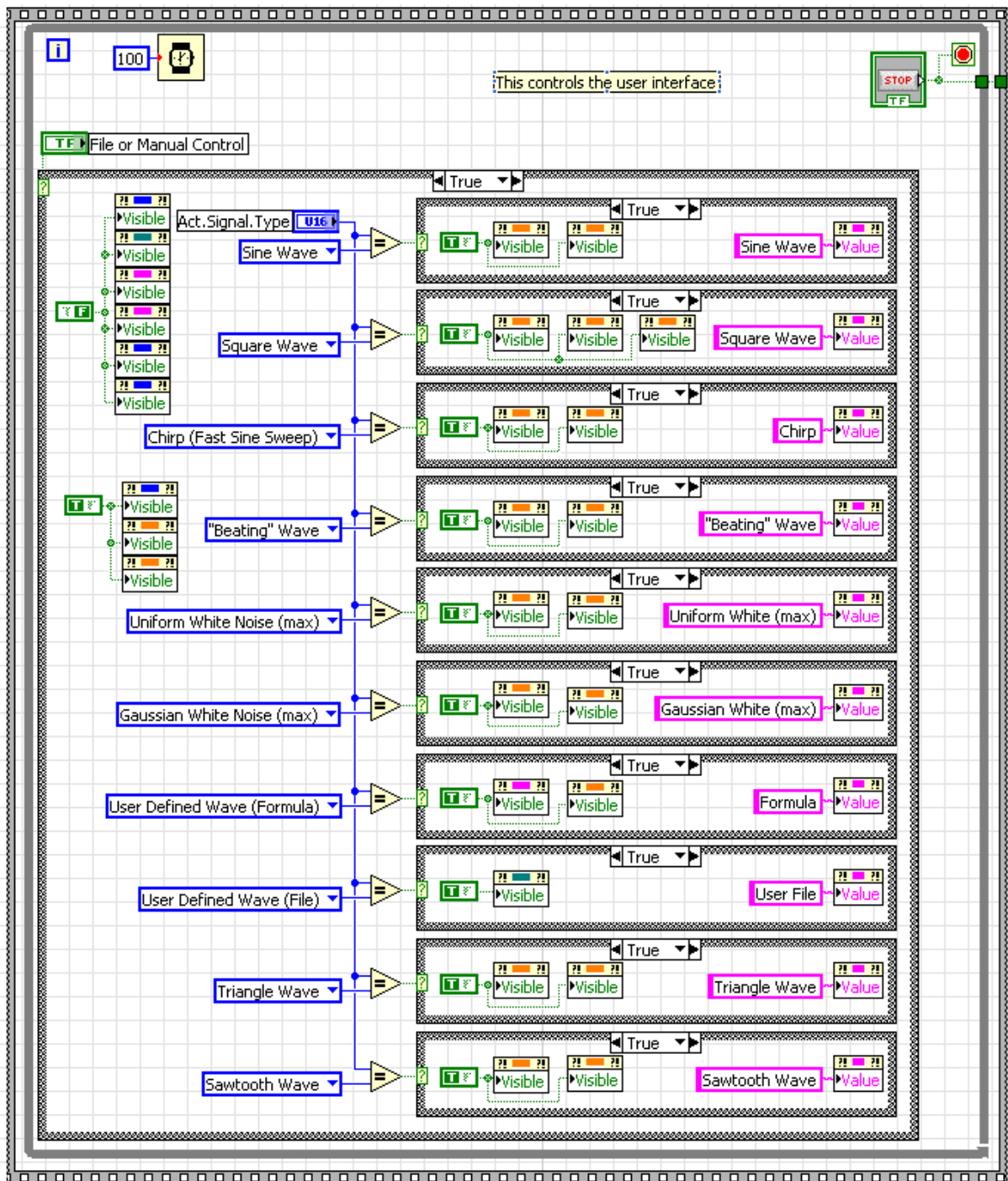


Figure 4.12: LabVIEW code designed to control user interface for a user-friendly selection of testing parameters.

Table 4.2: Motion Planner Control Code

Commands	Functions
DEL AIFOL	Delete existing Analog Input Following program
DEF AIFOL	Define Analog Input Following “AIFOL” program
ANIMAS1-1	Define analog input master as expansion I/O block 1, pin 1
FOLMAS+12	Master is set to follow an analog Input value
FFILT3	Set the following filter to 50 Hz to smooth following
FPFILT20	Set the following position filter to 20 Hz to smooth following
FOLRN1	Axis 1 will turn 1 counts for 1 count of ADC value
FOLRD1	The denominator of the ratio
FOLMD0	Master distance
D -	Make positive voltage values go towards the electromagnet
PSET0	Zero out motor and encoder positions
MA1	Absolute position mode
MC1	Continuous mode
DRIVE1	Turn on the drive
FOLEN1	Enable following
GO1	Start following
END	End program

voltage signals are sent to the actuator at 10000 Hz. Because this updating rate is faster than the updating rate of the actuator (2 ms), motion will occur without a “lag time” and not incur excess noise. If a lag time between DAQ and excitation were to exist, added characterization uncertainty of a physical simulation would result. This section of LabVIEW code is shown in Figure 4.13.

In order for the linear servo motor to respond to the analog voltage signals, a control code must be written in its native language (Parker Motion’s Motion Planner Software). The Motion Planner code is given and described in Table 4.2.

Equipment Safety Features

The Reconfigurable Test Setup control program contains three features specifically programmed to ensure longevity of the electromagnet and the linear servo motor: “zero padding,”

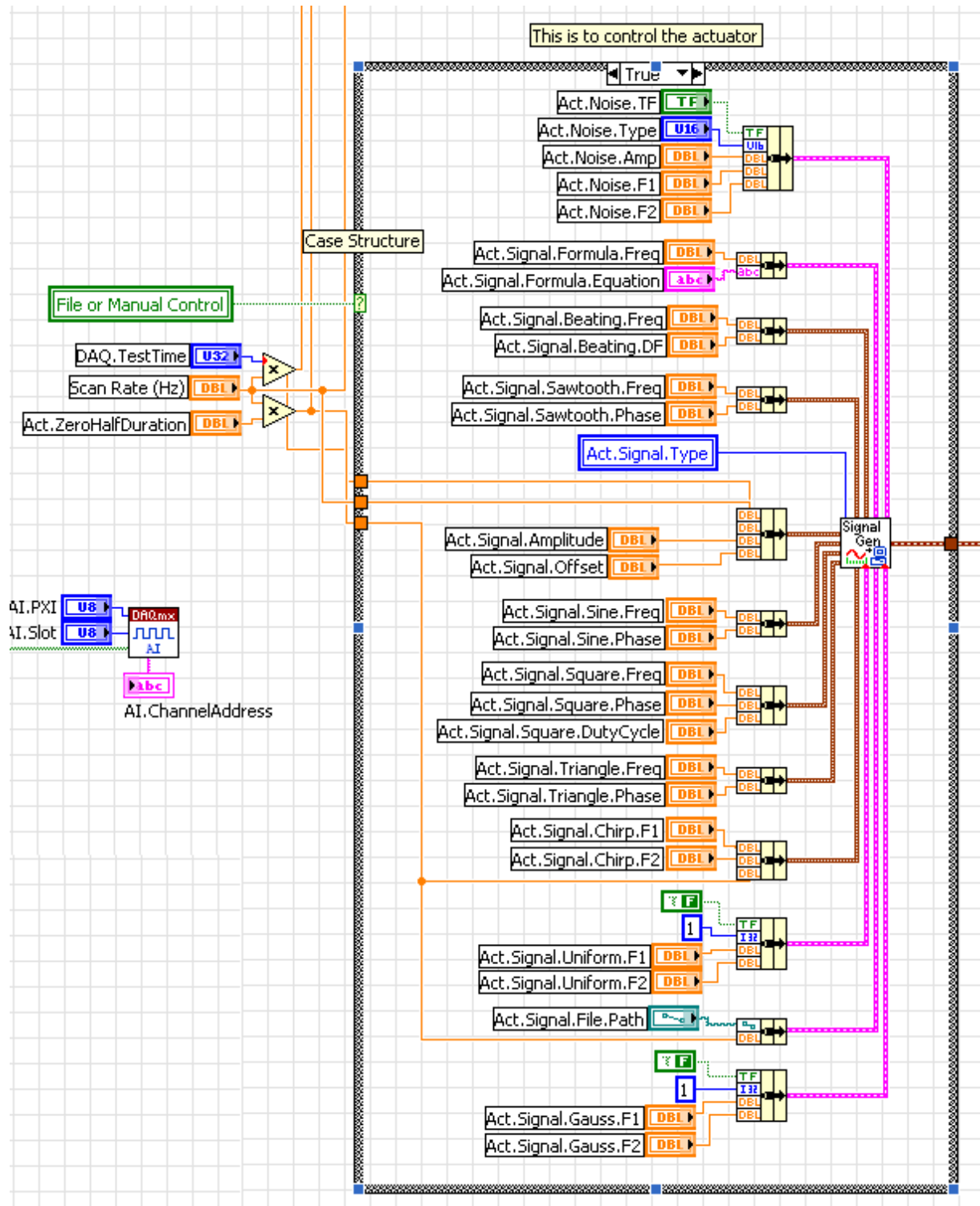


Figure 4.13: LabVIEW code designed output a variety of motion types. The analog output from this code is then sent to the linear servo motor, which will “follow” the sent signal.

“ramp up,” and “actuator relaxation time.” The function of the zero padding feature is to make sure that the actuator starts its motion from a set position - in this case, the middle of the range of motion of the electromagnet. Without this feature it would be possible to begin the test at the far ends of the electromagnet’s range of motion. Then through the course of the test, the linear servo motor would literally “slam” and eventually damage the electromagnet while the experiment was running.

The ramp up feature tapers the magnitude of the actuator motion so that the test does not begin with an instantaneous thrust. Such a movement could possibly damage the linear servo motor or the electromagnet. Another beneficial feature of the ramp up is that the actuator will end its motion at the same position as it began. Therefore when performing a series of tests, each individual motion plan will begin at the same starting position.

Lastly, the actuator relaxation time provides a “resting period” for the entire device in between tests. This is especially critical if the user is running a number of tests where voltage values are repeatedly delivered to the electromagnet in excess of 6 volts in magnitude (the value of 6 volts was found through experience and is for this electromagnet only). Repeated nonstop testing at these levels will raise the surface temperature of the electromagnet and possibly cause damage. By allowing a “cool down period,” the electromagnet has time to dissipate heat caused through its normal operation.

Data Acquisition Code

Analog input readings of voltage are recorded from the various sensors installed within the Reconfigurable Test Setup. Similarly, the linear servo motor’s motion is dictated by analog output voltage values. The timing of the analog input/analog output (AIAO) events is critical because should the two signals have different internal clocks, it would not be possible to correlate the sensor readings to a particular instance of actuator movement. Therefore, the sampling

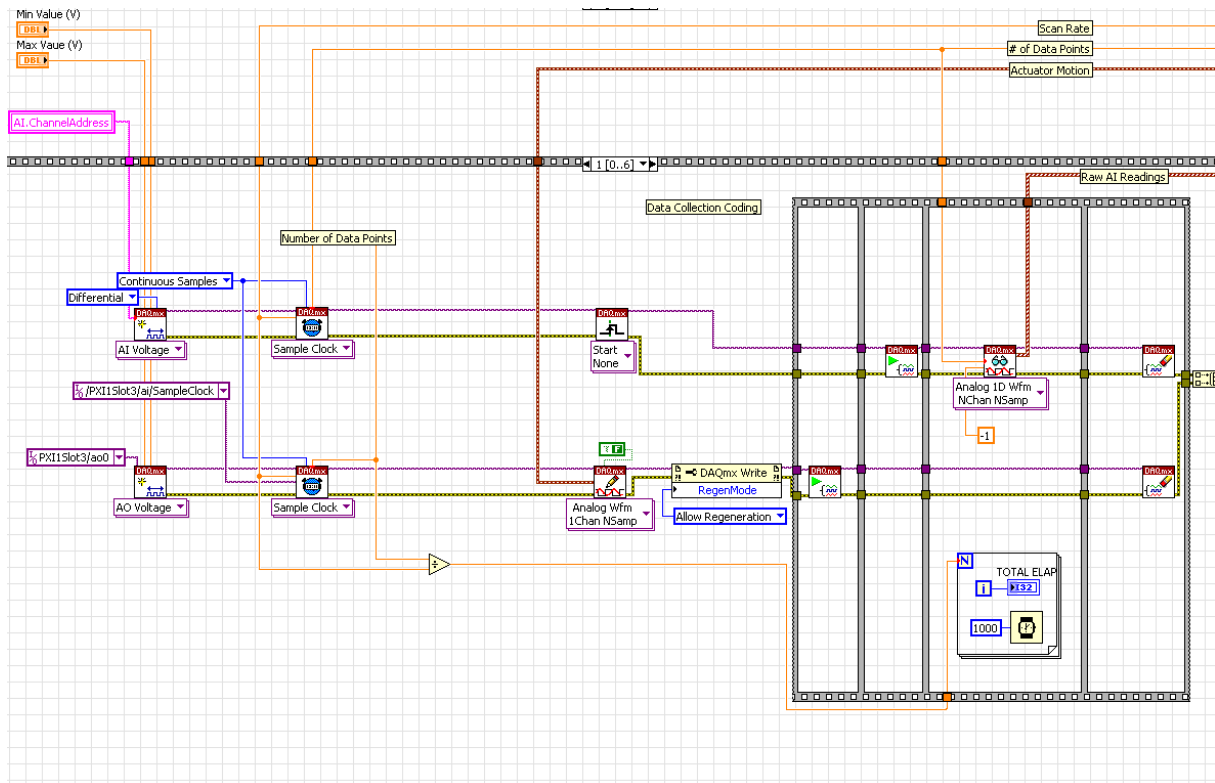


Figure 4.14: LabVIEW code designed to output and acquire analog voltage signals to and from an external device (the BNC 2120 Terminal Block).

rate of the entire AIAO process is constant through the course of a testing session. The upload rate to the linear servo motor has been set at 10000 Hz, which will deliver voltage signals faster than its 0.2 ms update rate. This section of LabVIEW code is shown in Figure 4.14.

Data Calibration

The sensors attached to the Reconfigurable Test Setup system record measurements in terms of voltage. These readings then must be converted into meaningful measurements. The “scale” converts voltage into the required units of the sensor’s output (for example cm/s for the linear velocity transducer (LVT)) while the “offset” provides the slope intercept. Current calibration factors are shown in Table 4.3. This section of LabVIEW code that calibrates the data is shown in Figure 4.15.

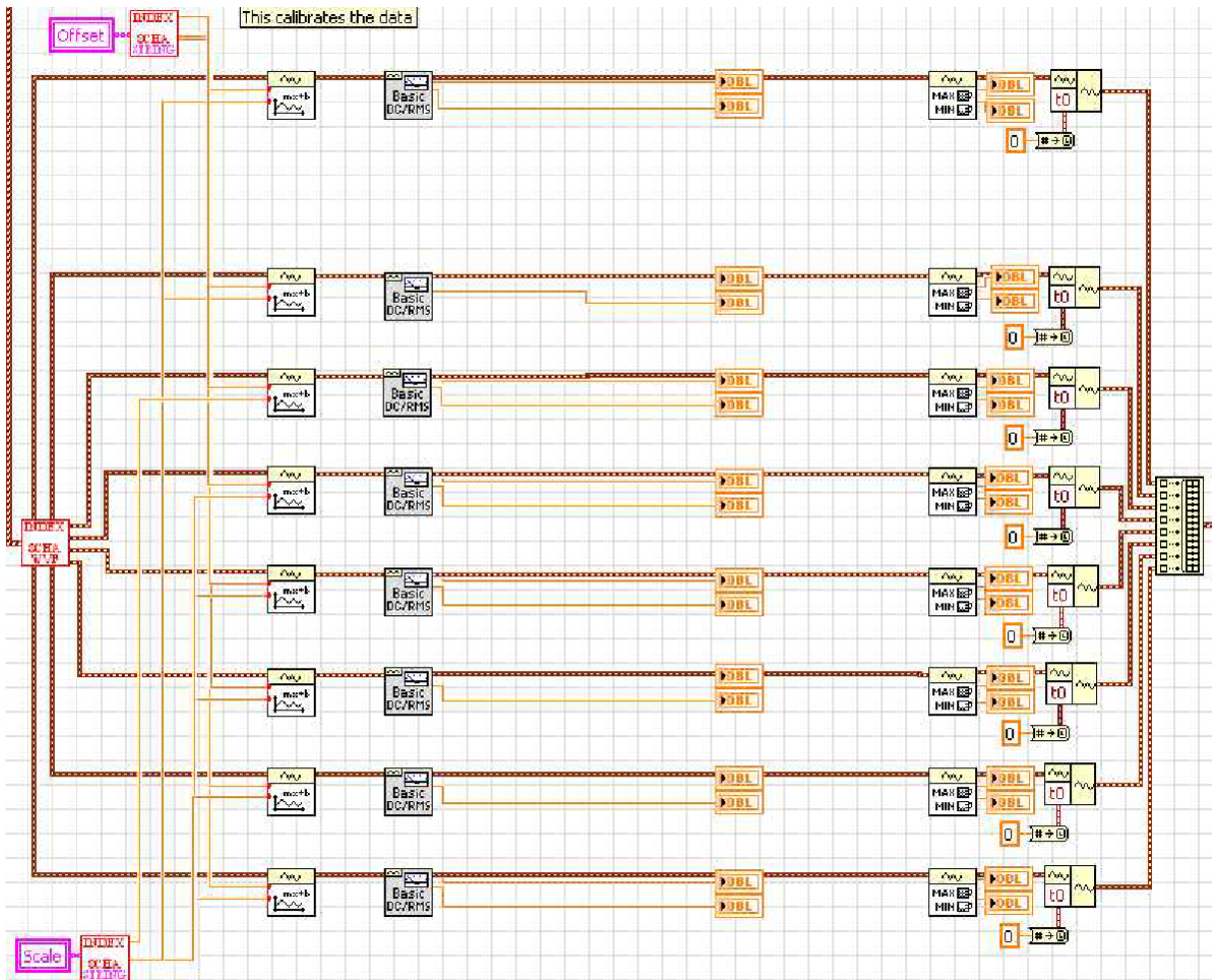


Figure 4.15: LabVIEW code designed to convert analog measurement signals into calibrated units.

Table 4.3: Reconfigurable Test Setup Control Code Calibration Factors

Channel	Channel Name	Units	Scale	Offset
0	Displacement	cm	0.28	0.00
1	Velocity	cm/s	1.04	0.00
2	Acceleration	g	1.00	-1.44
3	Input Force	N	-1.00	0.00
4	Restoring Force	N	-34.5	-0.75
5	Programmed Restoring Force	V	1.00	0.00

Graphical Analysis

Once the data is calibrated, it is organized into meaningful graphs and phase diagrams. Three phase plots are generated and displayed upon the user interface: velocity vs. displacement, displacement vs. restoring force, and velocity vs. restoring force. The code also generates a compiled plot of all sensor readings. Lastly a spectral density plot is generated, displaying the frequency components of acquired signals.

The primary benefit of the generation of these graphs is that it allows the researcher to view the characteristics at the conclusion of the performed test. This information is critical for troubleshooting purposes - especially the spectral density plot, which identifies if high-frequency noise is present in the recorded measurements. This section of LabVIEW code is shown in Figure 4.16.

4.2.2 Restoring Force Calculator Code

To simulate the physical restoring force of the Reconfigurable Test Setup, a sophisticated computer code was written in the C language. This program is referred to as the Restoring Force Calculator. In this section, its user interface and the nonlinear dynamic models currently programmed into the algorithm are described.

A great benefit of this system is the user has the ability to add new dynamic models into its library. Another key feature of the Restoring Force Calculator is its ability to sample data at a high rate. The accurate calculation of the instantaneous value of the restoring force is critical because the properties of a nonlinear dynamic model may change with slight variations of displacement and velocity. The process of reading velocity and displacement measurements and the subsequent calculation of the restoring force is repeated throughout the simulation, as

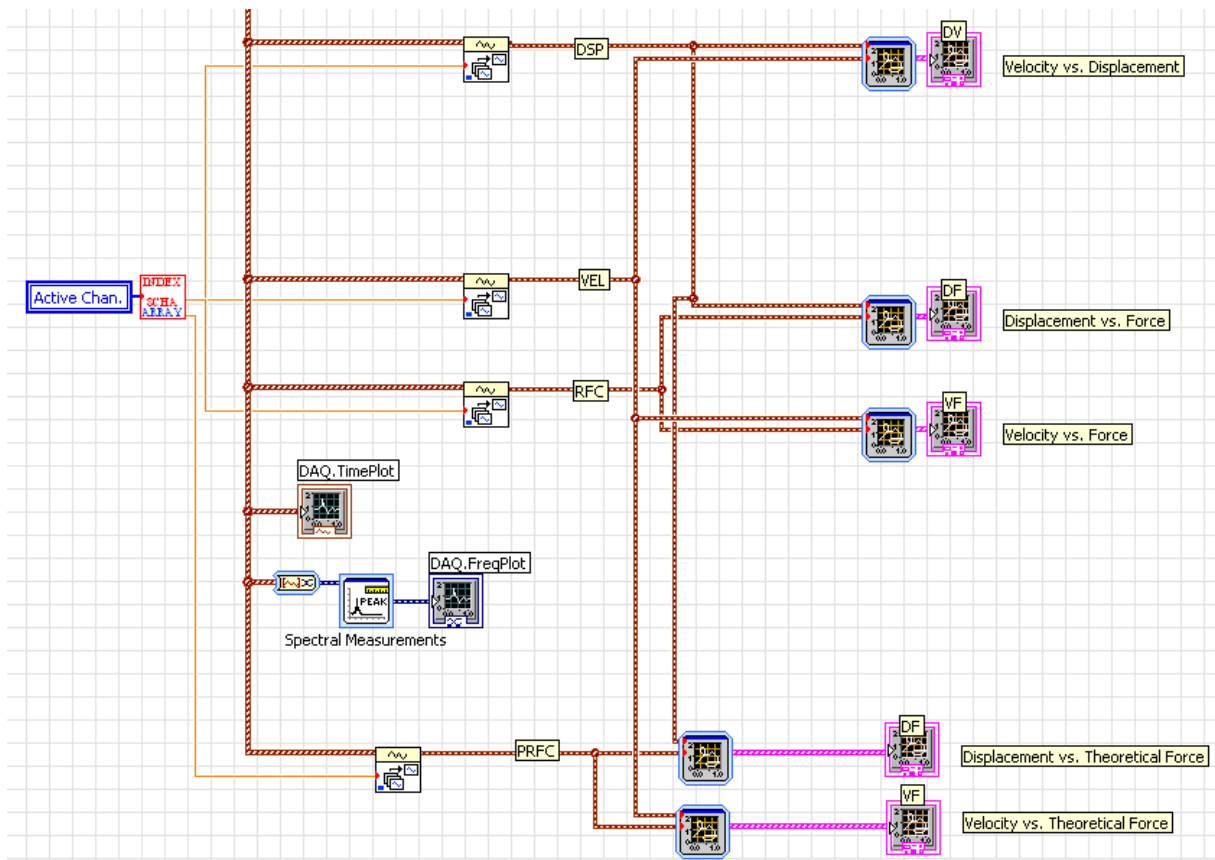


Figure 4.16: LabVIEW code designed to output recorded data into meaningful graphical analysis.

the current measurements are used to calculate the next value of the restoring force.

User Interface

The user interface is the top-level program for the device. Each feedback option is listed and the user simply needs to choose the appropriate nonlinear behavior type and the desired dynamic coefficients. After setting these values, the user is able to commence the physical simulation of the restoring force. The user interface for the Restoring Force Calculator is shown on the next page:

```

/*****
* This is the main control panel for the RECONFIGURABLE TEST SETUP *
*****/

#include <stdio.h>
#include <conio.h>
#include <math.h>
#include <time.h>
#include <assert.h>
#include "nidaqmx.h"
#include "feedback1.h"
#include "feedback2.h"
#include "feedback3.h"
#include "feedback4.h"

int main()
{
    float64    gap;
    float64    coef1;
    float64    coef2;
    float64    coef3;
    int        type;

    type=4;
    switch(type)
    {
        case 1:          //Linear and Cubic Stiffness Terms
        {
            coef1 = 0.75; // Values for linear part
            coef2 = 0.30; // Values for cubic part
            feedback1(coef1,coef2);
            break;
        }
        case 2:          //Gap-Space Nonlinearity
        {
            gap= 1.00;    // Gap size: 10.= 1 inch
            coef1 = 0.0;   // Values IN the gap
            coef2 = 1.0;   // Values beyond gap
            feedback2(gap,coef1,coef2);
            break;
        }
        case 3:          //Trilinear Nonlinearity
        {
            gap= 1.5;     // Gap size: 10.= 1 inch
            coef1 = 0.0;   // Values IN the gap
            coef2 = 2.0;   // Values beyond gap (to the right of the gap)
            coef3 = 1.0;   // Value before the gap (to the left)
            feedback3(gap,coef1,coef2,coef3);
            break;
        }
        case 4:          //Simplified Design Method
        {
            coef1 = 3.0;   // Value of C (damping coefficient)
            coef2 = 0.30;   // Value of n (degree of nonlinearity)
            coef3 = 0.05;   // Value of k (damper stiffness)
            feedback4(coef1,coef2,coef3);
            break;
        }
        default: printf("Bad input type = %d\n", type);
    }
    return 0;
}

```

Restoring Force Calculator

The Restoring Force Calculator codes are a series of routines that designate the nonlinear behavior of the restoring force electromagnet. The code features DAQ functions (to capture the current displacement and velocity values) as well as a number of error checks to ensure that the DAQ is functioning properly. The length of time to run the restoring force program may also be changed within these codes.

For safety of the restoring force modeler, all calculated feedback values are restricted to values capable of being safely replicated by the electromagnet (between -10 and 10 volts). The currently programmed feedback options are summarized in Table 4.4. They include: linear, Duffing, gap-space nonlinearity (to be introduced in Section 5), trilinear nonlinearity (a modification of the gap-space nonlinearity), and a nonlinear viscous damper (to be introduced in Section 6.2).

To display an example, the Restoring Force Calculator code written for a linear or Duffing model is shown on the next two pages:

```

/*****
* RECONFIGURABLE TEST SETUP FOR a linear/duffing model *
*****/

#include <stdio.h>
#include <conio.h>
#include <time.h>
#include <assert.h>
#include "nidaqmx.h"
#include "feedback1.h"

// POLYNOMIAL CASE
int feedback1(float64 coef1, float64 coef2)
{
    int32      error=0, read=0, write=0;
    TaskHandle taskHandle=0;
    TaskHandle taskHandle2=1;
    TaskHandle taskHandle3=3;
    TaskHandle taskHandle4=4;
    float64     datain1[1000]={0}, datain=0;
    float64     doffset=0, dtotal=0;
    float64     dataout1=0, dataout2=0;
    float64     disp, d4, d3, d2, d1, d0, fstiff;
    uInt32      data2[5005];
    char        ch, errBuff[2048]={'\0'};
    const char  triggerSource[] = "PFI0";
    const char  chan_in[]="Dev1/ai0";
    const char  chan_out[]="Dev1/ao0";
    int         TestLength = 1000000000;
    int32       icode=0;
    FILE        *out;
    int         Iicnt, icnt, i;

    // taskHandle4 creates and configures a timer to create digital pulses for output
    DAQmxErrChk (DAQmxCreateTask(" ", &taskHandle4));
    DAQmxErrChk (DAQmxCreateCOPulseChanFreq(taskHandle4,"Dev1/Ctr1","",DAQmx_Val_Hz,DAQmx_Val_Low,0.0,
    1000000.,.1));
    DAQmxErrChk (DAQmxCfgImplicitTiming(taskHandle4,DAQmx_Val_ContSamps,10000));
    DAQmxStartTask(taskHandle4);

    icnt=0;

    // taskHandle and taskHandle2 create the AI/AO channels
    DAQmxErrChk (DAQmxCreateTask(" ", &taskHandle));
    DAQmxErrChk (DAQmxCreateTask(" ", &taskHandle2));

    DAQmxErrChk (DAQmxCreateAIVoltageChan(taskHandle,chan_in,"",DAQmx_Val_Diff,-10.0,10.0,DAQmx_Val_Volts,
    NULL));
    DAQmxErrChk (DAQmxCreateAOVoltageChan(taskHandle2,chan_out,"",-10.0,10.0,DAQmx_Val_Volts,NULL));

    DAQmxStartTask(taskHandle);
    DAQmxStartTask(taskHandle2);

    /*****/

    d4 = 0; d3 = 0; d2 = 0; d1 = 0; d0 = 0;

    for (Iicnt = 0; Iicnt <= 999; Iicnt++)                //This is to calculate the offset
    {
        DAQmxReadAnalogScalarF64(taskHandle,-1.0, &datain1,NULL);

        for (i = 0; i < 999; ++i)
        {
            dtotal += datain1[i];
            doffset = dtotal/1000;
        }
    }
}

```

```

        d1 = datain1[999]; d2 = datain1[998];
        d3 = datain1[997]; d4 = datain1[996];
    }
}

/*****BEGIN TEST*****/
while(icnt++ < TestLength)
{
    if (icnt > 1)
    {
        //Recycling data points
        d4 = d3, d3 = d2, d2 = d1, d1 = d0;
    }

    DAQmxReadAnalogScalarF64(taskHandle,-1.0, &datain,NULL);

    d0 = datain;
    disp=0.25*d0 + 0.25*d1 + 0.25*d2 + 0.25*d3;

    /*****Generate the force in polynomial case*****/
    fstiff=coef1*disp+coef2*disp*disp*disp;

    dataout2 = fstiff*-1.0;

    if(dataout2 < -10.)
        dataout2 = -10.;
    if(dataout2 > 10.)
        dataout2 = 10.;

    DAQmxWriteAnalogScalarF64(taskHandle2,"YES",-1.0,dataout2,NULL);

}
read=0;

if( read>1 )
{
    printf("Outputting to file\n");
    out = fopen("c:/jpc/out2.txt","w");
    icnt=0;
    while(icnt++ < 5000)
    {
        fprintf(out,"%d  %u\n",icnt,data2[icnt]);
    }
}

Error:
if( DAQmxFailed(error) )
    DAQmxGetExtendedErrorInfo(errBuff,2048);
if( DAQmxFailed(error) )
    printf("DAQmx Error: %s\n",errBuff);
printf("End of program, press any key to quit now\n");
while( !_kbhit() ) {}
ch = _getch();
return 0;
}

```

Table 4.4: Current Nonlinear Feedback Types

Designation	Description or Equation
Simple Spring	Contains a linear stiffness term Input: k
Nonlinear Spring	Contains linear and cubic stiffness terms Inputs: k_1 and k_3
Spring with Gap (Bilinear)	User may specify the size of the gap as well as the stiffnesses inside and outside the gap Inputs: gap size, k_{inside}, and k_{outside}
Spring with Gap (Trilinear)	User may specify the size of the gap as well as the stiffnesses before, inside, and after the gap Inputs: gap size, k_{before}, k_{inside}, and k_{after}
Simplified Damper	Modeled by Equation 6.5. Inertia and stiffness terms required to physically simulate the damper Inputs: c, n, and k

5 PHYSICAL STUDY: CALIBRATION

The methodology presented in this research study is a new approach to the physical simulation of dynamic models. Once the Reconfigurable Test Setup was constructed, the accuracy, reliability, and limitations of the device must be quantified. In this chapter, a number of steps taken for calibration purposes are presented.

The restoring force determines the characteristics of dynamic systems. Because the goal of the Reconfigurable Test Setup is to have great flexibility in the modeling process, it is imperative that the computer code written to control the restoring force be accurate in the replication of the restoring force and robust enough to handle a number of nonlinear behaviors. To create the control program, the Microsoft Visual C program was utilized. C is a free-form, general purpose computer coding language that can be compiled into binary for rapid processing. It was chosen because of its popularity within the coding community (for quick implementation by a large number of users) and its high processing speed, which is crucial for the real-time computations performed by the Restoring Force Calculator.

The C program contains a user interface program where one can choose the type of restoring force capability the Reconfigurable Test Setup will have, as well the values of the parametric coefficients. Once chosen, a subroutine processes the measured displacement and velocity values and outputs a corresponding force value. The user also has the ability to add a number of subroutines to the project work file, essentially allowing the Reconfigurable Test Setup to replicate an endless number of dynamic models.

In the determination of the modeling accuracy of the restoring force apparatus, three restoring force measurements are acquired and compared. The “physically recorded” restoring force is a direct measurement from the restoring force gauge, which is located between the electro-

Table 5.1: Types and Sources of Restoring Force Measurements

Designation	Abbrev.	Source	Description
Physically recorded	RFC	Restoring force gauge	This value is measured directly from the restoring force gauge, detailing electromagnetic output.
Calculated	IRFC	C real-time calculation	After directly sampling displacement and velocity values, the restoring force is calculated via software and value calculated is then sent to the electromagnet.
Theoretical	THEO	Post-analysis calculation	This value is calculated after completion of the physical testing using measured displacement and velocity values as inputs into the desired dynamic equation. It will not contain noise and will serve as an idealized case.

magnet and the moving mass. It details the force coming from the electromagnet. It will be designated as the *physically recorded restoring force* (RFC). The “calculated” restoring force value is calculated by the Restoring Force Calculator. As displacement and velocity measurements are supplied, the Restoring Force Calculator performs its computations and outputs the value into the controller of the electromagnet. This value will be designated as the *calculated restoring force* (IRFC). The “theoretical” restoring force is computed after the testing is completed. This value is theoretically perfect, as the recorded displacement and velocity values input into the desired dynamic model. These values will be designated as the *theoretical restoring force* (THEO). Each type of restoring force value is summarized in Table 5.1. RFC and IRFC are shown pictorially in Figure 5.1.

A dynamic model of considerable interest within the structural dynamics field is the dead-space (or gap-space) nonlinearity. Characteristics such as these are commonly found in mechanical devices where a small “gap” in its physical components may cause a “dead-space” in the device’s output (Yun and Masri, 2008). A true gap-space nonlinearity will have a restor-

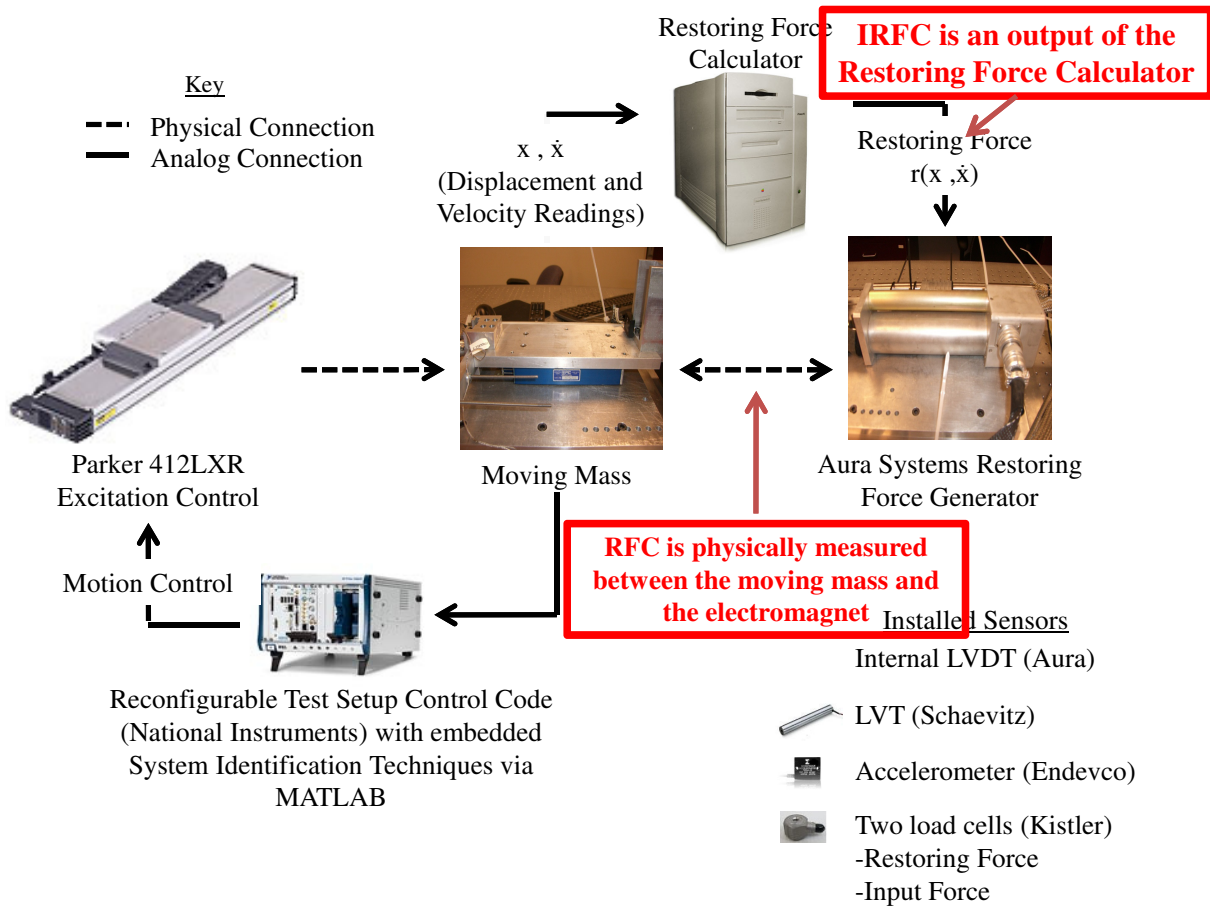


Figure 5.1: This is a modification of Figure 4.5 where the locations of RFC and IRFC have been superimposed. The physically recorded restoring force (RFC) is physically measured by a load cell located between the Restoring Force Electromagnet and the moving mass. The calculated restoring force (IRFC) is an output of the Restoring Force Calculator. The theoretical restoring force (THEO) is not calculated during the test and is therefore not shown. It is calculated post-analysis using physically recorded displacement and velocity values.

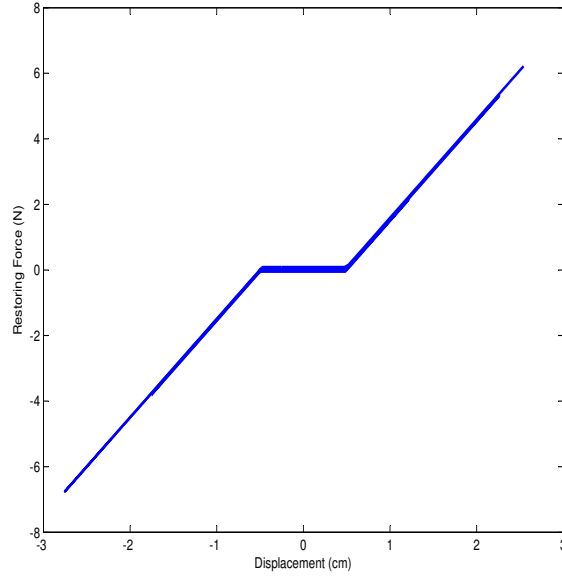


Figure 5.2: Displacement vs. restoring force phase plot for a gap-space nonlinearity. Characteristics such as these are commonly found in mechanical devices where a small gap between physical components can cause a “dead-space” for restoring force output. This type of dynamic model is able to be physically simulated by the Reconfigurable Test Setup.

ing output of zero in the “gap region.” However, it is also possible to have an altered stiffness, deemed a “trilinear dynamic model.” The motion for a true gap-space nonlinearity is described (for a gap in a linear spring) by

$$r(u(t), \dot{u}(t)) = \begin{bmatrix} k_1 u & \text{if } u < -gap \\ 0 & \text{if } -gap \leq u \leq gap \\ k_1 u & \text{if } u > gap \end{bmatrix}. \quad (5.1)$$

where gap is the size of the mechanical gap. A gap-space nonlinearity is shown (as a displacement vs. restoring force) in Figure 5.2. The physical simulation of a gap-space nonlinearity has long been a challenge for researchers; but with the Reconfigurable Test Setup, it is possible.

In Figure 5.3, three types of dynamic models created by the Reconfigurable Test Setup are displayed: linear, Duffing, and gap-space nonlinearity. Each has a restoring force solely

dependent upon displacement, thus a displacement vs. restoring force phase plot detail the governing system characteristics. Figures 5.3(a), (b), and (c) show three linear models with increasing stiffness values, which is demonstrated by the increasing slope of the restoring force. Figures 5.3(d), (e), and (f) show three Duffing models with increasing k_3 terms. In each model, k_1 remains the same. In Figure 5.3(d), the k_3 term is very small, meaning the resulting dynamic characteristics behave predominantly linear. On the other hand, Figure 5.3(f) has a much more dominant k_3 term, resulting in a much more nonlinear output. Gap-space models of increasing gap-size can be seen in Figures 5.3(g), (h), and (i).

5.1 Calibrating the Restoring Force Calculator

The Reconfigurable Test Setup device was calibrated to ensure test reliability. All measurement wires were properly shielded and grounded to prevent electrical noise. As described in Section 4.1.1, the controller of the electromagnet provides force and displacement oriented control, and the controller was calibrated by the manufacturer (Aura Systems) for force control.

The following sections describe a number of steps taken to improve and quantify the reliability of the Restoring Force Calculator.

5.1.1 Input Data Smoothing

To provide an accurate determination of the value of the restoring force in real-time, the Restoring Force Calculator samples displacement and velocity measurements at very high sampling frequency. This is done to ensure the real-time calculated force is being applied at a certain recorded displacement and velocity. However it is possible that the use of uncontrolled measurements from the sensors may leave the physical simulations more susceptible to measurement uncertainty (i.e. electrical spikes). In the initial calibration of the Reconfigurable Test Setup, only direct algorithm controls were utilized. Two approaches of input data processing considered: raw data and moving average.

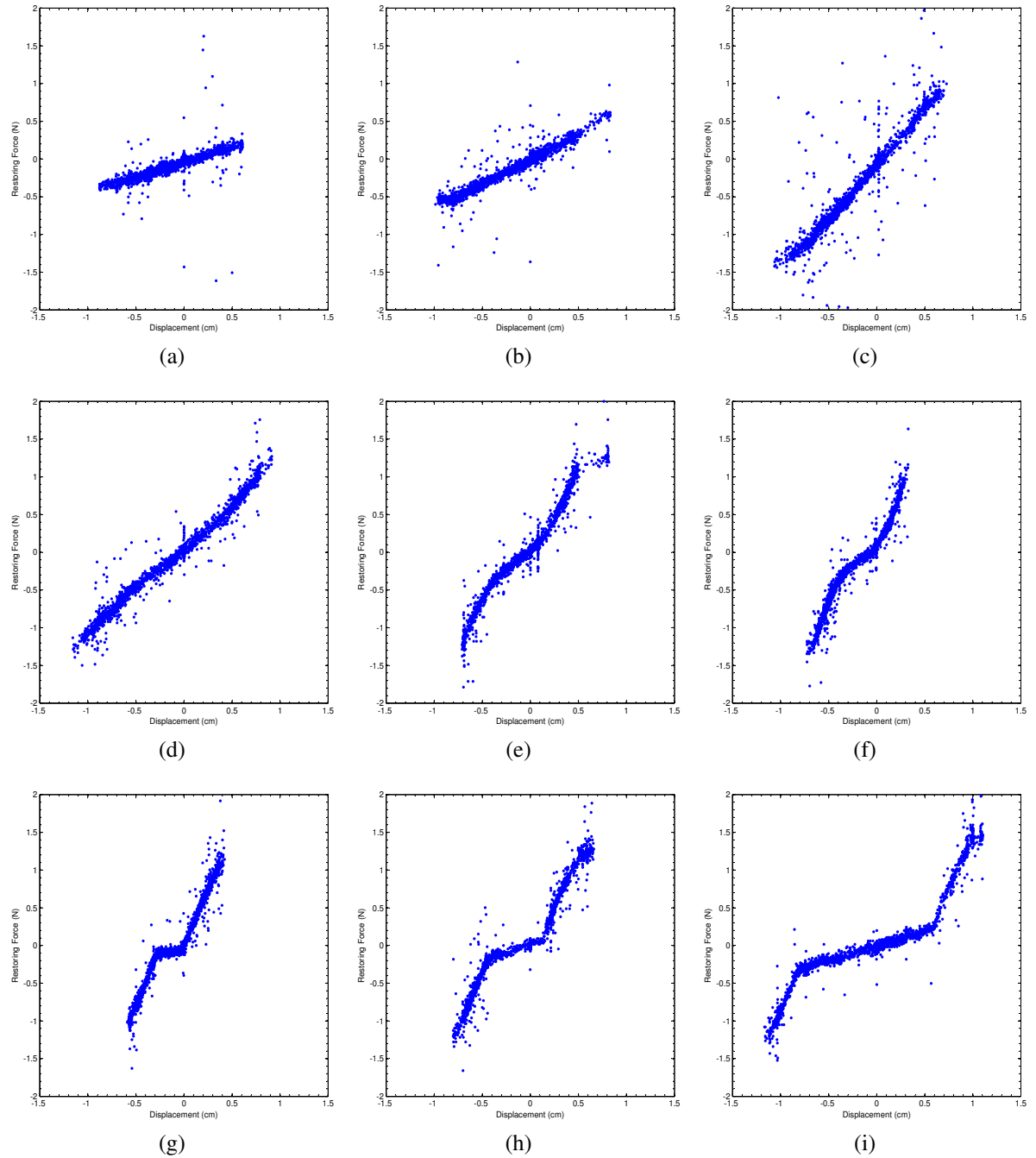


Figure 5.3: Sample nonlinear models created by the Reconfigurable Test Setup. Row 1 details three linear models with increasing stiffnesses; Row 2 displays three Duffing models with increasing k_3 terms; and Row 3 plots three gap space nonlinearities of various gap sizes.

The first type of filtering considered for implementation is moving average filtering, which smoothes data by replacing each data point with the average of the previously recorded steps. This process is given by the difference equation

$$m_{corr} = \frac{1}{N}(m_i + m_{i-1} + m_{i-2} + m_{i-3} + m_{i-4}) \quad (5.2)$$

where m_{corr} is the smoothed measurement value, i is the iteration number, and N is the number of filtered points (Proakis and Manolakis, 2006). For the determination of which filtering type provided the least amount of errors, N was taken as 5.

The second type of filtering considered for implementation is the moving median filtering, which is adept at eliminating outliers from data. Its process is described by

$$m_{corr} = \text{median}(m_i, m_{i-1}, m_{i-2}, m_{i-3}, m_{i-4}) \quad (5.3)$$

where $(m_i, m_{i-1}, \dots, m_{i-4})$ are sorted from least to greatest at each time step and the median is chosen. For comparison to moving average filtering, the median was selected out of the previous five recorded data points.

In this analysis, a Duffing model was utilized. Each test lasted 140 seconds and the models were excited with a broadband random force between 0.1 and 5 HZ. This process was repeated twenty times for each smoothing type considered: no smoothing (or “raw”), moving average, and moving median. In this analysis, the Restoring Force Calculator computed restoring force (IRFC) and theoretically calculated (THEO) values will be compared to determine which provided the most accurate smoothing. To measure the goodness of fit, mean square error (MSE) will be utilized, calculated by Equation 5.4.

Table 5.2: Restoring Force Calculator Smoothing over 20 Iterations

Filter Type	Mean MSE(%)	Average Loop Time (in ms)
No Smoothing	0.4933	0.000015
Moving Average	0.4058	0.000015
Median	0.4203	0.000016

$$MSE(\%) = 100 \times \frac{\sum_{i=1}^N (f_m^i - f_{th}^i)^2}{\sum_{i=1}^N (f_{th}^i)^2} \quad (5.4)$$

where i is the i^{th} data point, N is the total number of data points, f_m is the measured data set, and f_{th} is the theoretical value.

Discussion

Figure 5.4 details the results of the different smoothing types analyses, while Table 5.2 summarizes the mean-square analyses and details the average elapsed time per loop. Median average filtering provided similar MSE results to the moving average analysis. But due to the extra lines of code needed to “sort” data readings, the average time per loop was slightly larger. It was therefore decided to implement moving average filtering into each of the control algorithm codes.

Since it was determined that a moving average would be the smoothing type of choice (for this specific dynamic model and excitation combination), an investigation was made to determine the optimal number of terms to include. Therefore an analysis was conducted for weighted moving averages with ten different window sizes (one data point, two data points, ..., ten data points). Each test lasted over two minutes long and the models were subjected to broadband random excitation from a range of 0.1 to 5 Hz. Twenty data sets were recorded for each weighted average level. The mean MSE and corresponding standard deviations are shown in Table 5.3 and summarized in an error bar plot in Figure 5.5. As in the previous analysis,

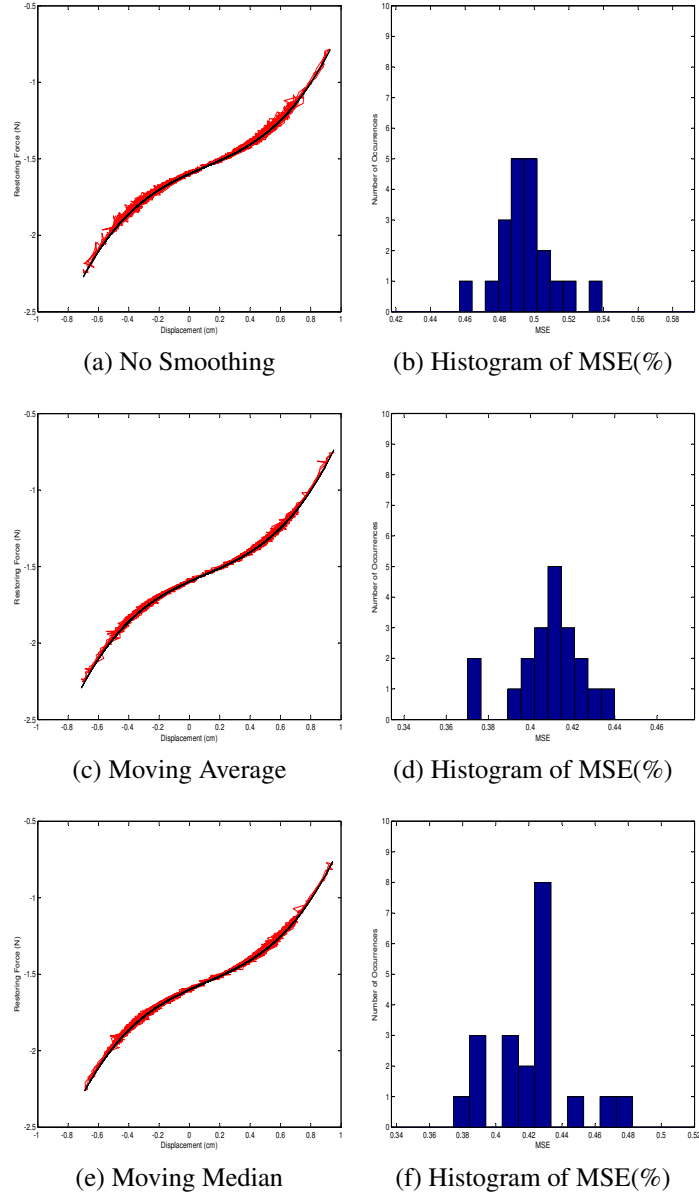


Figure 5.4: Duffing model created by the Restoring Force Calculator with different types of smoothing. In the figures on the left, the red dots represent the Restoring Force Calculator computation (IRFC) and the black line is a measure of the post-analysis calculated theoretical value (THEO). Figures on the right show the compiled results of the goodness of fit analyses over 20 iterations. Figures (a) and (b) are results using raw data points, Figures (c) and (d) are results using moving average filtering, and Figures (e) and (f) are results using median average filtering.

the Restoring Force Calculator computed restoring force (IRFC) and theoretically calculated (THEO) values will be compared to determine the optimal number of included weighted terms.

The results of the analysis show that the weighing of four data points proved to provide the best filtering results. Thus, Equation 5.2 must be taken where $N = 4$. It is theorized that too few data points leads to susceptibility to measurement noise and too many points cause an output lag when the model is excited at high frequencies.

In future studies, it is recommended that more advanced control algorithms be considered and evaluated. One method of particular interest is Spencer's 21-point moving average, a local cubic-polynomial smoother. A unique feature of Spencer's formula is the inclusion of negative weights, included to enhance "edge" smoothing. Unlike Equation 5.2 and 5.3 however, Spencer's formula requires data points before and after the smoothed point. Spencer's formula is given by (Gavin, 1993; Cleveland and Loader, 1994; Henderson, 1916):

$$\begin{aligned}
 m_{filt} = & \frac{1}{350}(60m_i + 57(m_{i-1} + m_{i+1}) + 47(m_{i-2} + m_{i+2}) + 33(m_{i-3} + m_{i+3}) + \\
 & 18(m_{i-4} + m_{i+4}) + 6(m_{i-5} + m_{i+5}) - 2(m_{i-6} + m_{i+6}) - 5(m_{i-7} + m_{i+7}) - \\
 & 5(m_{i-8} + m_{i+8}) - 3(m_{i-9} + m_{i+9}) - (m_{i-10} + m_{i+10})).
 \end{aligned}
 \tag{5.5}$$

To be a viable for implementation in the Reconfigurable Test Setup, two issues must be considered and resolved: lag time and future predictions. Lag time within the Restoring Force Calculator will hamper its abilities to update in real-time. Also because the Restoring Force Calculator and the Reconfigurable Test Setup Control Code (RTSCC) are housed in separate CPU's, a timing discrepancy will cause difficulty in data analysis. The use of Spencer's formula will also require the use of an accurate future value predictor. The future value forecasts must

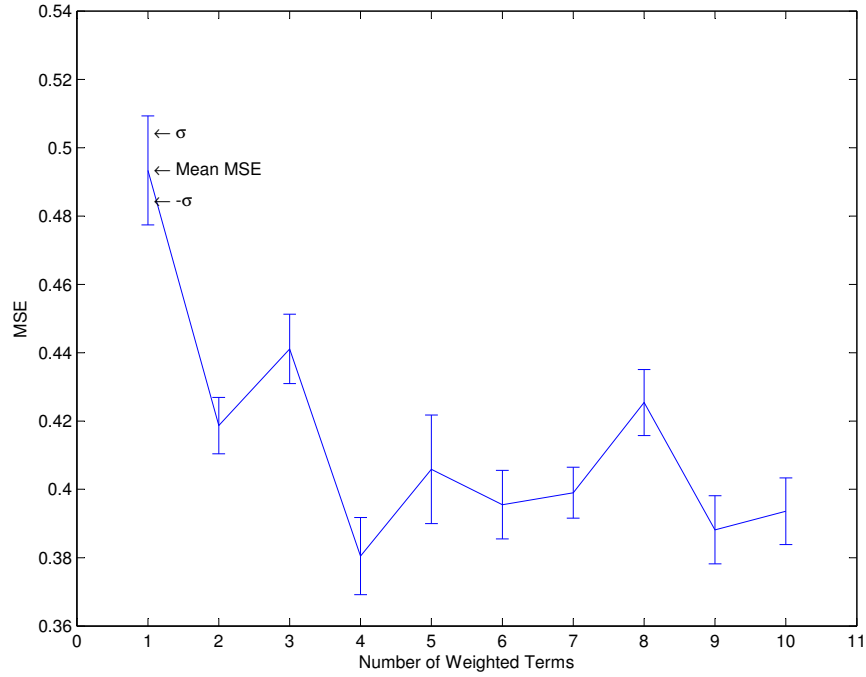


Figure 5.5: Compiled MSE values for a series of experimental tests to determine the optimal number of data points to include in the Restoring Force Calculator data smoothing process. Mean MSE error and corresponding standard deviations are graphed against the number of weighted terms included over 20 iterations. It can be seen that 4 points performed the best, as too few data points leads to susceptibility to noise and too many points cause an output lag when the model is excited at high frequencies.

be guaranteed for a variety of dynamic models otherwise faulty smoothing will result.

5.1.2 Interaction between the Restoring Force Electromagnet and the Linear Servo Motor

The interaction between the linear servo motor (which provides displacement-oriented input force) and the Restoring Force Generator is very complex. Because they are governed by separate controllers, coordination between the two is imperative so that conflict is minimized. For calibration, this interaction must be quantified.

As these two devices interact, small variations in displacement will result in fluctuations in the Restoring Force Calculator output (i.e. the value of IRFC) and correspondingly into the actual electromagnet output (RFC). It is theorized that this instability may be resolved by the

Table 5.3: Compiled MSE values and Standard Deviations to Determine the Number of Data Points to Include for Smoothing.

Terms Included	Mean MSE	Std. Dev.
1	0.4933	0.0160
2	0.4187	0.0083
3	0.4411	0.0102
4	0.3805	0.0113
5	0.4058	0.0159
6	0.3955	0.0100
7	0.3990	0.0075
8	0.4254	0.0097
9	0.3882	0.0100
10	0.3936	0.0098

utilization of a more resilient linear servo motor, as its position would be less influenced by the restoring force provided by the electromagnet thereby providing consistent output force for given displacement and/or velocity measurements.

In order to simulate a “stronger” linear servo motor, a series of gap-space models were considered with various stiffnesses: lower input stiffness would relate to a stronger motor and higher stiffnesses to a weaker motor. Five models were chosen with increasing linear stiffness ($k = 0.00, 0.50, 1.00, 2.00, \text{ and } 4.00$). Each model was subjected to broadband random excitation for 140 seconds and 20 data sets were assembled. A goodness of fit analysis will be performed between the Restoring Force Calculator computed restoring force (IRFC) and theoretically calculated (THEO) values. Recorded data is shown in Figure 5.6.

Discussion

As shown in Figure 5.7 and Table 5.4, the modeling error rises with the linear stiffness. This is seen in the linear areas beyond the gap, as the algorithm shows a progressively greater disbursement of output force. The results of the analysis prove that a more forceful linear servo motor will improve the modeling accuracy of the Reconfigurable Test Setup. As the approach

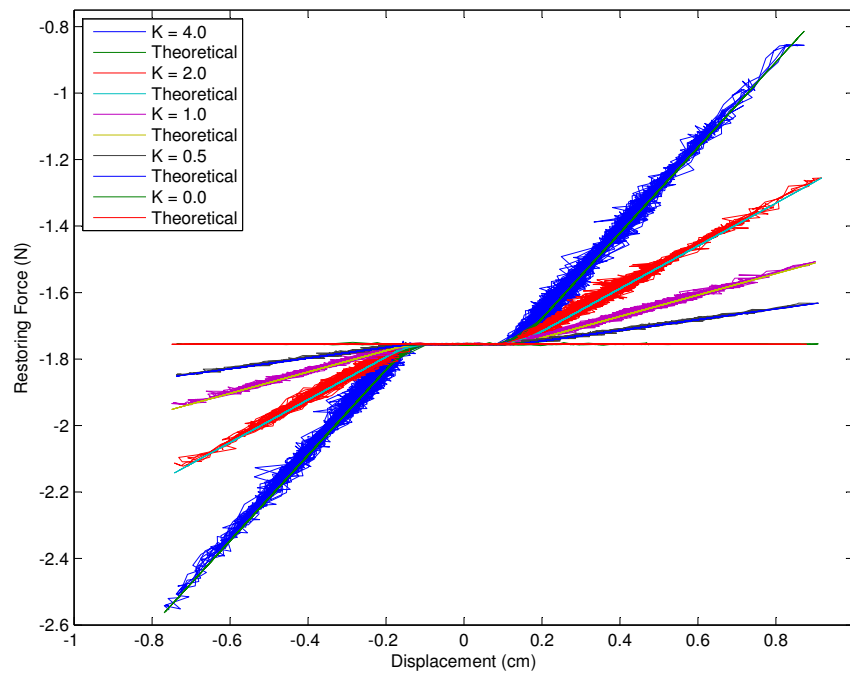


Figure 5.6: Gap-space models with different stiffness terms created by the Restoring Force Calculator. In this figure, the various models are compared to their theoretical values as well as with each other. As the stiffness is reduced (or the control of the actuator is increased), less noise is present in the measurements.

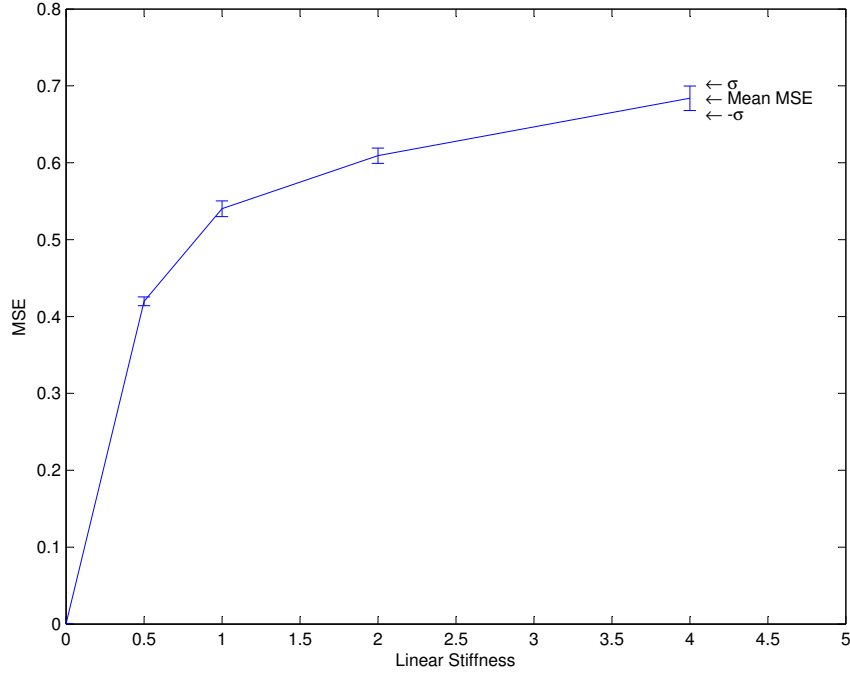


Figure 5.7: Mean and standard deviation mean square error of gap-space models over 20 iterations each. It is shown that with less output electromagnet force (hence simulating a stronger linear servo motor), the modeling accuracy of the Reconfigurable Test Setup is improved. It is therefore recommended that as future studies are planned, an improved linear servo motor be procured.

described in this study evolves, it is therefore recommended that a linear servo with greater displacement control and not susceptible to the electromagnetic output force be procured and utilized to provide the input force.

5.1.3 Effects of Excitation Frequency

In this investigation, the goal is to compare the Reconfigurable Test Setup's ability to replicate a nonlinear model undergoing different frequencies of excitation. A series of tests were conducted with a Duffing model undergoing a series of monotonic sinusoidal excitations: 0.5, 1.0, 2.5, and 5 Hz. Each test lasted a total 40 seconds, designed so that each excitation level had at least 15 cycles. In this analysis, a mean square error between theoretical restoring force (THEO) and Restoring Force Calculator computed restoring force (IRFC) will be used to de-

Table 5.4: Compiled MSE values Over 20 Iterations to Explore Linear Servo Motor and Electromagnet Interaction

Data Set	Linear Stiffness	Mean MSE	MSE Std. Dev.
Gap No. 1	0.0	0.0007	0.0000
Gap No. 2	0.5	0.4198	0.0058
Gap No. 3	1.0	0.5402	0.0102
Gap No. 4	2.0	0.6091	0.0099
Gap No. 5	4.0	0.6839	0.0160

termine each excitation frequency's goodness of fit. The results are shown in Figure 5.8 and Table 5.5.

Discussion

The error in the analysis rises as the excitation increases; although it must be noted that even at 5 Hz of excitation, the goodness of fit was still within 1%. It is possible that the upload rate of the Restoring Force Calculator is not fast enough and at high frequency levels of excitation, this effects of the “lag” is highlighted. It is also feasible that the linear servo motor experiences additional noise while performing motion at high frequency. Because the linear servo motor moving much faster, the interaction between it and the electromagnet also may cause added uncertainty.

The last possible theory for the additional amount of noise is due to the DAQ scan rate of the Reconfigurable Test Setup Control Code (RTSCC). For this test, it was set at 200 Hz. Figure 5.9 displays displacement vs. velocity phase plots under excitation frequencies of 1 and 5 Hz, respectively. At lower frequency excitation, a full phase plot is captured. However when the excitation is increase to 5 Hz, the phase plot appears “choppy.” This suggests that the chosen scan rate for this test was not fast enough.

With the above discussion in mind, it is difficult to precisely determine why the goodness of fit decreased as excitation frequency increased. In future studies, the source of additional error

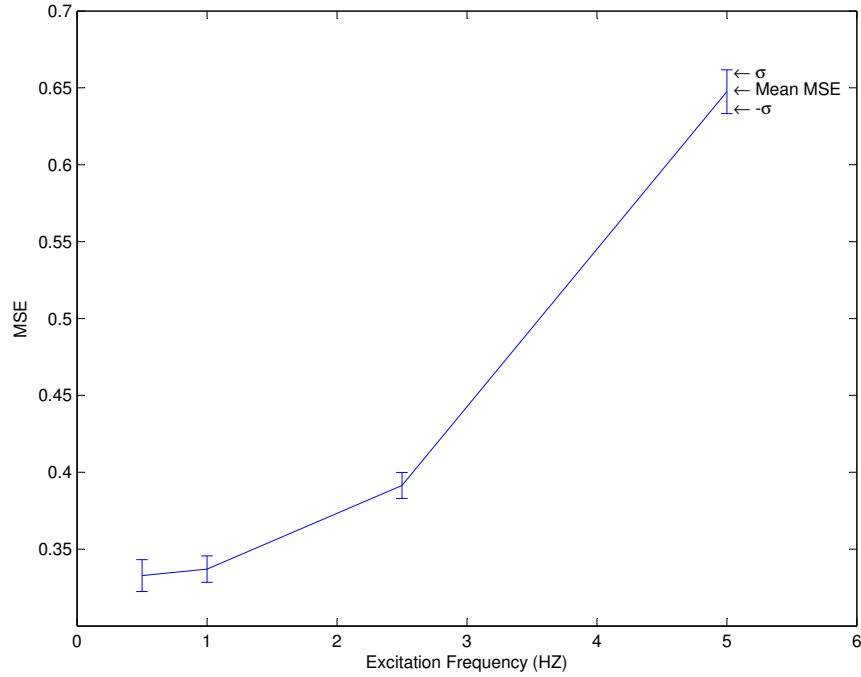


Figure 5.8: Mean and standard deviation mean square error of Duffing models of increasing excitation frequency. Data was compiled from a set of 20 iterations per frequency.

Table 5.5: Compiled MSE values (of IRFC and THEO restoring force values) over 20 Iterations to Explore the Effect of Excitation Frequency

Excitation Frequency (Hz)	Mean MSE	MSE Std. Dev.
0.50	0.3328	0.0104
1.0	0.3371	0.0086
2.50	0.3914	0.0085
5.00	0.6475	0.0143

must be identified and improved upon.

5.2 Electromagnet Calibration

To calibrate the restoring force electromagnet, known voltage values (-10 to 10 volts in 1 volt increments) were input into the Aura Control Box and the moving mass was excited with broadband random excitation for 30 seconds. This process was repeated for 20 iterations. Despite the range of excitation, because the input voltage remains constant for each trial, the

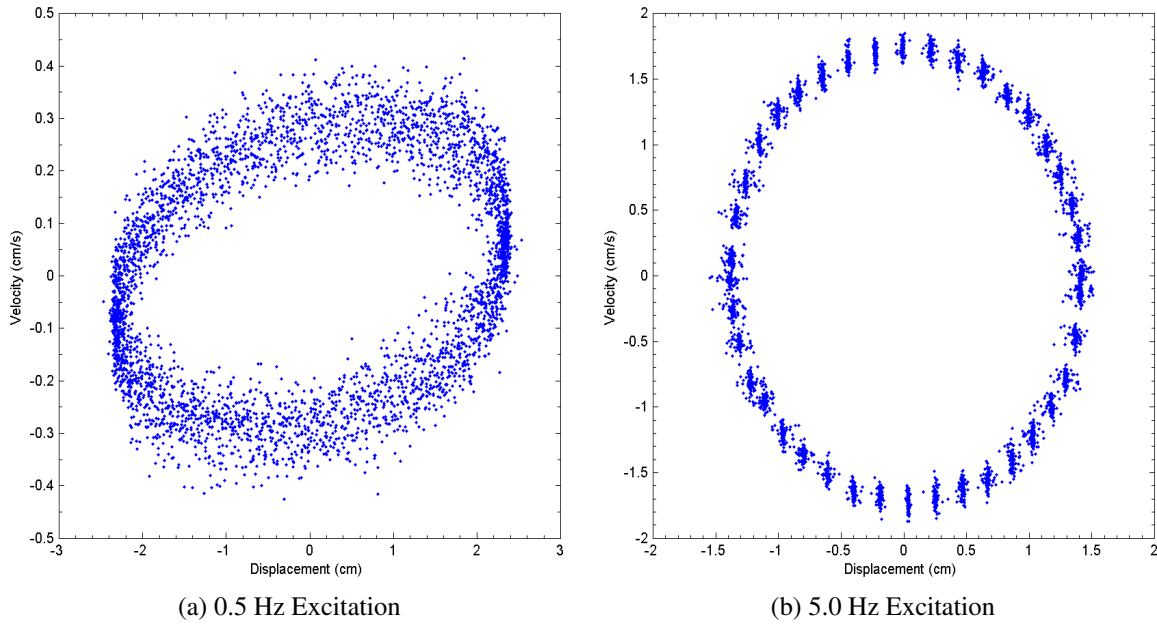


Figure 5.9: Displacement vs. velocity phase plots for a Duffing model undergoing different frequencies of excitation. The groupings of measurements in Figure (b) highlight the need for a higher DAQ scan rate in this test.

output of the electromagnet should also remain constant. The mean of the recorded data sets were compiled shown in Figure 5.10(a).

The results show that the electromagnet's force output behaves nonlinearly, a common occurrence in many actuators. To determine appropriate scale and offset values, the force output was restricted to its linear range (shown in Figure 5.10(b)) and a linear regression was performed. The conversion factor between input voltage and restoring force is given in Equation 5.6.

This analysis shows that the output of the electromagnet is not linear. In future studies, it is important that the chosen electromagnet be linear in its output force. With the current device, the its nonlinearity may cause physical simulation issues (i.e. an increase in Restoring Force Calculator computed value (IRFC) does not result in an exact increase in actual electromagnet simulated restoring force (RFC)).

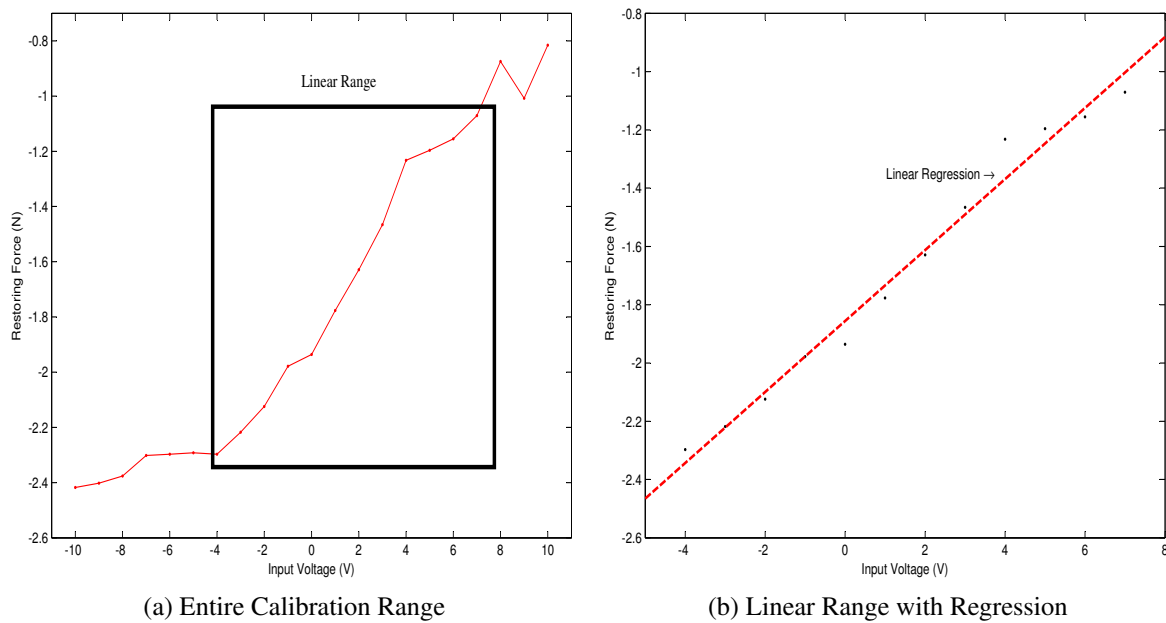


Figure 5.10: Plot of input voltage values and the corresponding measurements recorded by the restoring force gauge.

$$\text{Electromagnet Force Output} = 0.1218 * \text{Input Voltage} - 1.8561 \quad (5.6)$$

5.3 Actuator Noise and Post Filtering

In this analysis, the goal is determine if the linear servo motor or the electromagnet is contributing high frequency noise into recorded measurements. To perform the test, the accelerometer was utilized. During each of these tests, a broadband random excitation ranging from 0.1 to 5 Hz provided displacement orientated input motion for a length of two minutes.

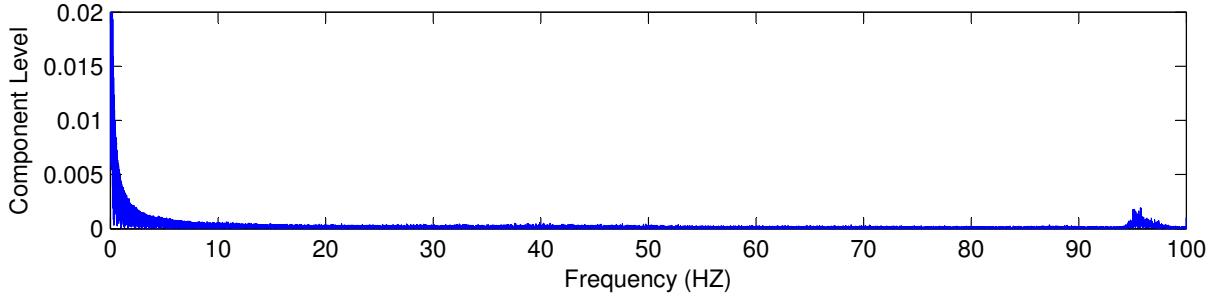
First, the accelerometer was placed upon the non-moving surface of the linear servo motor. In this way, the ambient vibration caused by its motion could be recorded. Then by performing a Fast Fourier Transform (FFT), a determination of the frequencies of the ambient vibrational noise was possible. The results are shown in Figure 5.11(a), where a signal between 90 and

100 Hz is clearly visible. Next, the accelerometer was placed upon the surface of the moving mass, but without an active restoring force (i.e. the restoring force electromagnet remained off). Thus acceleration measurements recorded data from only the motion of the linear servo motor. The FFT, shown in Figure 5.11(b), details a nearly uniform increase in frequency contributions from that of Figure 5.11(a). Last, with the accelerometer remaining upon the moving mass, the restoring force generator was activated. The FFT, shown in Figure 5.11(c), comprises of very similar frequency contributions as Figure 5.11(b).

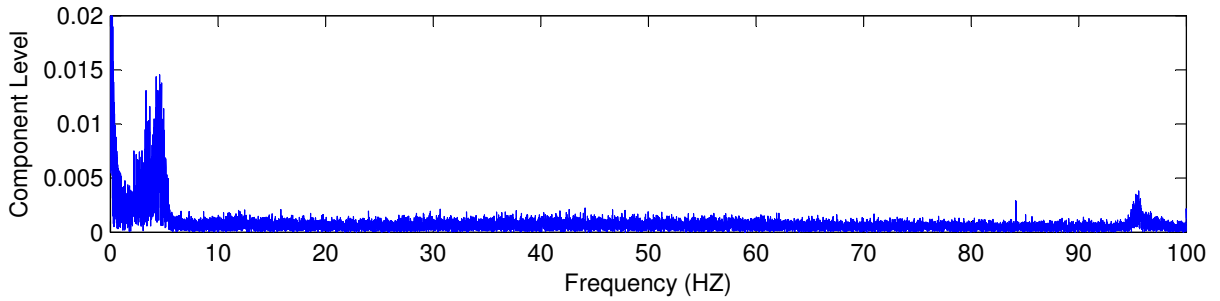
The results of Figure 5.11 demonstrate that the linear servo motor provides a considerable content of high frequency vibrational interferences into the measurement signal. The Restoring Force Electromagnet, on the other hand, does not.

Due to the presence of high frequency signal components in the physical measurements, post-processing may be utilized to filter out unwanted data interferences. In this study, a Band-pass Butterworth filter will be utilized. It includes both lowpass and highpass filtering abilities and the use of a Butterworth filter does not distort the measured response. The motion frequency of the broadband random excitement ranged from 0.1 to 5 Hz, therefore these frequency contributions are desirable. Therefore by setting the lowpass frequency to 0.01 Hz and the highpass to 30 Hz, desired response components will not be omitted.

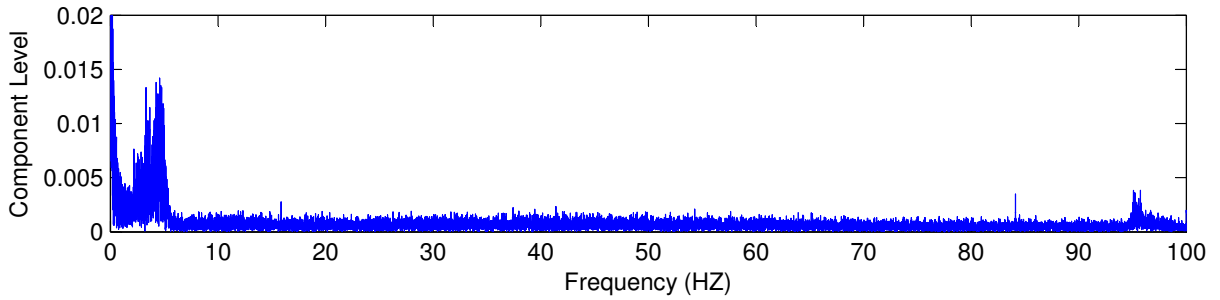
Figure 5.12 details the differences between an unfiltered and filtered recorded data set. Figure 5.12(b) shows the variety of high-frequency noise present in the measurements. By restricting the acceptable frequencies (Figure 5.12(d)), a much cleaner signal results.



(a) Actuator Ambient Noise



(b) Movement without Restoring Force



(c) Movement with Restoring Force

Figure 5.11: Fast Fourier Transforms (FFT) of acceleration measurements. Figure (a) was taken from the surface of the linear servo motor. Figure (b) was taken from the moving mass without engagement of the restoring force. Figure (c) was taken from the moving mass with an active restoring force. This analysis displays the presence of high frequency noise in the measurements. Notice that the activation of the restoring force generator causes little difference between signal components. Because the excitation frequencies vary from 0.1 to 5 Hz, it is theorized that through post-filtering with a Butterworth Filter between 0.01 and 30 Hz, a much cleaner signal will result.

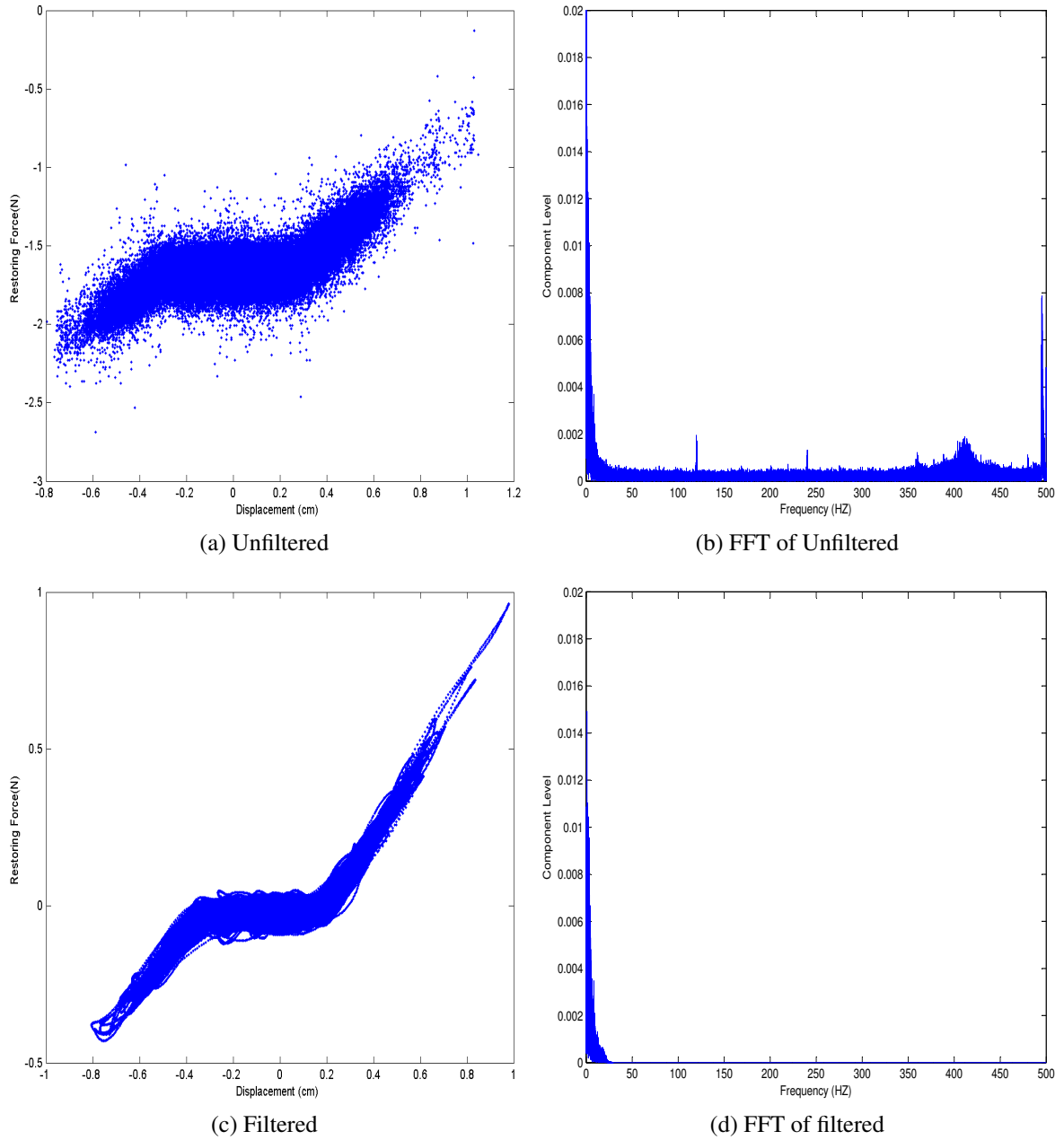


Figure 5.12: A gap-space nonlinear model shown before and after post processing with cutoff frequencies of 0.01 and 30.0 Hz. When comparing Figures (b) and (d), the utilization of the Butterworth Bandpass filter eliminates the contamination of high-frequency noise resulting in more distinctive characterization.

6 PHYSICAL STUDY: APPLICATIONS

The overall goal of this research project is to showcase that the Reconfigurable Test Setup is a viable tool for the physical creation of nonlinear dynamic data. In this chapter, a number of practical applications that the Reconfigurable Test Setup can be used for are presented and evaluated.

6.1 Damage Simulation

A possible use for the Reconfigurable Test Setup is to create physical data that can be used in a change detection analysis, one of the goals of structural health monitoring (SHM). According to Yun and Masri, the development of a reliable SHM methodology is imperative for two major purposes: (1) to avoid structural failure by detecting changes in the physical system commonly caused by deterioration, impact, and other structural modifications; and (2) to establish effective time schedules for routine maintenance. In a 2008 study, Yun and Masri demonstrated the normalized Chebyshev polynomials of the Restoring Force Method proved successful at detecting genuine systems changes (Yun and Masri, 2008). This analysis was also confirmed by the theoretical study discussed in Section 3.3.

Parameter Change without Time Dependency

To be able to reliably produce physical data that can be used in a change detection analysis, the MSE between the physically measured (RFC) and the Restoring Force Calculator computed restoring force (IRFC) must be similar for the two models. If this is the case, it is demonstrated that the Reconfigurable Test Setup can accurately replicate similar dynamic models.

Duffing models were physically created with a nonlinear stiffness term (k_3) of 0.30, dubbed the “unchanged” model. The unchanged model was excited with a broadband random force

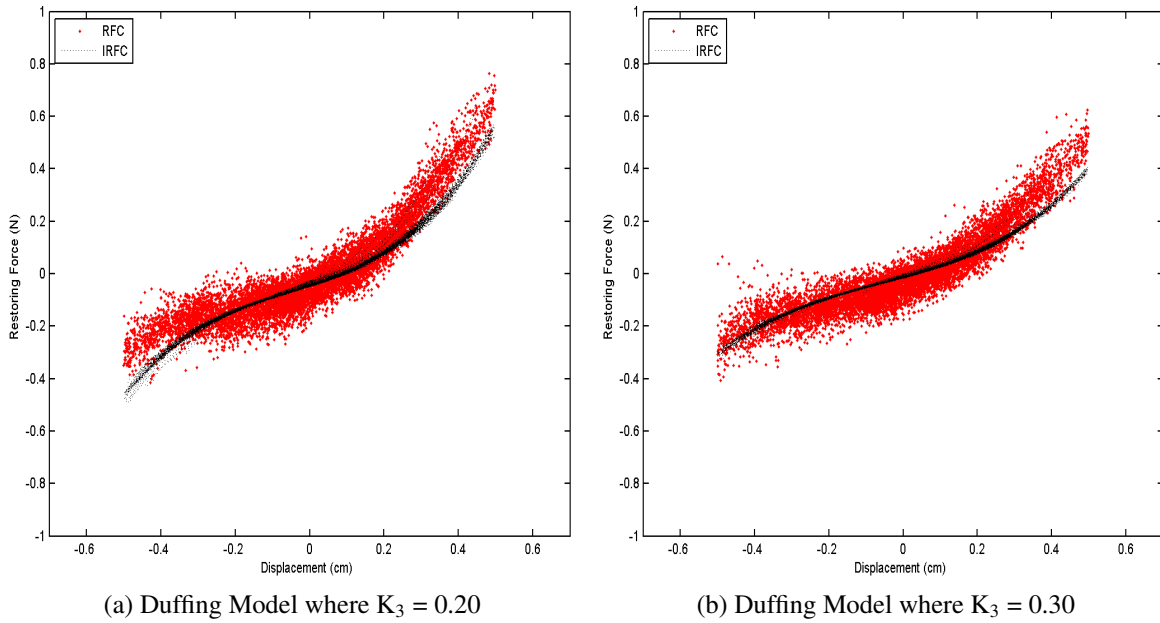


Figure 6.1: Duffing models physically created by the Reconfigurable Test Setup to demonstrate its ability to create physical data for change detection analysis. Over the course of 20 iterations, a Duffing model with k_3 of 0.30 had a mean MSE(%) of 14.02 compared to the Restoring Force Calculator computed value, while the Duffing model with $k_3 = 0.20$ had a mean MSE of 14.83. In each figure, the red dots represent physically recorded restoring force values (RFC) and the black line represents the Restoring Force Calculator computed value (IRFC).

for a period of one minute and 20 tests were performed. Then the nonlinear stiffness term was decreased to 0.20 and the process was repeated. The second model was dubbed the “changed” model. In each analysis, k_1 was set at 0.75. This process was repeated 20 times and the mean MSE was recorded.

It was found that the unchanged model had a MSE of 14.02% with a standard deviation of 1.4114% and the changed model had a MSE of 14.83% with a standard deviation of 0.8966%. Displacement vs. restoring force phase plots of the identified values can be seen in Figure 6.1.

Parameter Change with Time Dependency

In a real-world application, the deterioration of an installed energy dissipation device could

lead to a number of undesirable structural health outcomes, including catastrophic failure. In the past, much effort has been spent devising structural health monitoring approaches to alert critical maintenance personnel should a system change occur. However, it is very difficult to analyze the physical behavior of a structure under a damage case because of the inability to precisely control the deterioration rate.

Perhaps the most advantageous use of the Reconfigurable Test Setup test setup is its ability to physically simulate “damage” or “deterioration” scenarios of a nonlinear device. By inserting a “decay” or “growth” function (depending upon the intended damage expectation) into the Restoring Force Calculator, the deterioration rate can be precisely controlled and physical measurements recorded.

In a real world scenario, the deterioration of a nonlinear spring will lead to the softening of the parametric coefficients and the decaying of each (k_1 and k_3) was explored. To control the softening rate, the equation for experimental decay used in this analysis. It is given by the equation:

$$N(t) = N_0(A e^{-\lambda t} + B) \quad (6.1)$$

where $N(t)$ is the current value of the parameters (either k_1 or k_3 depending on the analysis), t is the algorithm loop number (i.e. time), N_0 is the original value of the coefficient, A is the scale factor, B is the offset, and λ is the decay rate (Hall and Selinger, 1981). The values of A , B , and λ were chosen such that the original coefficient would decay from its original value to 25% of its original value. Exponential decay was chosen so that the deterioration rate would decay rapidly at the beginning of the test and then slow considerably near the end.

The properties of the decay allow for the researcher to analyze the effects of a fast or slow deterioration with a single experimental setup. However because the decay rate is a nonlinear

Table 6.1: Comparison between Update Rates of “Decaying” and “Undecaying” Simulations

Type	Average Loop (ms)	Average Elapsed Time (s)
“Decaying”	0.000016	59.9553
“Undecaying”	0.000015	63.4797

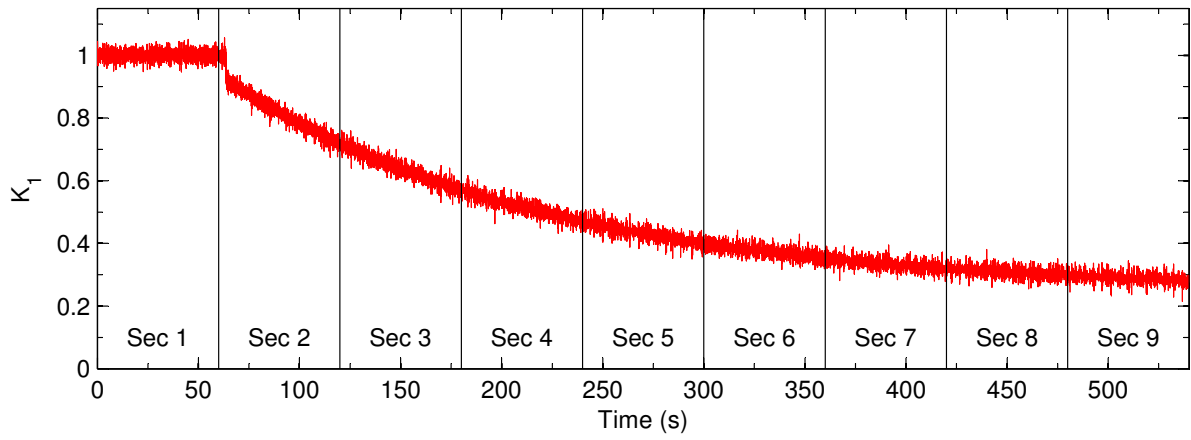
computation and a number of extra confining commands are required to allow for its computation, the elapsed time for update rate is dramatically reduced. To determine the effects of an increased processing loop, the “decaying calculation” simulation were recorded twenty times. For a basis of comparison, an “undecaying calculation” was also timed. The results are shown in Table 6.1.

Although the difference between average loop length is only 0.000001 ms, difference between the two over an elapsed time of sixty seconds is over 3.5 seconds. Because the updating rate is much slower, additional uncertainty is introduced into the control algorithm. This is an issue that further complicates the successful reproduction of a damage scenario.

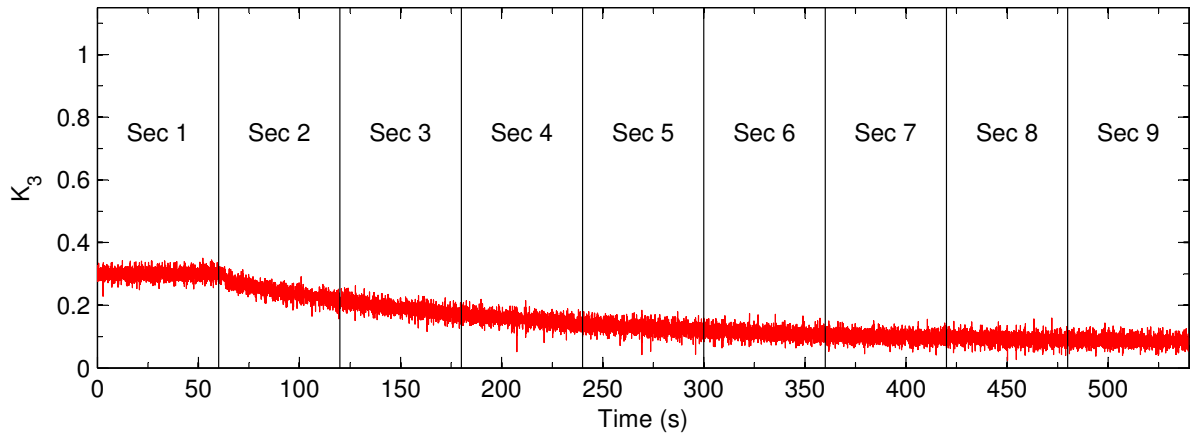
Two time-correlated damage condition analyses were performed: one with decay of the linear coefficient, and another with decay of the nonlinear coefficient. Each test was excited with a broadband random force and lasted 540 seconds. The recorded data was split into nine - sixty second increments. The time variation of the linear and nonlinear stiffness terms and corresponding section increments are shown in Figures 6.2(a) and 6.2(b).

Figures 6.3 and 6.4 show the variation of the nonlinear models as the coefficients decay. By viewing time lapsed phase plots, it is shown how the properties of the dynamic model change. The decrease of the linear coefficient results in increasing dominance of the cubic term. Thus, Figure 6.3 becomes increasingly nonlinear in its dynamic behavior. Conversely, the decay of the cubic term (Figure 6.4) leads to a much more linear shaped model.

In a physical study, the ability for the Reconfigurable Test Setup to decay its dynamic properties is very important for a variety of reasons. To perform a similar study without the recon-



(a) Decay of k_1



(b) Decay of k_3

Figure 6.2: Decaying rate of coefficients k_1 and k_3 .

figurable test setup, a number of factors will limit proper experimentation: (1) physical decay of an actual energy dissipation device is very difficult to achieve without actually damaging the item. This process would obviously be very expensive; (2) experimental quantification of the decay rate of a physical device will be unknown; (3) the actual decay of the device may take a long period of time.

The reconfigurable test setup has the ability to showcase the deterioration of its parameters and perform its deterioration in a controllable time window, making feasibility studies a more realistic option. The studies are also completely repeatable, so confidence levels (of the global effects of a deteriorated system) can be determined.

6.2 Physical Simulation of Nonlinear Viscous Damper

This chapter will demonstrate a practical application of the Reconfigurable Test Setup by modeling a nonlinear orifice viscous damper (hereinafter viscous damper), a very versatile energy dissipation device.

6.2.1 Background of Viscous Dampers

A viscous damper requires no auxiliary power, as they are completely self-contained. Originally developed for military and demanding industrial applications, a viscous damper is a device commonly installed on civil structures to passively dissipate energy generally produced by wind or seismic activities. Similarly, viscous dampers have shown the ability to provide sufficient damping at large velocities while limiting peak damper forces (Lin and Chopra, 2002).

The components of a viscous damper are shown in Figure 6.5 and generally consist of a piston rod, a chamber filled with a compressible silicon fluid, and a control valve. A high strength resin seal and a seal retainer keep the silicon fluids contained in the chambers (Soong and Dargush, 1997). Ultimately, the dynamic performance characteristics of a damper depend

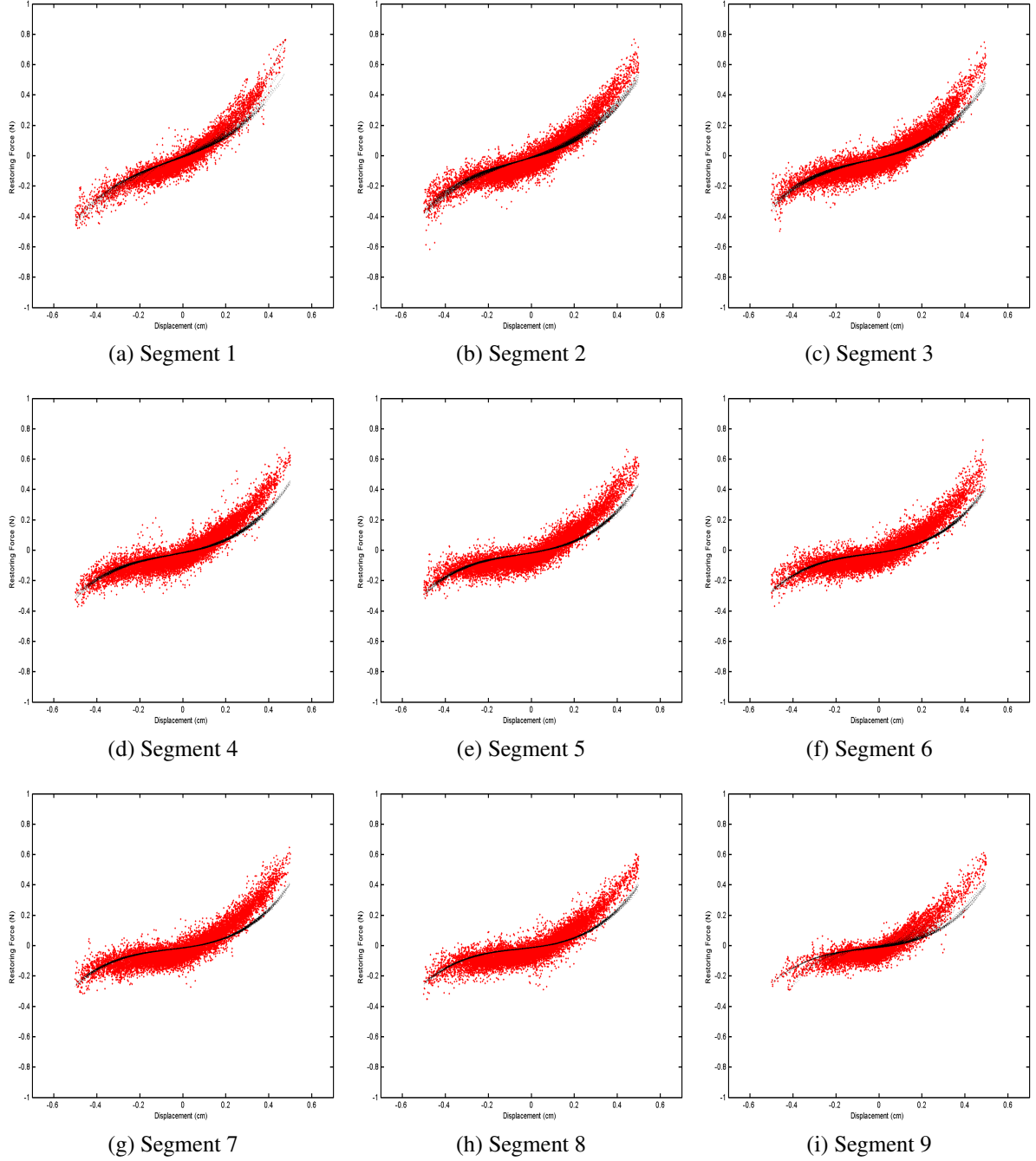


Figure 6.3: Time-lapse exponential decay of the linear stiffness term (k_1) of a nonlinear spring as modeled by the Reconfigurable Test Setup. The black line details the Restoring Force Calculator computed restoring force value (IRFC) and the red dots detail the physically recorded restoring force value (RFC).

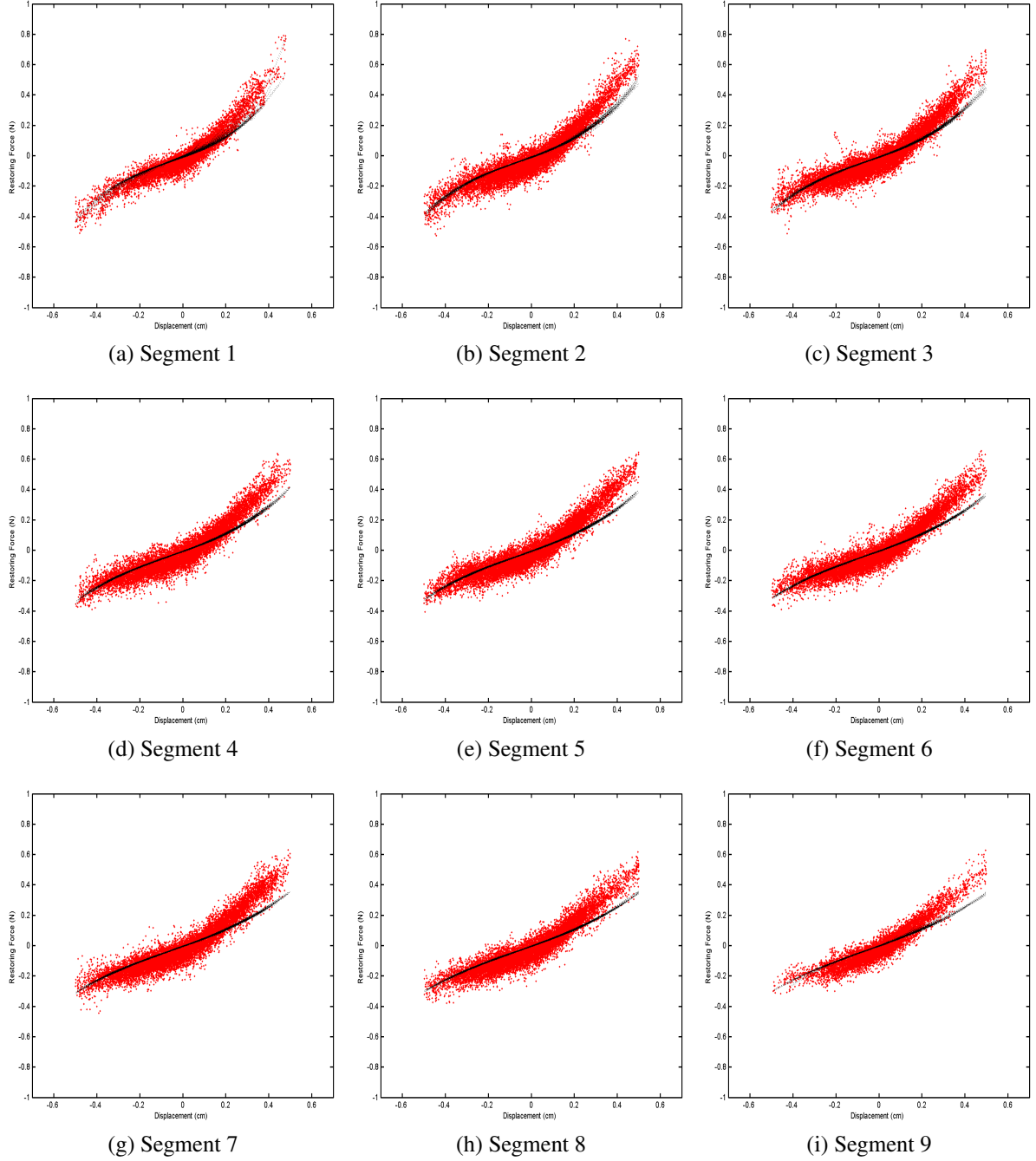


Figure 6.4: Time-lapse exponential decay of the cubic stiffness term (k_3) of a nonlinear spring as modeled by the Reconfigurable Test Setup. The black line details the Restoring Force Calculator computed restoring force value (IRFC) and the red dots detail the physically recorded restoring force value (RFC).

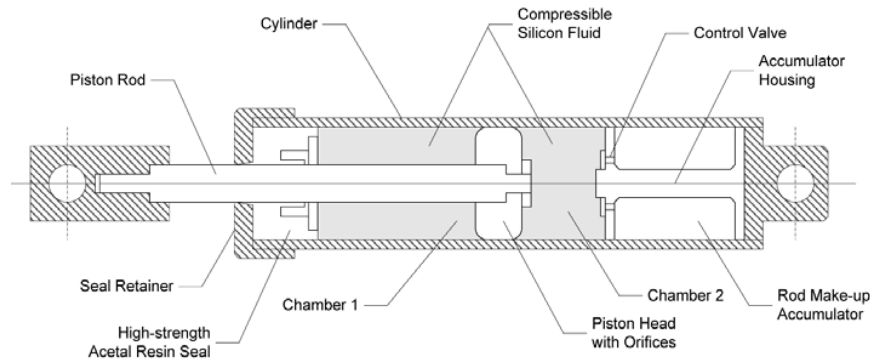


Figure 6.5: Components of a typical fluid orifice viscous damper (Soong and Dargush, 1997).

upon the configuration of the small orifices on its piston head. In order to dissipate an applied force, small orifices on the piston head require the fluid to pass through the orifices in tandem with the piston motion. Recently developed fluids have high strength, low viscosity, are stable over a broad temperature range, and are insensitive to impurities commonly introduced during manufacturing (Taylor, 1996).

Viscous dampers have a long life span, as they have been used for over 100 years in very demanding applications, notably in aerospace and military applications (Taylor, 1996). They can be installed on a new or retrofitted on an existing variety of structures, including (Yun et al., 2008):

- diagonal component of a truss.
- portion of a cable stay on a suspension bridge.
- portion of a tuned mass damper (for vibration reduction).
- portion of a base isolation system.

Because of their ability to mitigate forces, viscous dampers are becoming increasingly popular to incorporate into the design of large civil structures. Photographs of nonlinear viscous

dampers installed in a variety of in-field applications can be seen in Figure 6.6. Figure 6.6(a) is from the Pacific Bell North Area Operations Center. This building includes a total of 62 viscous fluid dampers each with a capacity of 130 kN. Together these devices will provide enough structural damping to withstand a catastrophic earthquake. The building is essential because it serves as the area's emergency facility (Soong and Dargush, 1997). Figures 6.6(b) and (c) are installed on the Richmond-San Rafael Bridge in San Francisco, California. On this project, 28 viscous fluid dampers each with capacities over 1000kN were installed on a bridge originally built in the 1950's. Their inclusion will allow the structure to withstand a "maximum credible earthquake" (Taylor Device, Inc.).

The use fluid viscous dampers also have a number of recent documented successes. In the aftermath of the March 2011 earthquake which heavily impacted Japan, Taylor Devices has reported that of the 22 buildings and bridges currently installed with dampers, each site has survived the earthquake without suffering any major structural damage (Clifford, 2011). Other notable uses of viscous dampers are found in (Spencer, 1999; Park and Koh, 2001; Wolfe et al., 2002; Agrawal et al., 2003; Li and Ou, 2008; Cheng et al., 2010).

A sizeable drawback of the use of viscous dampers is that its failure may result in a structural collapse. Because of the numerous dependencies upon a properly working device, *in-situ* viscous damper health evaluation is crucial (Borcherdt, 2005). Many current *in-situ* inspection practices involve a physical inspection. Although these tests are performed by an experienced professional, minimal knowledge can be gained regarding the performance capabilities by a visual inspection. The inspector will often only be able to determine that the structural connection is in good condition and that no viscous fluid leakage has occurred (Tasbihgoo, 2006). Therefore, either physical testing or on-site health monitoring of a damping system is vital to ensure the safety of the public.

For a large-scale viscous damper, physical testing is a very expensive process to remove



(a) Pacific Bell North Area Operations Center



(b) Side view of Richmond-San Rafael Bridge in San Francisco, CA



(c) Underneath view of Richmond-San Rafael Bridge in San Francisco, CA

Figure 6.6: Photographs of viscous dampers in various structural damping applications. (Photos courtesy of Taylor Devices, North Tonawanda, NY.)

the device from its field position and transport it to a testing laboratory. Additionally, few laboratories have the equipment or the size needed to properly test these large devices. In this section, it will be demonstrated how the dynamic signature of the large-scale viscous damper can be simulated by the compact reconfigurable test setup.

6.2.2 Simplified Mathematical Modeling

The restoring force of a nonlinear viscous damper can be modeled as (Wolfe et al., 2008):

$$f(t) = C \text{sgn}(\dot{u}) |\dot{u}|^n + p(u, \dot{u}, \ddot{u}, T) + \epsilon(t) \quad (6.2)$$

where $f(t)$ is the damping force, c is the damping coefficient, n is the exponent that defines the damping nonlinearity ($n = 1$ for linear; $n < 1$ for softening; and $n > 1$ for hardening), T is the internal temperature of the damper, and $\epsilon(t)$ is a random identification residual. The signum function extracts the sign of a number (-1 for $\dot{u} < 0$, 0 if $\dot{u} = 0$, and 1 for $\dot{u} > 0$). This equation is also applicable for design purposes (Hart and Wong, 2000; Minyamoto and Hanson, 2002). However because the behavior of a damper is a function of a number of parameters, a simpler method describing its motion for *in-situ* applications is desirable.

The dynamic properties of a viscous damper specified by the manufacturers must meet acceptable design requirements. Although numeral quality-assurance test procedures have been developed, the guidelines published by the Highway Innovative Technology Center (HITEC) remain the most popular in practice (HITEC, 1996, 1999b,a). The Reconfigurable Test Setup modeling application will focus upon a number of static, dynamic, and stability tests for various energy dissipation devices.

A viscous damper's damping characteristics follow a nonlinear constitutive law at relatively low frequency expressed as

$$f(t) = C \text{sgn}(\dot{u}) |\dot{u}|^n \quad (6.3)$$

and is referred to as the Simplified Design Method. Damper manufacturers use this equation to specify the energy dissipation capacity of the damper, by specifying the damping ratio, c , and its nonlinearity parameter, n , which defines the hysteresis loop shape (Lin and Chopra, 2002). To determine the device's frequency dependency, HITEC testing guidelines specify a series of monotonic sinusoidal tests at different frequencies and a constant displacement amplitude. The parameters of the model are identified by Equation 6.3 which is valid when the inertia ($m\ddot{u}$) and the stiffness (ku) terms are insignificant and the frequency of the excitation is low.

Should these assumptions be untrue, other possible modeling equations include:

$$f(t) = m\ddot{u} + C \text{sgn}(\dot{u}) |\dot{u}|^n \quad (6.4)$$

and

$$f(t) = m\ddot{u} + C \text{sgn}(\dot{u}) |\dot{u}|^n + ku \quad (6.5)$$

where m is the mass of the damper piston and k is the identified linear stiffness. The first equation compensates for numerical instabilities during analytical testing. These issues typically are not encountered in practice because the mass of the piston is negligible compared to the mass of the overall structure. The second equation takes into account the stiffness of the damper, as recent research has shown can significantly contribute to the force applied by the damper (Yun et al., 2008; Wolfe, 2002). Displacement can play a key role in the determining of a viscous damper's output force due to its internal design (Wolfe et al., 2008).

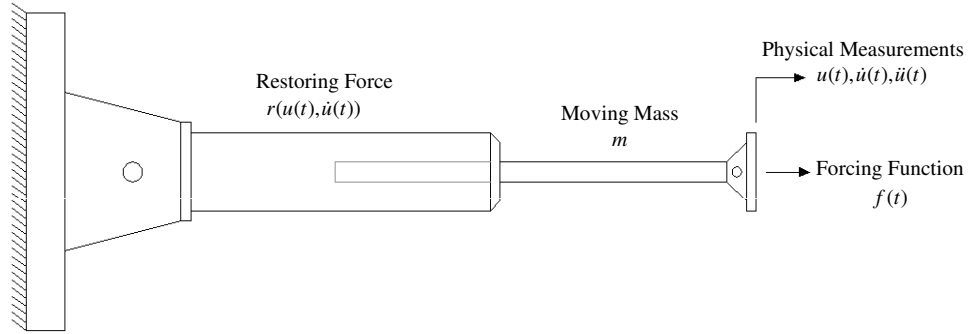


Figure 6.7: Simplified mathematical model of a nonlinear viscous damper.

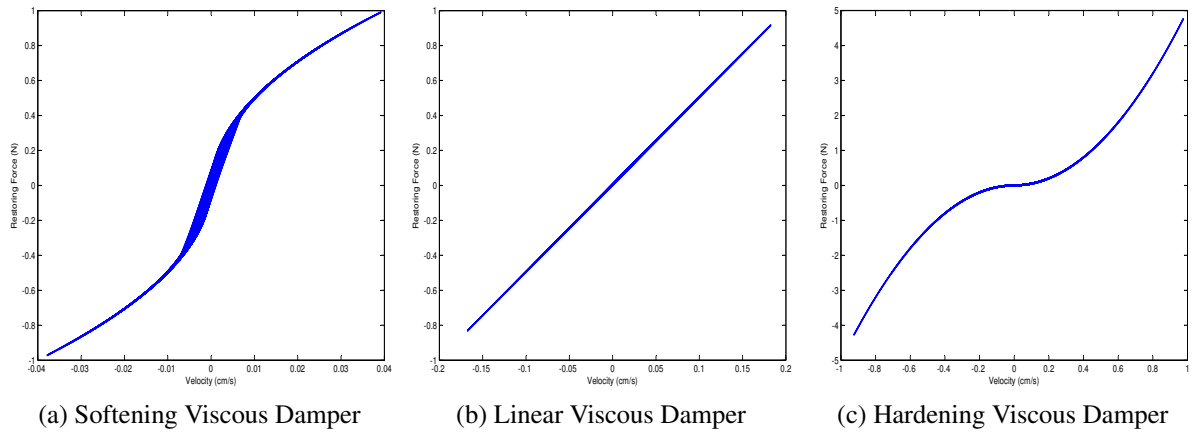


Figure 6.8: Velocity vs. restoring force phase plots for (a) softening, (b) linear, and (c) hardening nonlinear viscous dampers. A softening damper will have a n less than 1, a linear damper will have a n equal to 1, and a hardening damper will have a n greater than 1.

The industry standard, however, for the *design* and *modeling* of viscous dampers remains with Equation 6.3. Figure 6.7 details how the damper test assembly can be configured to function as a simplified mathematical model. As shown, a nonlinear viscous damper will display a nonlinear relationship between velocity and restoring force very similar to Figure 2.1 (Tasbihgoo et al., 2007). Figure 6.8 detail the shapes of: (a) a softening viscous damper; (b) a linear viscous damper; and (c) a hardening linear damper.

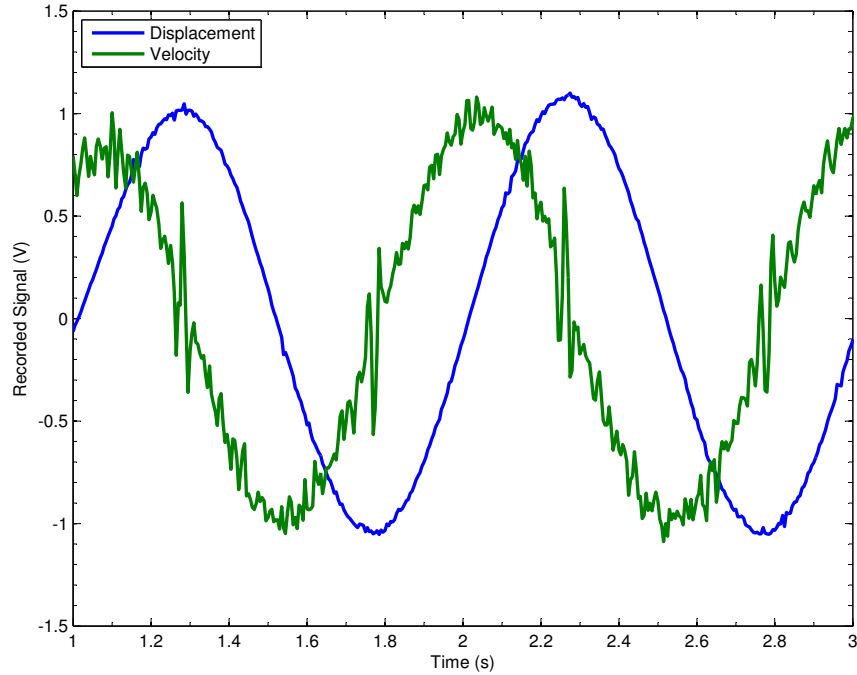


Figure 6.9: Recorded displacement and velocity measurements of a nonlinear damper undergoing monotonic sinusoidal excitation. When velocity nears zero, the interaction between the restoring force generator and the linear servo motor becomes uncertain. It is theorized that a “stronger” linear servo motor will limit the modeling instability.

6.2.3 Velocity Dependent Modeling using the Reconfigurable Test Setup

The physical modeling of a solely velocity-dependent dynamic model is somewhat different than a displacement-dependent model. The primary reason for the difference is because unlike displacement, velocity is a derived measurement value and is therefore much more susceptible to small changes in magnitude and sign. The faults of the current setup at modeling a nonlinear damper are best demonstrated in Figure 6.9, which displays recorded displacement and velocity over time. In this particular example, the damper is being excited by a monotonic sinusoidal excitation. When the linear servo motor reaches the peak of its path and velocity approaches zero, instability exists within the dynamic simulation. This causes uncertainty in the system until the input force begins moving at a higher magnitude velocity. This instability could be resolved by an increased stiffness term, but the equation of dynamic motion will be altered.

A possible remedy to the uncertainty of the modeling of nonlinear dampers at low velocities is the application of a broadband random force. As discussed in HITEC (1996), it is much more advantageous to excite a damper under a variety of frequencies. This is also beneficial in viscous damper modeling with the Reconfigurable Test Setup as the use of a broadband random excitation will result in rapid changes in velocity due to frequent, random changes in frequency.

In Figure 6.10, a variety of velocity-dependent nonlinear models physically simulated (RFC) by the Reconfigurable Test Setup are displayed. Because each model is solely dependent upon velocity, the velocity vs. restoring force phase plots detail the governing system characteristics. Each has been excited by a broadband random force ranging from 0.1 to 5 HZ. Similarly, a Bandpass Butterworth post-processing filter (ranging from 0.01 to 30 HZ) has been applied.

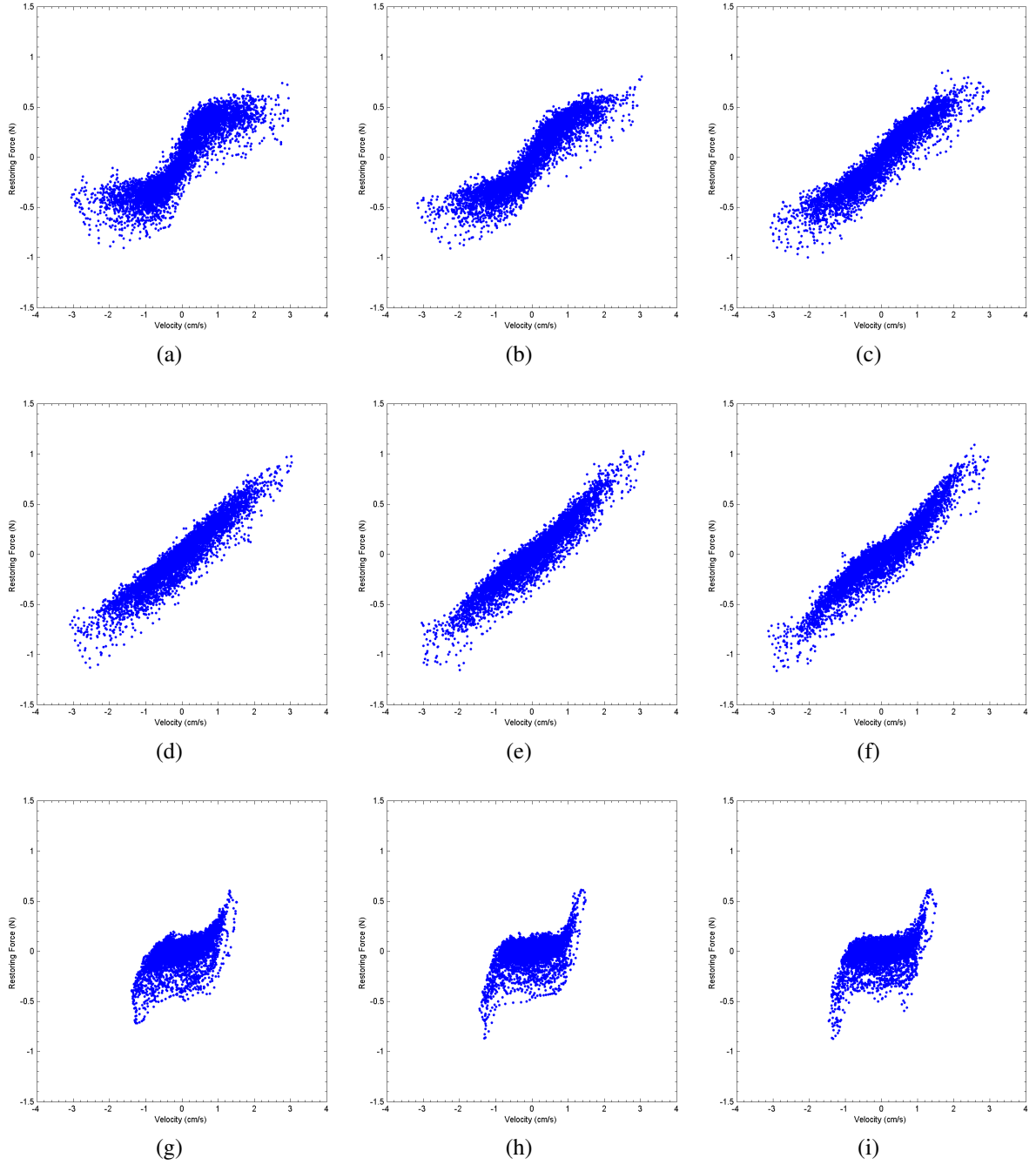


Figure 6.10: A number of nonlinear damping models physically simulated (RFC) by the Reconfigurable Test Setup system. Row 1 details three “softening” models ($n = 0.25, 0.50, \text{ and } 0.75$, respectively); Row 2 displays a linear damper (Figure 6.10d) and two increasingly “hardening” models ($n = 1.25$ and 1.50 respectively); and Row 3 plots three highly nonlinear damping models ($n = 3, 5, \text{ and } 6$ respectively).

7 SUMMARY AND CONCLUSIONS

7.1 Summary

The overall goal of this study was to develop and present a robust and versatile system that is able to replicate the dynamic properties of a variety of physical systems. The major components of the apparatus include a reprogrammable restoring force generator and corresponding restoring force calculator, a sophisticated data acquisition system with a number of direct-measurement sensors, and a linear servo motor capable of providing a variety of excitation types.

To explore the effects of uncertainty upon dynamic model creation and system identification, a number of dynamic models were synthetically created using software. Parametric and nonparametric system identifications were then performed on the data. System uncertainty, when present only on the input force vector, did not affect the identified coefficients, but error was present in the force recreation. It was demonstrated that measurement uncertainty had both undesirable effects upon the system identification and recreation of the force. A study was also presented to verify the change detection ability of orthogonal basis functions with a reduced order model.

Much effort was devoted to calibrating the Reconfigurable Test Setup. It was discovered that real-time smoothing with a weighted average improved the accuracy of the Restoring Force Calculator. Additionally, the procurement of a more “sturdy” linear servo motor would decrease the uncertainty in the electromagnet/linear servo motor interaction, thus improving repeatability and accuracy of the physical simulation. It was also demonstrated that the frequency of excitation had little effect upon the accuracy. Lastly it was established that the electromagnet has a nonlinear relationship between input voltage and output force. Considerable simulating

improvements can be achieved with an electromagnet with a linear output relationship.

Despite the number of improvements needed on the current configuration of the test setup, it was demonstrated that the Reconfigurable Test Setup is capable of physically simulating a variety of dynamic models. In this study, two possible uses were demonstrated: change detection and physical system deterioration. Because the control of these models are easily reprogrammable with software, the setup also has the ability serve as a cross-cutting tool in a variety of research purposes including: system identification, health monitoring, stochastic quantification, and model validation.

A discussion was presented regarding the current modeling techniques of velocity-dependent nonlinear dynamic models, specifically a nonlinear viscous dampers. It was demonstrated the test setup has the ability to physically model a range of dampers. However due to the nature of precisely controlling a model heavily dependent upon a derived measurement state, further calibration of the test setup is required.

The work presented in this study demonstrate a number of potential uses of the Reconfigurable Test Setup as a viable tool for the simulation and identification of problems involving single degree of freedom dynamic phenomena. The Reconfigurable Test Setup shows great potential as a research tool for those working in the applied mechanics, educational, or research fields.

7.2 Challenges Presented in the Physical Simulation of Restoring Properties with Software

The creation of a device capable of reproducing the physical restoring properties of a dynamic model with software is a very challenging endeavor. As this project is an introductory study, a number of challenges have been met. Although a number of solutions methods to these difficulties have been proposed, they are by no means perfected. With further analysis into these

issues, a more reliable test-setup will result.

The method does however, show great promise in its abilities and real-world functionalities. But with the ideology's introduction into in-field applications, comes the added difficulty of performing experimentation outside the confines of a laboratory. The following is a list of difficulties that must be overcome for a reliable real-time simulation device:

1. Input measurements must be free of measurement noise.

- Physical simulation of restoring properties is highly dependent upon directly recorded measurements. The presence of measurement noise leads to great error introduction into output results. Further complicating the matter is the fact that velocity and displacement measurements are utilized in real time to calculate the value of the restoring force.
- Because a degree of noise will be present in all physically recorded measurements, the researcher must take steps to ensure contamination is kept to a minimum. Wires must be shielded and grounded. Real-time filtering is an option that shows promise but its implementation will not reduce computation time. In this study real-time weighted averaging was explored and it was determined for a displacement-dependent nonlinearity, a four-term weighted average proved most accurate.

2. Synchronization between timing clocks of Restoring Force Calculator and data acquisition control must be achieved.

- Recorded displacement and velocity measurements are sent directly to both devices. A lag between the two will cause a discrepancy between the calculated output force (which is based upon displacement and velocity readings) and recorded displacement and velocity readings. The lag will create hysteretic results.

- Synchronization is increasingly crucial as the reconfigurable test setup is used for more complex analysis types. For instance in a deterioration study, the current coefficient needs to be recorded along with measured restoring force so the two can be quantitatively compared. Desynchronization will lead to additional error. The achievement of synchronized clocks is crucial for reliable damage simulation based upon software. A possible solution to the issue of synchronization is the consolidation of the data acquisition, excitation, and Restoring Force Calculator codes into a single CPU.

3. Input force must not be affected by restoring force.

- For repeatability purposes, it is critical that the input force is not affected by the restoring force output. Failure to do so will lead to unwanted hysteresis effects.
- Through experience in working with the apparatus, a visual inspection of an operating test will show no obvious signs of its motion being affected. However small variations are easily noticed in displacement/force interactions shown by phase plots - particularly when the forcing motion changes frequencies and amplitudes of excitation. Because of the nature of the dynamic models, the input force/restoring force interaction is increasingly critical to limit with velocity dependent dynamic models.

4. Algorithm update rate must remain as fast as possible.

- The updating rates of the reconfigurable setup's components must be maximized so that real-time updating of the dynamic model is possible. However, an increasingly high updating rate also introduces more uncertainty into the analysis. Therefore, a balance between modeling accuracy and updating rate must be reached.

5. Restoring force generator must be specifically designed for dynamic modeling.

- The restoring force generator (the controller and electromagnet) utilized in this study was originally designed to be operated in a manufacturing environment. Because this was its intended use, high output force precision and controller updating rate were not top criteria in its design considerations. Thus the physical modeling accuracy of the current test setup is limited by the controller's performance. In future studies, a custom device with output accuracy and updating rate as chief design features is recommended for usage.
- Similarly, the device's output force does not follow a linear calibration, which is essential for accurate physical simulation.

6. Superfluous vibrations must be minimized.

- A number of measures were taken keep vibrations to a minimum, including: performing the experimentation on an industrial device whose purpose is to limit vibration (an optical table), shielding connection wires, and lowpass filtering the analog signal sent to the input. Despite these efforts high-frequency vibrations were still present in the test setup, primarily due to the linear servo motor. For enhanced modeling accuracy, these interferences must be diminished.

7.3 Future Studies Planned using the Reconfigurable Test Setup

A number of future studies with the Reconfigurable Test Setup are planned for the development of a wide range of experimental nonlinear dynamic studies. As an immediate need, the device will require further calibration to increase accuracy and reliability of the force output. The current configuration must also be improved, as noted by the shortcomings discussed in Section 7.2.

Although deterioration of system parameters was discussed in this study, a possible application of the device is the ability to have the system parameters of the restoring force as random

variables, so that the uncertainty effects upon the dynamic response can be studied experimentally.

The deterioration and random variable methodologies can also be applied to a physical structure, as the methodology introduced by the Reconfigurable Test Setup can be taken into the field. In this way, the propagation effects of the uncertainty can be determined through the coupled structure. Since the deterioration rate or uncertainty bounds are either known or able to be determined, the effects upon the attached structure can also be experimentally quantified.

7.3.1 Sample Applications

The Reconfigurable Test Setup has the potential to be a valuable tool for experimental studies in a wide range of engineering fields. In this section, three real-world applications using the Reconfigurable Test Setup are described.

Deterioration of a Viscous Damper installed on a Bridge

Civil Engineering Application

As described in Section 6.2.1, viscous dampers are becoming increasingly popular to incorporate into the design of large civil structures due to their ability to mitigate dynamic forces. For this reason, the study of nonlinear viscous dampers and other devices of this type is imperative. In the past, much effort has been spent to devise reliable structural health monitoring approaches to detect changes in the properties of these devices.

However, significant efforts must also be placed upon analyzing the additional forces incurred by surrounding structural members as a result of a damper's deterioration. For experimental quantification and analysis, the Reconfigurable Test Setup can be installed upon the actual structure to perform a deterioration study. Figure 7.1 details the locations of viscous

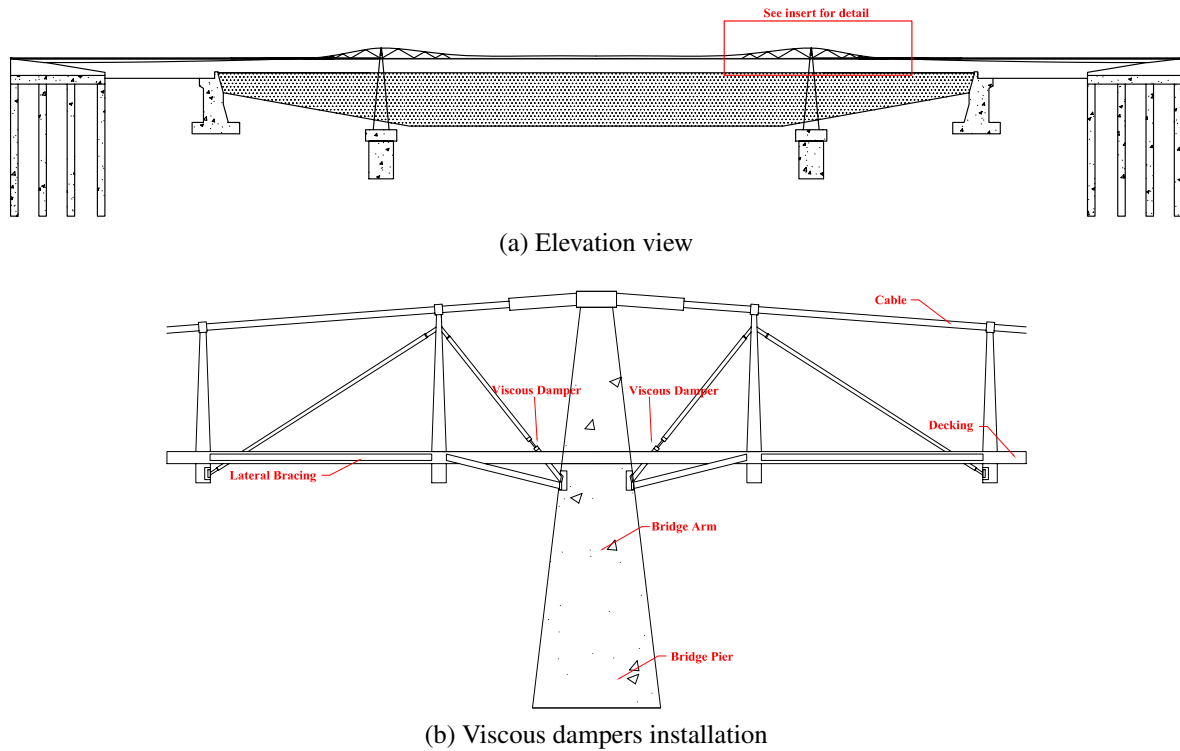


Figure 7.1: Installation of viscous dampers upon a long-span bridge. Figures drawn from plans originally designed by Arup (2011).

dampers installed upon a generic, long-span bridge. Using the design criteria from the installed viscous dampers, the Reconfigurable Test Setup can physically simulate its attributes and deteriorate in a controlled manner. In this way, the stochastic effects of complex nonlinear dynamic components that propagate through adjacent components can be experimentally quantified.

With the knowledge gained from this type of study, “critical elements” can be identified for design modification. Additionally, the bridge maintenance plan may be able to be modified, allowing for the maintenance budgets to be more efficient.

Design of an Automobile Suspension

Mechanical Engineering Application

The Reconfigurable Test Setup is able to physically simulate a wide range of nonlinear phe-

nomena. Thus, it can be used to aide and verify engineering *designs*. An example of this application can be considered for the design of an automotive shock absorber, shown in a simplified model in Figure 7.2.

One engineering design application example would be if an automobile designer wanted to determine what damper properties would provide the smoothest driving experience when installed in parallel with an existing spring. In a traditional study, the engineer in charge of the project would likely gather a number of available dampers and attach the spring to each one. Then the two devices would be subjected to a load and the results would be analyzed. The process would repeat itself numerous times and the “best fit” would be chosen. Undoubtedly the procedure will yield a result, but the process would be very time consuming and the chosen solution would come from the physical devices actually analyzed.

On the other hand, the pre-existing spring could attached in parallel to the Reconfigurable Test Setup and the excitation of a rough-road test could be applied to the system. The researcher would have the ability to easily vary the damping characteristics of the apparatus, determine which work best, and select a physical damper with the similar characteristics. In this way, a wide range of system characteristics could be evaluated in a time efficient manner with a single test setup.

Recoil Study of a Mounted Turret

Military Application

Many military-use devices, such as tanks, turreted artillery, and missile launching components are subject to severe impulse loads when delivering their payload. To ensure proper functioning of the device, these forces must be dissipated effectively. According to Chen and Wereley (2004), active damper fluids (such as magnetorheological or electrorheological) are preferred over passive alternatives (such as viscous fluids) due to superior performance in dissi-

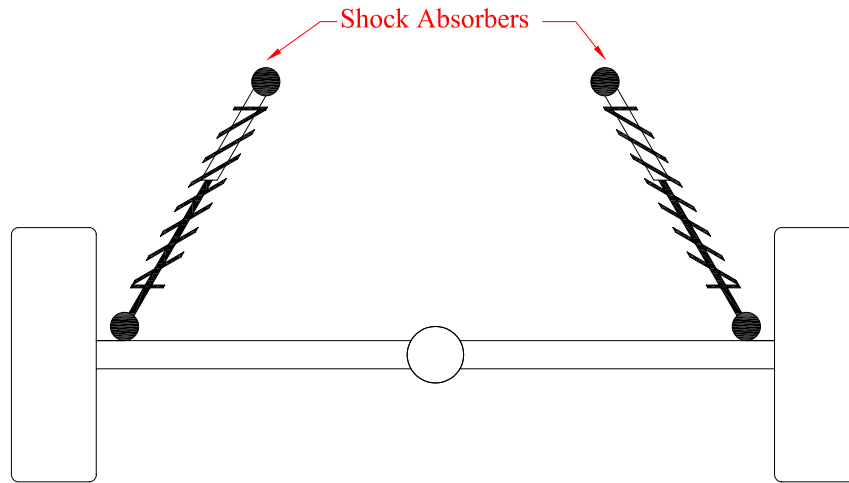


Figure 7.2: Elevation view showing the location of shock absorbers installed on a vehicle chassis.

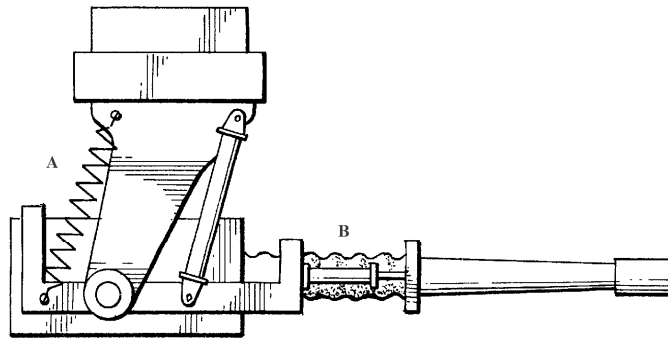


Figure 7.3: Model of a mounted turret (Chen and Wereley, 2004).

pating large impulse loads. Figure 7.3 details a model of a typical mounted turret where energy dissipation is provided by the spring (labeled as “A”) and a passive damper (labeled as “B”) (Chen and Wereley, 2004).

General military convention suggests with decreased recoil, increased target accuracy and firing rate can be achieved. In the weapon design and prototyping phase, the use of the Reconfigurable Test Setup would allow a military researcher to experimentally couple a range of active damping system characteristics with a certain caliber weapon. As the two are experimentally combined and evaluated, a more efficient design can be explored.

8 APPENDIX

The Reconfigurable Test Setup approach introduced in this research project will be the basis of conference paper to be presented at the 6th International Conference on Bridge Maintenance, Safety and Management (IAMBAS 2012). The conference will be held from July 8-12, 2012, in Villa Erba, Lake Como, Italy. Included is the accepted abstract for this paper, entitled “Non-linear Dynamic Modeling with a Reconfigurable Test Setup.”

Also included are two conference papers that have been coauthored during my graduate research. They will be introduced at the International Symposium on Innovation & Sustainability of Structures in Civil Engineering (ISISS 2011). The conference will be held from October 28-30, 2011 at Xiamen University, Xiamen, China. Included are the full versions of the conference papers, entitled “A Non-Parametric Identification Methodology for Large-Scale Nonlinear Dynamic Systems with Uncertain Measurements” and “System Identification and Classification of Stochastic Change Detection of Uncertain Nonlinear Systems with Reduced-Order Models,” respectively.

Nonlinear Dynamic Modeling with a Reconfigurable Test Setup

Aaron Rank¹, Hae-Bum Yun¹, and Sami Masri²

¹ Department of Civil, Environmental and Construction Engineering, University of Central Florida

² Viterbi School of Engineering, University of Southern California

Experimental nonlinear dynamics is an important area of study in the field of structural engineering and structural health monitoring. A great challenge is the inability of a physical device to have complete freedom to simulate a wide range of nonlinearities. As a result, many researchers have longed for a versatile, but accurate, test apparatus capable of validating nonlinear modeling, system identification, and stochastic analysis studies.

The objective of our study is to develop a reconfigurable test setup as a tool to be used in a wide range of nonlinear dynamic studies. The main components include a moving mass whose restoring force can accurately be controlled and reprogrammed (with software) based upon directly measured displacement and velocity readings at each time step. The device offers control over nonlinear characteristics (coefficients) and the equation of dynamic motion. The advantage of having such an experimental setup is the ability to simulate various types of nonlinearities with the same test setup. As a result, data collected can be used to help validate dynamic models or system identification methods.

To display a practical application of the device, a case study is presented to physically simulate an orifice viscous damper, commonly used in vibration mitigation in bridges and buildings. For a large-scale viscous damper, physical testing is needed to ensure proper working functionality; however it is a very expensive process and few laboratories have the equipment needed to properly test these large devices. Conversely with the use of the compact reconfigurable test setup, the dynamic signature of the large-scale viscous damper can be simulated with pre-collected data.

The apparatus is a useful tool for researchers and designers, allowing for physical data collection for system identification or uncertainty quantification purposes.

A NON-PARAMETRIC IDENTIFICATION METHODOLOGY FOR LARGE-SCALE NONLINEAR DYNAMIC SYSTEMS WITH UNCERTAIN MEASUREMENTS

Hae-Bum Yun¹, Aaron Rank¹, Sami F. Masri², and Gianmario Benzoni³

¹ Department of Civil, Environmental and Construction Engineering, University of Central Florida, Orlando, Florida 32816, USA

² Department of Civil and Environmental Engineering, University of Southern California, Los Angeles, CA 90033, USA

³ Department of Structural Engineering, University of California, San Diego, CA 92093, USA

Abstract: In the field of structural dynamics, the data recorded by measurement sensors are often polluted by measurement uncertainty, commonly referred to as “noise.” The effect of the measurement uncertainty is frequently oversimplified to be simple additive Gaussian noise in many studies. In addition, for civil structures, such as large-scale nonlinear viscous dampers, stochastic quantification, which requires the collection of a large number of data sets, is often infeasible due to high costs associated with repeated physical testing even in laboratories equipped with large loading frames. A methodology is proposed for change detection of a dynamic model in the presence of uncertain measurements with limited physical data. It was demonstrated that reliable change detection is possible with the Restoring Force Method, a non-parametric system identification technique, because: (1) small changes of a nonlinear system are detectable; (2) physical interpretations are possible; and (3) the uncertainty of detected changes are quantifiable without *a priori* system characteristic knowledge.

Keywords: large-scale viscous damper, change detection, non-parametric identification, data resampling, Restoring Force Method, Bootstrap Method

1. INTRODUCTION

A number of types of uncertainty may exist in the field of structural dynamics that have an adverse effect upon system identification. These uncertainties can generally be classified into two broad categories: *measurement uncertainty* and *system parameter uncertainty*. This study pertains to measurement uncertainty, commonly referred to as “noise.” In real-world applications, measurements are taken by sensors which are often polluted by noise from a variety of sources. In many cases of *in-situ* monitoring, only a limited set of data (e.g., displacement or acceleration) is measured, depending on the measurement feasibility, and other necessary response states are numerically obtained through digital signal processing techniques. In such cases, the effects of measurement noise are not simply additive, and propagate throughout the response states.

Due to recent innovations in web-based communication and remote sensing, the practicality of a real-time remote monitoring system is feasible for civil infrastructure projects. For robustness, the designed change detection methodology should be able to deal with complicated noise effects. In addition, for full-scale (nonlinear) viscous dampers, stochastic quantification requires a large data set and often is infeasible due to high costs associated with repeated physical testing.

The objective of this study is the proposal of a methodology for change detection of a dynamic model in the presences of limited physical data. Overall, the proposed methodology will provide contributions to the health monitoring field in the following three ways:

- Enabling the interpretation of physical significance of detected changes, one can quantify the significance of the changes at the full-structure level as well as at the component level. This attribute

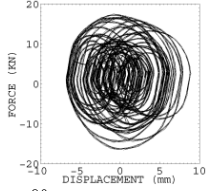
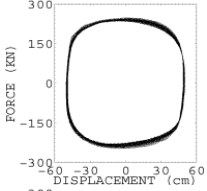
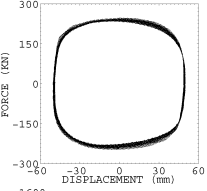
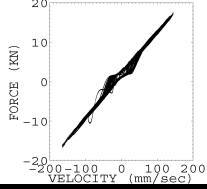
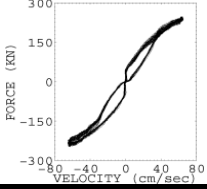
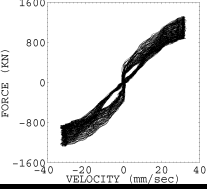
remains even when the dampers' evolving properties change into different classes of nonlinearity, due to various types of deterioration.

- With more reliable condition assessment methodologies, one can minimize unnecessary removal of undamaged dampers. Damper removal from civil structures is time-consuming and expensive due to their large physical size.
- Since the methodology proposed in this study employs non-parametric and data-driven system data processing techniques, the same approach is applicable to other types of nonlinear components, such as different types of energy dissipating devices, base isolators, and nonlinear joints.

2. Experimental Study

Three different large-scale nonlinear viscous dampers were tested at two different test facilities: the 66.7 kN viscous damper was tested at the University of California, Berkeley (designated as Damper A), and the 2001.6 kN and 2891.3 kN viscous dampers were tested at the University of California, San Diego (designated as Damper B and C, respectively). The testing protocols of each are outlined in Table 1.

Table 1. Nonlinear viscous dampers used in this study

Parameters	Damper A	Damper B	Damper C
Recorded Measurements	Acceleration, Force	Displacement, Force	Displacement, Force
Damping Characteristics	Linear	Nonlinear	Nonlinear
Time-Invariancy	Time-invariant	Time-invariant	Time-varying
Stiffness Response			
Damping Response			

3. Non-Parametric System Identification

A non-parametric SI approach, the Restoring Force Method (RFM), was chosen to be utilized in this study due to its ability to characterize a wide range of nonlinearities (Masri and Caughey, 1979). Using RFM, the restoring force of a single-degree-of-freedom nonlinear dynamic system can be modeled as

$$r(x, \dot{x}) = \sum_{i=0}^P \sum_{j=0}^Q \bar{C}_{ij} \bar{T}_i(\bar{x}) \bar{T}_j(\bar{\dot{x}}) \quad (1)$$

where $r(x, \dot{x})$ is the restoring force of the nonlinear dynamic system, \bar{C}_{ij} is the normalized Chebyshev coefficient, T_i is the i^{th} order Chebyshev polynomial, P and Q are the highest input modeling orders of the Chebyshev polynomial of the normalized displacement (\bar{x}) and velocity ($\bar{\dot{x}}$), respectively, within the range of $[-1, 1]$. Once the normalized Chebyshev coefficients are identified, they can be converted into the equivalent power series coefficients:

$$r(x, \dot{x}) = \sum_{i=0}^P \sum_{j=0}^Q \bar{C}_{ij} \bar{T}_i(\bar{x}) \bar{T}_j(\bar{\dot{x}}) = \sum_{i=0}^P \sum_{j=0}^Q \bar{a}_{ij} \bar{x}^i \bar{\dot{x}}^j = \sum_{i=0}^P \sum_{j=0}^Q a_{ij} x^i \dot{x}^j \quad (2)$$

Thus, three kinds of equivalent coefficients are available using the RFM: normalized Chebyshev coefficients (\bar{C}_{ij}), normalized power series coefficients (\bar{a}_{ij}) and de-normalized power series coefficients (a_{ij}). The basis

functions for \bar{C}_{ij} are orthogonal, while the basis functions for \bar{a}_{ij} and a_{ij} are non-orthogonal. The orthogonality of the basis functions significantly influences the stochastic properties of the identified coefficients, and as well as the performances of the system change detection capability (Yun and Masri, 2008).

4. Statistical Change Detection

4.1. Identification of Viscous Dampers

The classification of a nonlinear, time-varying system (Damper C) requires partitioning of the measured response. As shown in Fig. 1, the time history was broken into 8 segments (where 10 cycles of response were recorded in each). Deterministic studies were performed upon each of the dampers and it was demonstrated that RFM was applicable to each and physical interpretations could be made without *a priori* knowledge. (Yun *et. al*, 2009).

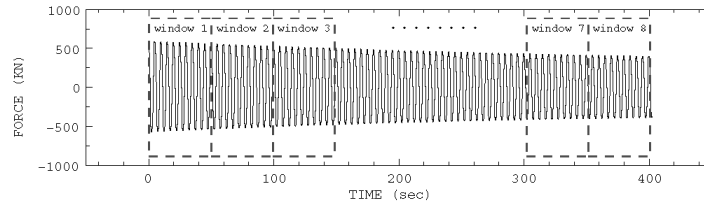


Fig. 1. Partitioning of the time history of the measured force of Damper C for system identification.

4.2. Uncertainty estimation of damper identification

A Monte Carlo simulation was performed to generate 3,000 unique data sets where 5% additive zero-mean Gaussian noise was introduced in terms of the root-mean-square (RMS) of the recorded measurement state. Since only acceleration or displacement was recorded during the tests, the velocity was numerically obtained to estimate the restoring force of the viscous damper. Consequently, the noise was propagated throughout the numerically obtained velocity – resulting in non-additive-Gaussian-noise. Additive and non-additive Gaussian noise is compared in Fig. 2. After the synthetic introduction of noise, system identifications of each damper were performed with RFM. A sample system identification for Damper C is shown in Fig. 3.

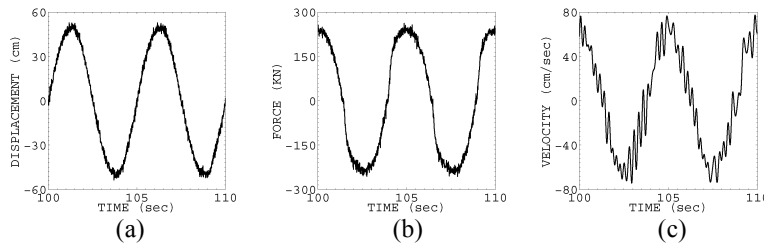


Fig. 2. Noisy response time histories. (a) and (b) detail measured displacement and force polluted with 5% zero-mean additive Gaussian random noise. (c) The velocity is obtained through numerical differentiation of the polluted displacement, detailing the noise effects are much more complicated than simple additive noise.

Fig. 4. shows the statistical correlation between identified coefficients. Although no correlation is seen between first order damping (\bar{a}_{01}) and linear stiffness (\bar{a}_{10}), a strong bias is seen between the linear (\bar{a}_{01}) and cubic damping (\bar{a}_{03}). Examination of Figs. 4(c) and (d) illustrate that no significant statistical correlations are observed between the identified normalized Chebyshev coefficients. Thus, the normalized Chebyshev coefficients of the RFM (\bar{C}_{ij}) prove to be a valid change indicator because statistical independence is preserved due to its orthonormal basis function (Yun *et. al*, 2009).

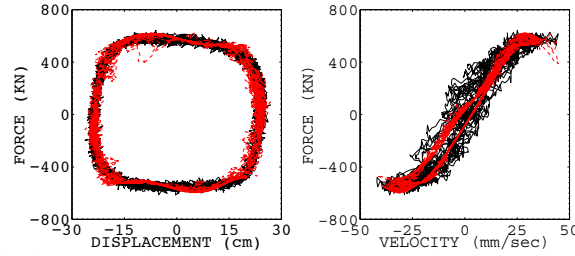


Fig. 3. A sample identification result for the noisy measurement data using the Restoring Force Method.

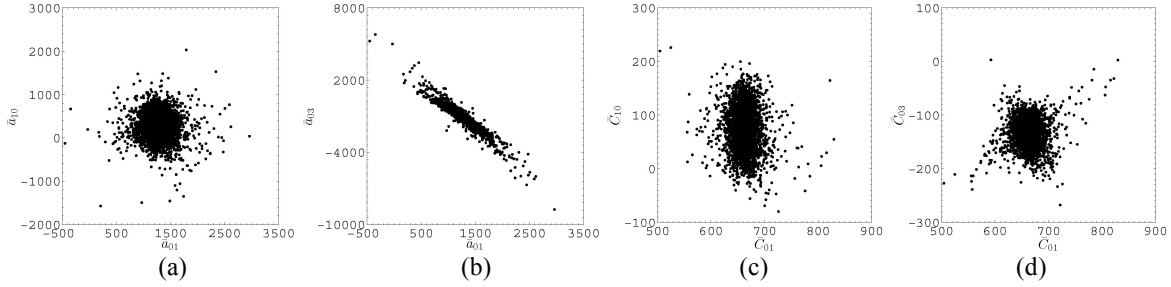


Fig. 4. Sample scatter plots of the normalized power series coefficients (\bar{a}_{ij}) and normalized Chebyshev coefficients (\bar{C}_{ij}) of the noisy response of a nonlinear, time-variant damper.

The distribution of the identified, normalized Chebyshev coefficients for Damper C were obtained. The distribution of the most dominant coefficient, \bar{C}_{01} , is shown in Fig. 5. As the measured response decreases with time, so does the mean of the identified coefficients. The standard deviation, however, remains relatively constant throughout the. In an in-field monitoring application, by assembling the distribution of the identified coefficients:

- One can accurately check if a genuine system change has occurred through comparison of the mean of the identified coefficients;
- One can interpret physical meaning of detected system change. In this particular example, it is shown that the actual changes are due to the degradation of damping rather than stiffness without physical knowledge of the degrading damper; and
- The uncertainty of system change detection is quantifiable through comparison of the standard deviation. The orthogonality of the Chebyshev polynomials allows avoiding computationally challenging *multiple integral* including the coefficients of all series expansion terms. Instead, *single integral* for each coefficient term can be performed for statistical testing.

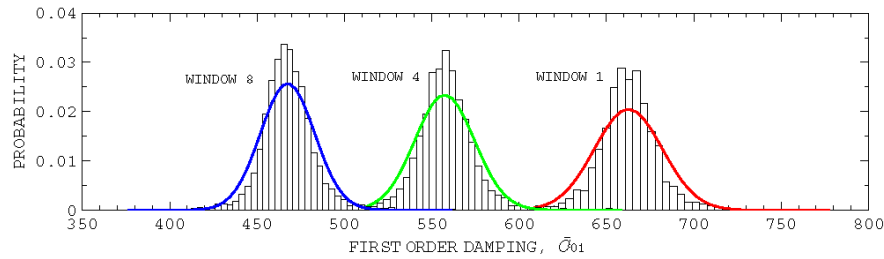


Fig. 5. Histogram and probability density functions of \bar{C}_{01} for different time windows.

5. Data Recycling

5.1. The Bootstrap Method

The uncertainty quantification presented in Section 4 required a very large data set. However, collecting sufficient data sets of large-scale viscous dampers for reliable statistical estimation is very difficult and expensive. The Bootstrap method is a statistical data recycling technique for the uncertainty estimation of identification parameters. This method is commonly used where the estimation of parameter uncertainty is

needed, but an insufficient amount of data is available for a statistically reliable uncertainty quantification. Excellent introductory literature on the Bootstrap method can be found in Davison and Hinkley (1997).

5.2. Resampling of Data Process

Single data sets of Dampers A, B, and C were recycled with the Bootstrap method using the following procedures. However, different procedures are required depending upon whether force and displacement (Damper A) or force and acceleration (Dampers B and C) were measured. The procedures are summarized in Fig. 6.

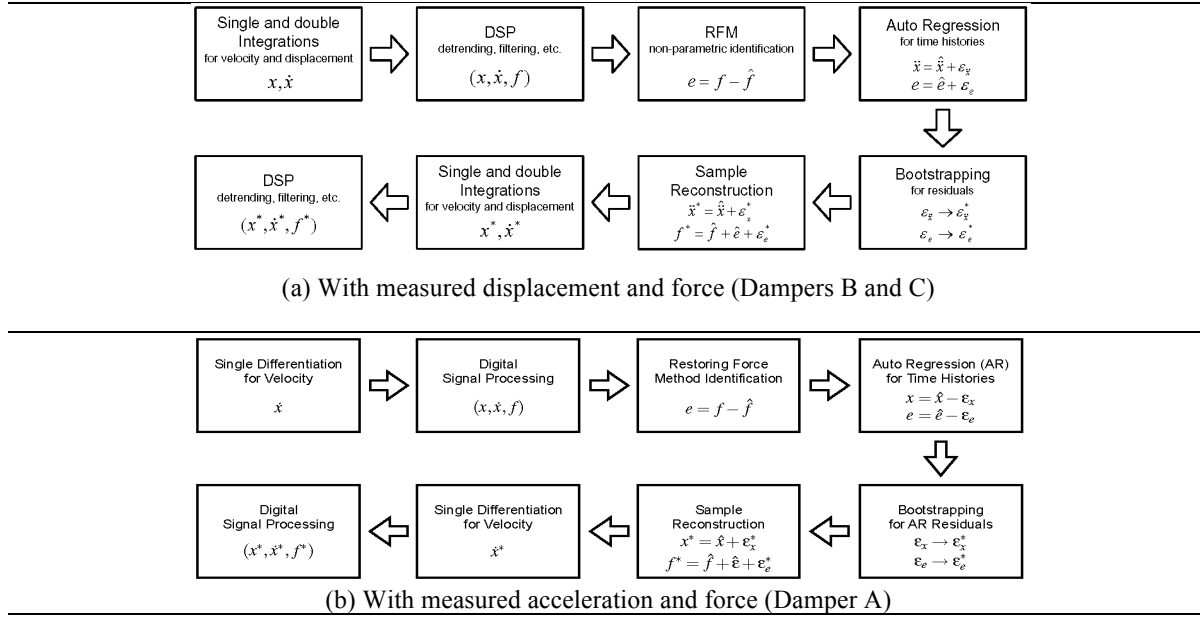


Fig. 6. Bootstrap resampling procedures with measured (a) displacement and force and (b) acceleration and force

5.3. Comparison of Recycled and Physically Recorded Data

A sample comparison between the original and Bootstrap-resampled data is shown in Table 2. For displacement and force initial measurements, the recycled data show slightly larger dispersion than the original data. However, as shown in Table 3, the error estimates with the Bootstrap method are larger than those with physical tests – meaning the Bootstrap method yields more conservative results.

For acceleration and force initial measurements, the range of the Bootstrap-resampled velocity is nearly identical to the physically recorded velocity in the velocity-force plot. However, the resampled displacement is approximately twice that of the physically recorded displacement, giving strong indications of a statistical biasness as the secondary integration is performed. It is therefore recommended the Bootstrap method only be used should displacement and force be the physically recorded measurements.

6. Conclusion

The methodology discussed in this paper is applicable to various nonlinear systems with uncertainty because no *a priori* knowledge is required. The normalized Chebyshev coefficients (of the RFM) can be used as an indicator to detect and quantify the uncertainty bounds of system changes. Physical interpretations of the detected changes are also possible. Bootstrapping data was also explored with noisy measurements and it was found that system identification could be estimated reasonably accurately, provided displacement and force are measured.

Table 2. A comparison of the original and Bootstrap-resampled data. The upper half of the table displays displacement-force plots, while the lower half shows the velocity-force plots.

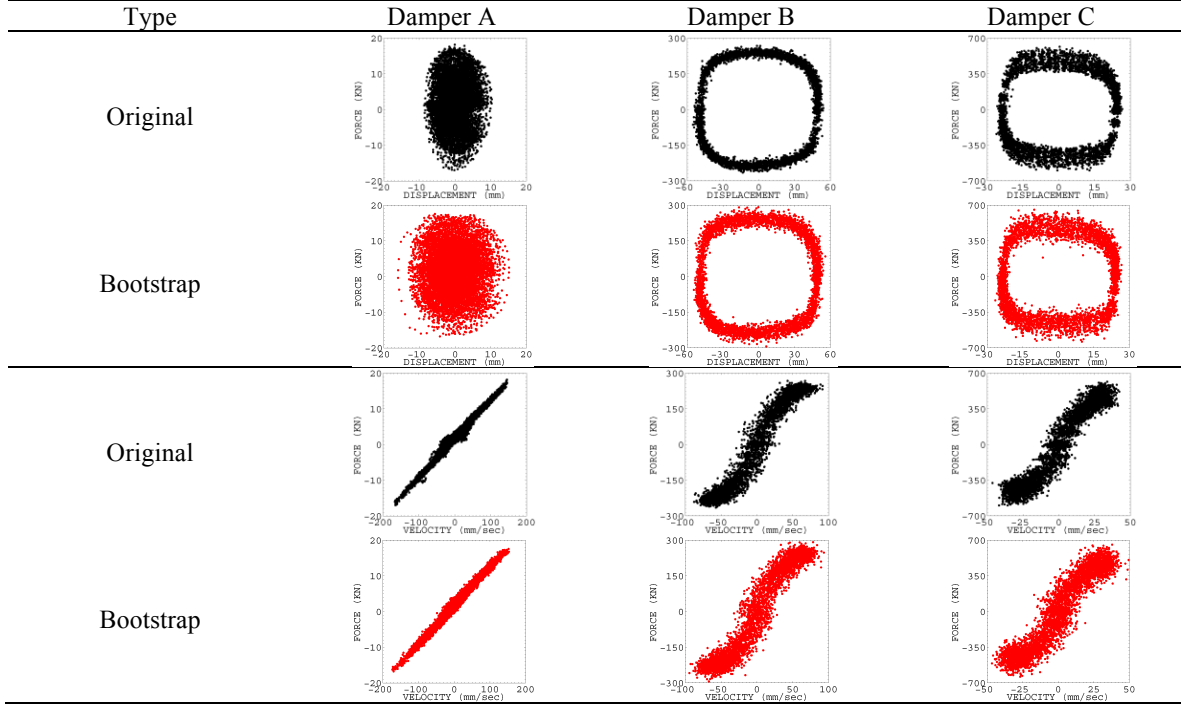


Table 3. Bootstrap estimations of errors for the coefficients identified using the Restoring Force Method

Type	Damper A			Damper B			Damper C		
	Physical	Bootstrap	Ratio	Multiple	Bootstrap	Ratio	Physical	Bootstrap	Ratio
\bar{C}_{10}	0.19	0.32	1.68	14.26	17.35	1.22	32.17	42.14	1.31
\bar{C}_{01}	0.16	0.31	1.94	8.60	12.22	1.42	17.17	26.21	1.53
\bar{C}_{30}	0.14	0.32	2.29	14.09	18.63	1.32	28.40	37.81	1.33
\bar{C}_{03}	0.10	0.20	2.00	9.14	12.49	1.37	20.71	27.47	1.33
\bar{a}_{10}	0.69	1.44	2.09	115.28	149.10	1.29	245.46	311.77	1.27
\bar{a}_{01}	0.74	1.64	2.22	86.03	104.55	1.22	198.68	235.09	1.18
\bar{a}_{30}	2.32	4.76	2.05	360.35	474.97	1.32	786.05	983.70	1.25
\bar{a}_{03}	2.26	5.67	2.48	322.88	395.84	1.23	669.23	823.17	1.23

REFERENCES

- Davison, A. C., Hinkley, D.V. *Bootstrap Methods and Their Application*. Cambridge University Press, New York, 1997.
- Masri, S.F, Caughey, T.K. (1979) A nonparametric identification technique for nonlinear dynamic problems. *Journal of Applied Mechanics Transactions on ASME* 46:2, 433-447.
- Yun, H.-B. and Masri, S. F. (2008). Stochastic change detection in uncertain nonlinear systems using reduced-order models: system identification. *Smart Materials and Structures*, 17:1, 1-13.
- Yun, H.-B., Masri, S. F., Wolfe, R. W., and Benzoni, G. (2009). "Data-driven methodologies for change detection in large-scale nonlinear dampers with noisy measurements." *Journal of Sound and Vibration*, 322(1-2), 336–357.

SYSTEM IDENTIFICATION AND CLASSIFICATION OF STOCHASTIC CHANGE DETECTION OF UNCERTAIN NONLINEAR SYSTEMS WITH REDUCED-ORDER MODELS

Aaron Rank¹, Hae-Bum Yun¹, and Sami F. Masri²

¹ Department of Civil, Environmental and Construction Engineering, University of Central Florida,
Orlando, Florida 32816, USA

² Department of Civil and Environmental Engineering, University of Southern California, Los Angeles,
CA 90033, USA

Abstract A reliable structural health monitoring (SHM) methodology is proposed to detect relatively small changes in uncertain, time-varying, nonlinear systems. Using a nonlinear magneto-rheological (MR) damper, effective system changes and uncertainties were precisely controlled over the course of 4000 physical tests. The tested MR damper was identified with the Restoring Force Method (RFM), a non-parametric system identification method involving two-dimensional orthogonal polynomials. Classification results shows that the identified coefficients with orthogonal basis functions can be used as reliable indicators for detecting small, genuine system changes with reduced-order models. An optimal design procedure is also proposed and for the classification of detected system changes. The use of the MR damper to create physical change detection data, while suitable in this study, does not have complete freedom to simulate a wide range of nonlinearities. To allow for the physical modeling of a wide range of nonlinear models, the authors also introduce an experimental setup whose restoring force can accurately be controlled and reprogrammed (with software) based upon directly measured displacement and velocity readings at each time step.

Keywords: magneto-rheological damper, Restoring Force Method, Support Vector Machines, change detection, non-parametric identification, system uncertainty

1. Introduction

The structural health monitoring (SHM) for a complex physical system presents a number of challenges including: the structure's nonlinear dynamic characteristics, system parameter and measurement uncertainties, and the need to reliably detect small changes in system characteristics. Moreover, in many field applications, the physical complexity of timely deteriorating dynamic systems is unknown, so that mathematical models with reduced-order complexity are commonly used.

The significance of modeling error can be classified according to the relationship of the system complexity, $O(\mathbf{p})$, and the model complexity, $O(\mathbf{q})$. If the true system parameters, \mathbf{p} , are uncertain, the relationship between $O(\mathbf{p})$ and $O(\mathbf{q})$ can be represented in one of the following states:

- i. $O(\mathbf{p}) > O(\mathbf{q})$: the system complexity is greater than model complexity (underfitting);
- ii. $O(\mathbf{p}) = O(\mathbf{q})$: the system complexity is equal to than model complexity (perfect fitting);
- iii. $O(\mathbf{p}) < O(\mathbf{q})$: the model complexity is greater than system complexity (overfitting).

In practice because \mathbf{p} is often unknown, system identification is rarely perfect fitting. Mita and Hagiwara (2003) demonstrated when the system identification is either underfitting or overfitting, the identified \mathbf{q} is generally *statistically biased* rendering change detection inaccurate.

To develop a reliable structural health monitoring methodology applicable for in-field applications, these obstacles must be overcome. The method must: (1) be versatile enough to deal with timely deteriorating

systems, whose physical characteristics are unknown after deterioration; (2) have the ability to detect system changes using reduced-order models; (3) allow for physical interpretations of the changes; and (4) have the capability of uncertainty quantification where depending on the confidence level of damage detection, appropriate action can be taken.

With the above discussion in mind, the objective of this study is to develop a reliable change detection methodology for uncertain nonlinear systems.

2. Experimental Study

The properties of a semi-active magneto-rheological (MR) damper are controllable through changing the magnitude of the input current fed to the damper's electromagnet. A total of 4000 tests were performed with different means and standard deviation of input current. During the tests, the displacement (x), velocity (\dot{x}), and force (f) were measured separately. A schematic of the instrumentation system architecture is shown in Fig. 1.

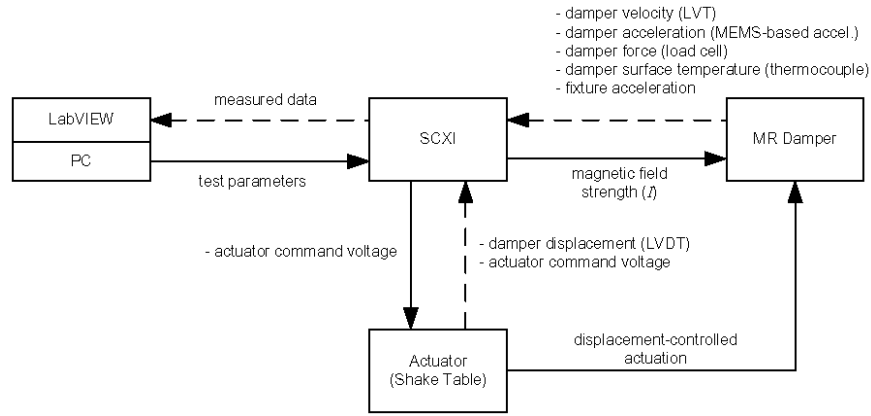


Fig. 1. Schematic of the instrumentation system architecture for the magnetorheological (MR) damper test apparatus.

3. Introduction to the Restoring Force Method

A non-parametric system identification (SI) approach, the Restoring Force Method (RFM), was used in this study due to its ability to characterize a wide range of nonlinearities (Masri and Caughey, 1979). Using RFM, the restoring force of a single-degree-of-freedom nonlinear dynamic system can be modeled as

$$r(x, \dot{x}) = \sum_{i=0}^P \sum_{j=0}^Q \bar{C}_{ij} \bar{T}_i(\bar{x}) \bar{T}_j(\bar{\dot{x}}) \quad (1)$$

where $r(x, \dot{x})$ is the restoring force of the nonlinear dynamic system, \bar{C}_{ij} is the normalized Chebyshev coefficient, \bar{T}_i is the i^{th} or j^{th} order Chebyshev polynomial, P and Q are the highest input modeling orders of the Chebyshev polynomial of the normalized displacement and velocity, respectively, within the range of $[-1, 1]$. Once the normalized Chebyshev coefficients are identified, they can be converted into the equivalent power series coefficients:

$$r(x, \dot{x}) = \sum_{i=0}^P \sum_{j=0}^Q \bar{C}_{ij} \bar{T}_i(\bar{x}) \bar{T}_j(\bar{\dot{x}}) = \sum_{i=0}^P \sum_{j=0}^Q \bar{a}_{ij} \bar{x}^i \bar{\dot{x}}^j = \sum_{i=0}^P \sum_{j=0}^Q a_{ij} x^i \dot{x}^j \quad (2)$$

Thus, three kinds of equivalent coefficients are available using the RFM: normalized Chebyshev coefficients (\bar{C}_{ij}), normalized power series coefficients (\bar{a}_{ij}), and de-normalized power series coefficients (a_{ij}). The basis functions for \bar{C}_{ij} are orthogonal, while the basis functions for \bar{a}_{ij} and a_{ij} are non-orthogonal.

4. MR Damper Identification

4.1. Physical interpretations without a priori knowledge

The MR damper used in this study had very complicated nonlinearities: a hysteretic nonlinearity due to the viscous action of the MR fluid combined with a dead-space nonlinearity due to a mechanical gap in the damper near the damper's neutral position (i.e., $x \approx 0$) and the viscous nonlinearity due to the MR damper characteristics within the remaining displacement range.

The MR damper was identified with the model orders of O(5/20) and O(20/20) to investigate the effects of model-order reduction. Fig. 2 shows the velocity-force plot of the measured and identified response with modeling orders of 5 and 20 (Fig. 2 (a)-(c), respectively). It is demonstrated that with a 5th order analysis the majority of the traces of the hysteresis and damping softening-related nonlinearity in the velocity-force plot can be identified. However, the details of the traces (largely due to the dead-space nonlinearity) fail to be identified. Using the basis functions of the Chebyshev polynomials, "smooth" (or continuous) nonlinearities can be identified using a relatively small number of the series expansion terms. However, for a discontinuous nonlinearity, such as the dead-space nonlinearity, a relatively large number of the series expansion terms are usually needed of the same basis functions. Fig. 2 (d) shows that with a higher modeling order, the discontinuous nonlinearity is fairly accurately identified. In SHM applications, the system complexity, $O(\mathbf{p})$, is generally unknown, so that the identification results using reduced-order models would be statistically biased, which results in unreliable system condition assessment.

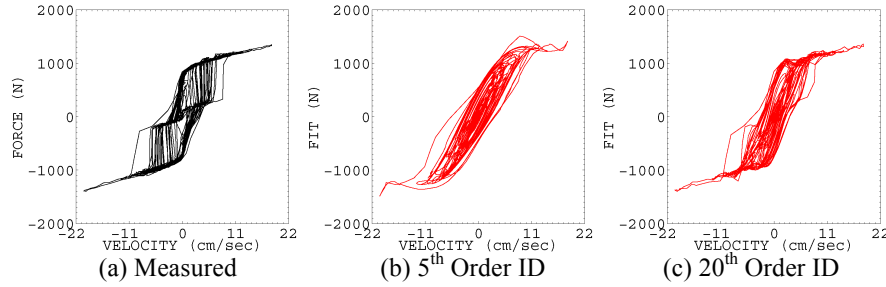


Fig. 2 - A sample identification result for the MR damper using the Restoring Force Method with different model complexities.

4.2. Physical interpretations without assuming system models

Greater system identification accuracy can be achieved with a higher modeling order. However, in the area of change detection, focus must be placed upon the major properties of the device. The unbiasedness of the identified coefficients using the orthogonal basis functions is critical for implementing the change detection in uncertain nonlinear systems: the probability of the identified coefficients should be a function of the system uncertainty, not a function of the model complexity. When the unbiasedness is guaranteed, the identified coefficients of a reduced-order model can be safely used for change detection. Consequently, change detection could be observed even with the model complexity of $O(\mathbf{p}) \neq O(\mathbf{q})$.

According to Yun and Masri (2008), the identified restoring forces for reduced-order and higher-order models can be expressed as

$$\hat{r}_h = \hat{r}_l + \hat{r}_e = \hat{\phi}_l \psi_l + \hat{\phi}_e \psi_e = \hat{\phi}_h \psi_h \quad (3)$$

where \hat{r}_l and \hat{r}_h are the restoring force components identified with a reduced-order model and higher-order model, respectively, \hat{r}_e is the residual between \hat{r}_l and \hat{r}_h , $\hat{\phi}_l$ and $\hat{\phi}_h$ are the identified model parameters for the higher-order and reduced-order models, respectively, $\hat{\phi}_e$ is the identified model parameters for the residual, ψ_h and ψ_l are the basis functions for the higher and reduced-order models, and ψ_e is the basis function for the restoring force residual. The identified model parameters can be estimated as

$$E[\hat{\phi}_h] = \frac{\langle \hat{r}_h, \psi_l \rangle}{\langle \hat{r}_l, \psi_l \rangle} = \frac{\langle \hat{\phi}_l \psi_l + \hat{\phi}_e \psi_e, \psi_l \rangle}{\langle \psi_l, \psi_l \rangle} = \hat{\phi}_l \frac{\langle \psi_l, \psi_l \rangle}{\langle \psi_l, \psi_l \rangle} + \hat{\phi}_e \frac{\langle \psi_e, \psi_l \rangle}{\langle \psi_l, \psi_l \rangle} = \hat{\phi}_l + \hat{\phi}_e \psi_e \quad (4)$$

where $\langle \bullet \rangle$ is the inner product of two functions, $\psi_l = 1$, and $\psi_e = \frac{\langle \psi_e, \psi_l \rangle}{\langle \psi_l, \psi_l \rangle}$. Therefore, the biasness of the reduced-order model parameter ($\hat{\phi}_h$) depends on the significance of the term $\hat{\phi}_e \psi_e$. For the RFM, the orthogonality of the Chebyshev polynomial basis functions is guaranteed with the normalized displacement and velocity within the range of [-1, 1]. Consequently, the identified \bar{C}_{ij} become unbiased because ψ_l and ψ_e are orthogonal, and $\hat{\phi}_e \psi_e = 0$. Consequently, $E[\hat{\phi}_h] = \hat{\phi}_l$ is unbiased when ψ_l and ψ_e are orthogonal.

Fig. 3 shows a comparison of term-wise identification results, with two different modeling orders, for the normalized Chebyshev polynomial basis functions. In the figure, the first row shows the term-wise identification results with the O(5/20) for the linear damping (a), cubic damping (b) and linear stiffness terms (c), and the second row shows the same term-wise identified restoring forces with the O(20/20) and the results with O(5/20) and O(20/20) are nearly identical.

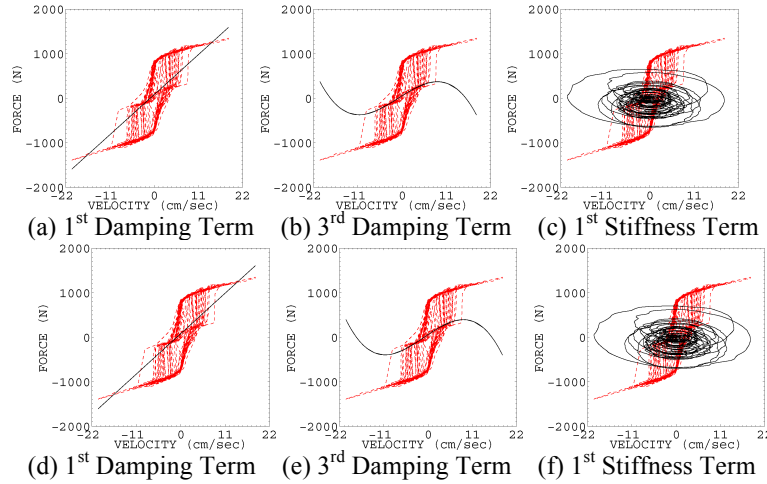


Fig. 3. Term-wise identification results with the modeling orders of O(5/20) (a-c) and O(20/20)(d-f) with the normalized Chebyshev polynomial basis functions.

Table 1 shows the stochastic effects of the model-order reduction on identified coefficients with the Chebyshev and power series polynomials. The comparison shows clearly that the identified Chebyshev coefficients are not biased with respect to the model complexity. Thus, the use of the RFM's Chebyshev polynomials with reduced-order models can reliably be used to detect changes in the system (Yun and Masri, 2008).

Table 1. Stochastic effects of model-order reduction on the coefficient identification with orthogonal and non-orthogonal basis functions after 4000 tests. The (%) column shows the percentage of $\frac{O(5/20)}{O(20/20)}$.

Chebyshev polynomials (orthogonal)						
Term (i,j)	Mean			Std. Dev.		
	O(5/20)	O(20/20)	(%)	O(5/20)	O(20/20)	(%)
(0,1)	1618.9	1637.2	98.9	53.5	54.2	98.6
(1,0)	624.1	668.2	93.4	43.2	48.0	90.0
(0,3)	14.6	15.6	93.9	17.3	17.2	100.7
Power series polynomials (non-orthogonal)						
(0,1)	3612.9	4615.9	78.3	167.7	1036.3	16.1
(1,0)	1210.8	1163.7	104.0	115.6	968.1	11.9
(0,3)	-5026.6	-24603.5	20.4	467.5	39334.8	1.19

The unbiasedness of the identified coefficients using the orthogonal basis functions is important for health monitoring because change detection is observed even at lower-ordered identification. Fig. 4 shows that even with only two identified coefficients (\bar{C}_{10} and \bar{C}_{01}), bivariate probability density functions can still accurately represent physical changes in the MR damper.

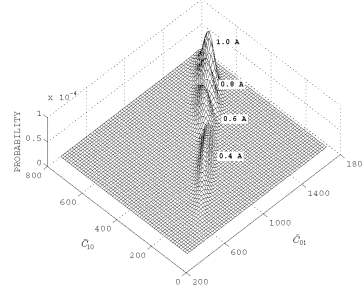


Fig. 4. Bivariate Gaussian distributions of the identified Chebyshev coefficients of two dominant terms

4.3. Classification of change detections

A reliable change detection method must be able to classify the detected changes. In this study, four different input currents and 2 different standard deviations were delivered to the MR damper, allowing for eight classification possibilities.

Support vector classification (SVC) was conducted on the identified orthogonal and non-orthogonal basis functions to detect effective changes (input current and standard deviation) of the MR damper. In Fig. 5, plots (a) and (b) shows the results of the orthogonal and non-orthogonal based coefficients, respectively, and plot (c) details normalized computation time. In plots (a) and (b), the \circ and \blacktriangle represents a lower and higher system uncertainty level, respectively.

By this comparison, it is clear the orthogonal coefficients were more robust and accurate in system change detection. Regardless of model order, orthogonal basis coefficient provided a higher classification. Additionally, classification precision continued to rise as the modeling order increased meaning that they can be used as excellent indicators for detecting (small) effective changes. With this information, an optimal classifier design procedure can be designed subject to three thresholds: classification precision, model order, and computation time can be established for a particular health monitoring case (Yun and Masri, 2009).

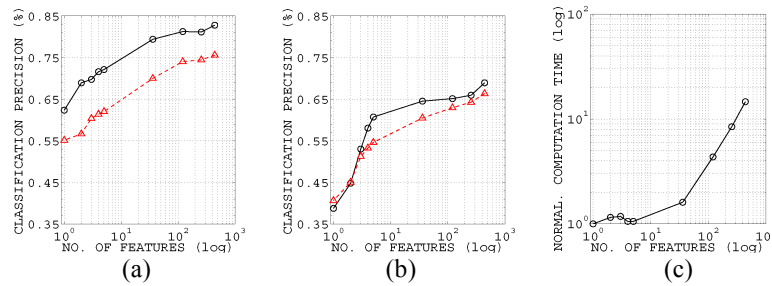


Fig. 5. The precisions of the support vector classification (SVC) for (a) orthogonally and (b) non-orthogonally based coefficients. In these comparisons, physical damper parameters with two different uncertainty levels are compared (\circ represents a higher level of uncertainty than \blacktriangle). The number of features is the number of terms of the series expansions used in the classification. (c) Details the system identification dependence upon computation time, normalized with respect to the smallest time.

5. Novel Reconfigurable Testing Approach

A great limitation on the system uncertainty study is that the MR damper does not have complete modeling

freedom. It would be very beneficial to have a versatile, but accurate, reconfigurable test apparatus capable of replicating a wide range of nonlinear behavior. An ongoing study by the authors seeks to develop such a device where the restoring force can accurately be controlled and reprogrammed based upon directly measured displacement and velocity readings at each time step. The device offers control over nonlinear characteristics and the equation of dynamic motion. A sample of restoring force vs. displacement phase plots created with the reconfigurable test setup is seen in Fig. 4.

The advantage of having such an experimental setup is the ability to simulate various types of nonlinearities with the same test setup. Similarly, controlled system uncertainties can be incorporated into the output of the restoring force, allowing for the realistic simulation of structural damage or deterioration.

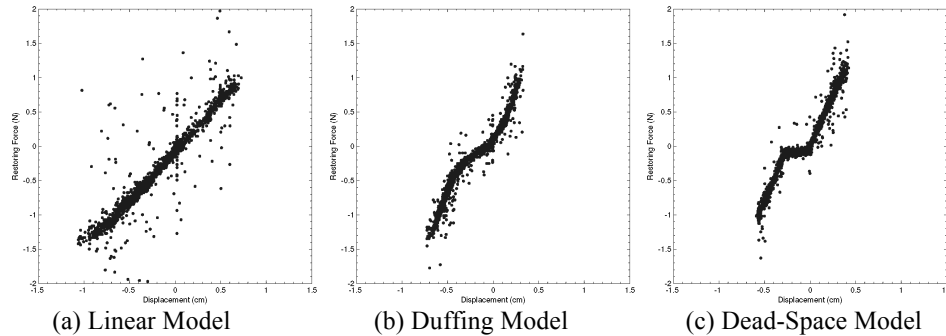


Fig. 4. Restoring force vs. displacement phase plots created by a reconfigurable test setup. A versatile device such as this will allow for a wide variety of system uncertainty studies. The creation of the device is an ongoing research project by the authors.

6. Conclusions

This methodology is applicable to various nonlinear systems for change detection analysis because no *a priori* knowledge of physical characteristics of target systems is required. The normalized Chebyshev (orthogonal) coefficients of the RFM can be used as an indicator because they are statistically unbiased, able to detect system changes, and physical interpretation is possible. Detection errors were also analyzed to evaluate the performance of the developed health monitoring methodology. An optimal design procedure was also proposed to classify system changes.

The magnetorheological damper used to create physical change detection data proved useful in this study. However, its equation of dynamic motion is limited to that of a nonlinear damper. For the physical creation of a wide range of nonlinear models, the authors also introduced an experimental setup whose restoring force can accurately be controlled and updated in real-time based upon directly measured displacement and velocity readings.

References

- Masri, S.F, Caughey, T.K. (1979) A nonparametric identification technique for nonlinear dynamic problems. *Journal of Applied Mechanics Transactions on ASME* 46:2, 433-447.
- Mita, A. and Hagiwara, H. (2003) Damage diagnosis of a building structure using support vector machine and modal frequency patterns. *Smart Systems and Nondestructive Evaluation for Civil Infrastructures* edited by Shih-Chi Liu, 50:57, 118-123.
- Yun, H.-B. and Masri, S. F. (2008). Stochastic change detection in uncertain nonlinear systems using reduced-order models: system identification. *Smart Materials and Structures*, 17:1, 1-13.
- Yun, H.-B. and Masri, S. F. (2009). Stochastic change detection in uncertain nonlinear systems using reduced-order models: classification. *Smart Materials and Structures*, 18:1, 1-12.

LIST OF REFERENCES

- Agrawal, A. K., Yang, J. N., and He, W. L. (2003). "Applications of Some Semiactive Control Systems to Benchmark Cable-Stayed Bridge." *Journal of Structural Engineering*, 129(7), 884–894.
- Ang, A. H.-S. and Tang, W. H. (1975). *Probability Concepts in Engineering Planning and Design, Basic Principles*. Wiley.
- Arup (2011). "The Millennium Bridge Project Page.
- Ayyub, B. M. and Klir, G. J. (2006). *Uncertainty Modeling and Analysis in Engineering and the Sciences*. Chapman and Hall/CRC.
- Balthazar, J. M., Gonçalves, P. B., and Brasil, R. M. R. L. F. (2008). "Uncertainties in Nonlinear Structural Dynamics." *Mathematical Problems in Engineering*, 2008, 1–5.
- Borcherdt, R. D. (2005). "The Race to Seismic Safety: Protecting California's Transportation System." *Earthquake Spectra*, 21(2), 613–615.
- Caffrey, J. P., Masri, S. F., Tasbihgoo, F., Smyth, A. W., and Chassiakos, A. G. (2004). "A Re-Configurable Test Apparatus for Complex Nonlinear Dynamic Systems." *Nonlinear Dynamics*, 36(2-4), 181–201.
- Chen, P. and Wereley, N. (2004). "Magnetorheological damper and energy dissipation method.
- Cheng, S., Darivandi, N., and Ghrib, F. (2010). "The design of an optimal viscous damper for a bridge stay cable using energy-based approach." *Journal of Sound and Vibration*, 329(22), 4689–4704.

- Cleveland, W. S. and Loader, C. (1994). "Smoothing by Local Regression : Principles and Methods." *Report no.*, AT&T Bell Laboratories, Statistics Department, Murray Hill, NJ.
- Clifford, C. (2011). "Making buildings safer with earthquake shock absorbers.
- Datta, K. B. and Mohan, B. M. (1995). *Orthogonal Functions in Systems and Control (Advanced Series in Electrical and Computer Engineering)*. World Scientific Publishing Company, Singapore.
- Gavin, J. (1993). "Moving weighted average graduation using kernel estimation." *Insurance: Mathematics and Economics*, 12(2), 113–126.
- Hall, P. and Selinger, B. (1981). "Better estimates of exponential decay parameters." *The Journal of Physical Chemistry*, 85(20), 2941–2946.
- Hart, G. and Yao, T. (1976). "System identification in structural dynamics." *Journal of Engineering Mechanics*, 103(6), 1089–1104.
- Hart, G. C. and Wong, K. (2000). *Structural Dynamics for Structural Engineers*. John Wiley & Sons.
- Henderson, R. (1916). "Note on graduation by adjusted average." *Actuarial Society of America*, 17, 43–48.
- HITEC (1996). *Guidelines for the Testing of Seismic Isolation and Energy Dissipating Devices. CERF Report No. 96-02*. American Society of Civil Engineers, cerf repor edition.
- HITEC (1999a). *Evaluation Findings for Taylor Devices Fluid Viscous Damper. CERF Report No. 40402*. American Society of Civil Engineers, cerf repor edition.

- HITEC (1999b). *Summary of Evaluation Findings for the Testing of Seismic Isolation and Energy Dissipating Devices. CERF Report No. 40404*. American Society of Civil Engineers, cerf repor edition.
- Ibrahim, R. and Pettit, C. (2005). “Uncertainties and dynamic problems of bolted joints and other fasteners.” *Journal of Sound and Vibration*, 279(3-5), 857–936.
- Koekoek, R., Lesky, P. A., and Swarttouw, R. F. (2010). *Hypergeometric Orthogonal Polynomials and Their Analogues*. Springer.
- Li, H. and Ou, J. (2008). “Recent Advances In Structural Vibration And Failure Mode Control In Mainland China : Theory , Experiments And Applications.” *Engineering Conference*, 137–143.
- Lin, W.-H. and Chopra, A. K. (2002). “Earthquake response of elastic SDF systems with non-linear fluid viscous dampers.” *Earthquake Engineering & Structural Dynamics*, 31(9), 1623–1642.
- Mason, J. and Handscomb, D. C. (2002). *Chebyshev Polynomials*. Chapman and Hall/CRC.
- Masri, S., Smyth, A., Chassiakos, A., Caughey, T., and Hunter, N. (2000). “Application of neural networks for detection of changes in nonlinear systems.” *Journal of Engineering Mechanics*, 126(July), 666.
- Masri, S. F. and Caughey, T. (1979). “A Nonparametric Identification Technique for Nonlinear Dynamic Problems.” *Journal of Applied Mechanics*, 46(2), 433 – 447.
- Mendel, J. M. (1995). *Lessons in Estimation Theory for Signal Processing, Communications, and Control (2nd Edition)*. Prentice Hall.
- Minyamoto, K. and Hanson, R. D. (2002). “U. S. design of structures with damping systems.” *Proceedings of Structural Engineers World Congress (SEWC)*, Yokohama, Japan.

- Nayeri, R. D., Tasbihgoo, F., Wahbeh, M., Caffrey, J. P., Masri, S. F., Conte, J. P., and Elgamal, A. (2009). "Study of Time-Domain Techniques for Modal Parameter Identification of a Long Suspension Bridge with Dense Sensor Arrays." *Journal of Engineering Mechanics*, 135(7), 669.
- Park, W. and Koh, H. (2001). "Application and r&d of active, semi-active and hybrid vibration control techniques for civil structures in Korea." *7th International Seminar on Seismic Isolation, Passive Energy Dissipation and Active Control of Vibrations of Structures*, Assisi, Italy.
- Proakis, J. G. and Manolakis, D. K. (2006). *Digital Signal Processing (4th Edition)*. Prentice Hall.
- Soong, T. T. and Dargush, G. F. (1997). *Passive Energy Dissipation Systems in Structural Engineering*. Wiley.
- Spencer, B. F. (1999). "New applications and development of active, semi-active and hybrid control techniques for seismic and non-seismic vibration in the USA." *Structure*, 1994.
- Tasbihgoo, F. (2006). "Analytical and Experimental Studies in the development of Reduced-Order Computational Models for Nonlinear Systems," PhD thesis, University of Southern California.
- Tasbihgoo, F., Caffrey, J., and Masri, S. F. (2007). "Development of data-based model-free representation of non-conservative dissipative systems." *International Journal of Non-Linear Mechanics*, 42(1), 99–117.
- Taylor, D. P. (1996). "Fluid Dampers for Applications of Seismic Energy Dissipation." *Eleventh World Conference on Earthquake Engineering*. Elsevier Science Ltd., Paper Number: 798.
- Thorlabs (2010). "Theory of Tabletop Vibration.

- Wolfe, R. (2002). “Analytical and experimental studies of structural health monitoring of non-linear viscous dampers,” PhD thesis, University of Southern California.
- Wolfe, R. W., Masri, S., Tasbihgoo, F., Angeles, L., Benzoni, G., and Diego, S. (2008). “Fidelity of Reduced-Order Models for Large-Scale Nonlinear Orifice Viscous Dampers.” *Structural Control and Health Monitoring*, 15, 1143 – 1163.
- Wolfe, R. W., Masri, S. F., and Caffrey, J. (2002). “Some structural health monitoring approaches for nonlinear hydraulic dampers.” *Journal of Structural Control*, 9(1), 5–18.
- Worden, K. (1990). “Data processing and experiment design for the restoring force surface method, part I: Integration and differentiation of measured time data.” *Mechanical Systems and Signal Processing*, 4(4), 295 – 319.
- Wright, P. K. (2000). *21st Century Manufacturing*. Prentice Hall.
- Yun, H., Nayeri, R., Tasbihgoo, F., Wahbeh, M., Caffrey, J., and Wolfe, R. (2008). “Monitoring the collision of a cargo ship with the Vincent Thomas Bridge.” *Structural Control and Health Monitoring*, (April 2007), 183–206.
- Yun, H.-B. and Masri, S. F. (2008). “Stochastic change detection in uncertain nonlinear systems using reduced-order models: system identification.” *Smart Materials and Structures*, 17(1), 015040.
- Yun, H.-B. and Masri, S. F. (2009). “Stochastic change detection in uncertain nonlinear systems using reduced-order models: classification.” *Smart Materials and Structures*, 18(1), 015004.
- Yun, H.-B., Masri, S. F., Wolfe, R. W., and Benzoni, G. (2009). “Data-driven methodologies for change detection in large-scale nonlinear dampers with noisy measurements.” *Journal of Sound and Vibration*, 322(1-2), 336–357.

- Yun, H.-B., Tasbihgoo, F., Masri, Caffrey, J., Wolfe, R., Makris, N., and Black, C. (2008).
“Comparison of Modeling Approaches for Full-scale Nonlinear Viscous Dampers.” *Journal of Vibration and Control*, 14(1-2), 51–76.
- Zill, D. G., Late, and Cullen, M. R. (2006). *Advanced Engineering Mathematics*. Jones & Bartlett Pub.